13th International Eclogite Conference
Petrozavodsk, Karelia, Russia
June 24–27th, 2019

IEC-13
Petrozavodsk
Russia

EARLY PRECAMBRIAN ECLOGITES of the Belomorian Province, Fennoscandian Shield

Field Guidebook

IEC

Institute of Geology, Karelian Research Center, RAS
Geological Institute, Kola Science Centre, RAS
Geological Institute, RAS

EARLY PRECAMBRIAN ECLOGITES

of the Belomorian Province, Fennoscandian Shield

Field Guidebook

Organizers and editors
of the Field Guidebook:

Alexander Slabunov,
Institute of Geology KarRC RAS, Petrozavodsk, Russia

Victor Balagansky,
Geological Institute KSC RAS, Apatity, Russia

Andrey Shchipansky,
Geological Institute RAS, Moscow, Russia

Petrozavodsk
2019

УДК 552.48:551.71/.72(1-924.14/.16)(036)
ББК 26.31
Е11

Early Precambrian Eclogites of the Belomorian Province, Fennoscandian Shield. Field Guidebook /
Е11 A.I. Slabunov, V.V. Balagansky, A.A. Shchipansky (Eds.). – Petrozavodsk : KRC RAS, 2019. – 81 p.

ISBN 978-5-9274-0853-5

Early Precambrian eclogites are widespread in the Belomorian Province of the Fennoscandian shield. There are three points of view on the their age: 1) Archean and Paleoproterozoic; 2) solely Mesoarchean; 3) solely Paleoproterozoic. The goal of this field trip is to show all these types of eclogites including Archean and Paleoproterozoic (from the authors' point of view) eclogites, eclogitized Paleoproterozoic coronitic gabbroids, Archean zoisitites and their structural position in the Gridino, Salma (Uzkaya Salma and Shirokaya Salma) and Kuru-Vaara areas of the Belomorian Province. The geological excursions provide a good opportunity for the participants and the reader to exanimate these contradicting points of view immediately at beautiful outcrops on islands of the White Sea, on the benches of the Kuru-Vaara quarry and in the walls of road pits in the Salma area.

This Field Guidebook is of interest for geologists, petrologists and geochronologists who study the early evolution of the Earth and HP-UHP metamorphic processes.

552.48:551.71/.72(1-924.14/.16)(036)
ББК 26.31

Financial support of the Conference by the Ministry of Science and Higher Education of the Russian Federation

ISBN 978-5-9274-0853-5

CONTENTS


Ab → Jd+Q
Cpx20 ≠ Pmin
Cpx+Q
Cpx5+B
5%
Pl+Cpx
Cpx5
T
S
Ab
D

GEOLOGICAL REVIEW

ARCHEAN-PALEOPROTEROZOIC CRUSTAL EVOLUTION OF THE BELOMORIAN PROVINCE (FENNOSCANDIAN SHIELD) AND THE TECTONIC POSITION OF ECLOGITES

Slabunov, A.I.[1], *Balagansky, V.V.*[2], *Shchipansky, A.A.*[3]

[1] Institute of Geology, Karelian Research Center, Russian Academy of Sciences, 185910 Petrozavodsk, Pushkinskaya 11, Russia
[2] Geological Institute, Kola Science Center, Russian Academy of Sciences, 184209 Apatity, Fersmana 14, Russia
[3] Geological Institute, Russian Academy of Sciences, Russia 119225 Moscow, Staromonetniy 35, Russia

The Belomorian province, an Early Precambrian mobile belt, is located in the central part of the Archean core of the Fennoscandian shield and intervenes between the Archean Kola Province in the northeast and the Archean Karelian craton in the southwest (Figs. 1.1 and 1.2). This is believed to extend southeast at least 350 km beneath the sedimentary cover of the Russian platform (Bogdanova et al., 2005). The continental crust of the Belomorian Province was formed during the Meso- and Neoarchean Belomorian accretionary-collisional orogeny (Glebovitsky et al., 1996; Bibikova et al., 1999, 2004;

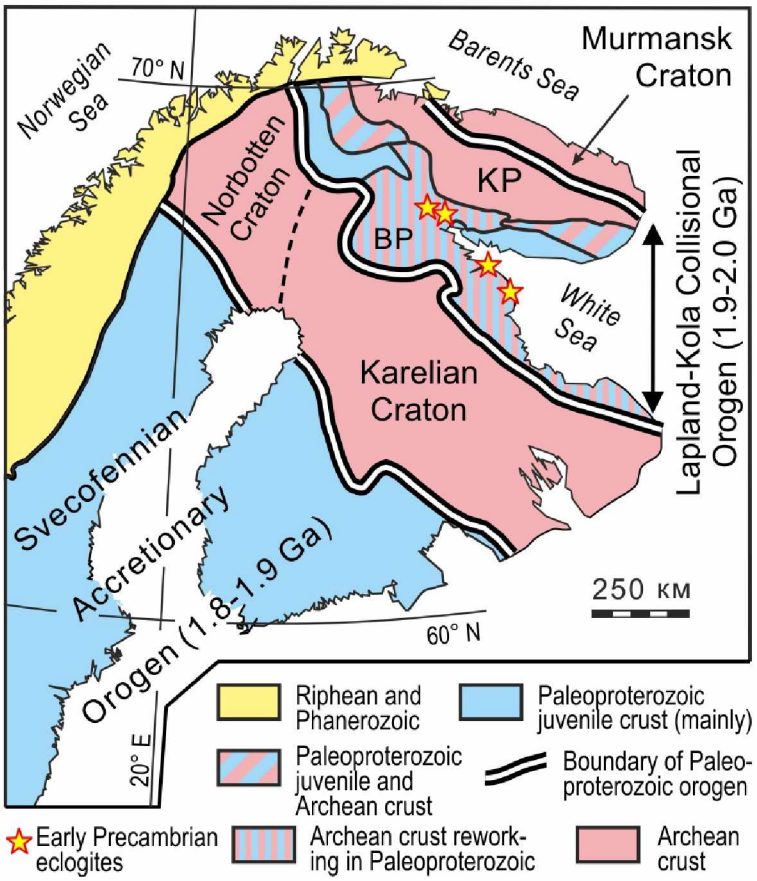

Fig. 1.1. Major tectonic units of the Fennoscandian shield (BP and KP, Belomorian and Kola provinces, respectively)

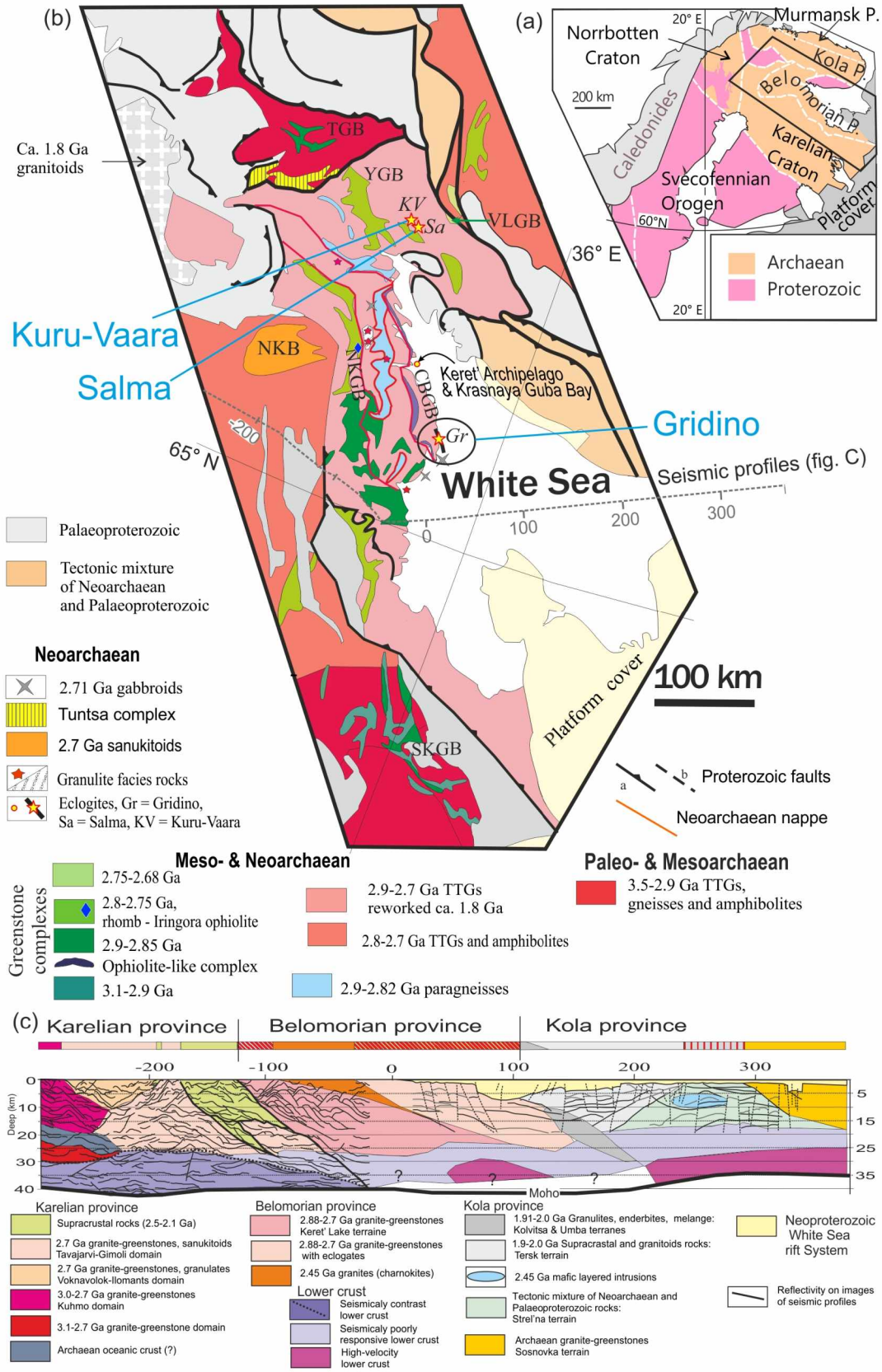

Fig. 1.2. (a) Location of the geological scheme shown in (b); (b) Geological scheme of the Belomorian province, Fennoscandian Shield (modify after Slabunov, 2008). **Paragneiss belt:** ChPB = Chupa; **Greenstone belt:** KGB = Keret'; NKGB = North Karelian; YGB = Yona greenstone belt; VLGB = Voche-Lambino greenstone belt; **Constituent part (structure) of geenstone belt**: Kh = Khizovaara; Ke = Keretozero; Ki = Kichany; Ka = Kolikorva; Ch = Chelozero; **Eclogite-bearing complex:** Gr = Gridino; Sa = Salma. (c) Geological deep section along seismic profiles DSS–CDP Kalevala–Kem'–White Sea (Sharov et al., 2010)

Slabunov, 2008; Mints et al., 2015). The Belomorian province was under the influence of a 2.40–2.45 Ga superplume (Bogdanova, 1996; Kulikov et al., 2010; Stepanova, Stepanov, 2010) and a *ca.* 2.1 Ga continental rifting (Stepanova et al., 2014). Then the Belomorian Province was the southwestern foreland of the Paleoproterozoic Lapland-Kola collisional orogen and was reworked during the Lapland-Kola orogeny (Daly et al., 2001, 2006; Balagansky, 2002). Hence, the Belomorian province is a deep Archean crust considerably exhumed shortly after the peak of the Paleoproterozoic collision (<1.90–1.92 Ga).

The Belomorian province is a tectonic collage consisting of several thrust-bounded sheets (nappes) as shown by geological mapping (Miller, Milkevich, 1995) and deep seismic profiles (Fig. 1.2 b-c) (Sharov et al., 2010). Neoarchean (*ca.* 2.7 Ga) nappes were probably responsible for the province structure (Miller, Milkevich, 1995; Glebovitsky et al., 1996) and Paleoproterozoic Lapland-Kola collision made this structure much more intricate (Glebovitsky, 2005; Daly et al., 2006; Mints et al., 2010b; Mudruk et al., 2013).

The Belomorian province consists of dominantly of Meso- and Neoarchean TTG rocks and subordinate amphibolites and paragneisses of the same age (2.90–2.65 Ga). The most ancient rocks are represented by ≥2.9 Ga dismembered remnants of a supra-subduction zone (SSZ) ophiolite (Fig. 1.2), a constituent part of the Late Mesoarchean Seryak mafite-ultramafite complex (Slabunov et al., 2019). Multiply foliated and migmatized TTG gneisses have developed from igneous protoliths from 2.88 Ga to 2.72 Ga, while their Sm-Nd model ages (t_{DM}) range from 2.93 to 2.72 Ga, indicating a lack of older crustal sources (Slabunov et al., 2006a, b; Slabunov, 2008). Archean high-grade amphibolite and paragneiss belts make up *ca.* 15–20 % of the province area (Fig. 1.2b) and consist of rocks geochemically close to island-arc volcanics, fore-arc basin sediments, and dismembered SSZ ophiolites, as well as molassa-type rocks. Five generations of greenstone complexes were formed at 2.88–2.82 Ga, 2.8–2.78 Ga, *ca.* 2.75 Ga, *ca.* 2.72 Ga and not later than 2.66 Ga, and two paragneiss complexes at 2.89–2.82 and 2.78 Ga ago.

The most prominent characteristic feature of the Belomorian province is the occurrence of eclogites (Fig. 1.2b) mentioned in papers already in the first half of the 20th centure (Eskola, 1921; Sudovikov, 1939). A modern stage of studying eclogites has been started after the discovery of these rocks first in the Gridino area (Volodichev et al., 2004) and in the Kuru-Vaara and Salma area, southwestern Kola Peninsula (Mints et al., 2010b), and then on islands of the Keret Archipelago and the Krasnaya Guba Bay (Figs. 1.1 and 1.2b). Two distinct types in age of eclogites have been reported from the Belomorian province, Meso- to Neoarchean (Volodichev et al., 2003, 2004; Slabunov et al., 2006a, b; Mints et al., 2010a, b; 2015; Li et al., 2015; Dokukina, Konilov, 2011; Konilov et al., 2011; Dokukina et al., 2014; Shchipansky et al., 2012a, b) and Paleoproterozoic (Volodichev et al., 2004, 2008; Travin, Kozlova, 2005, 2009; Kozlovsky, Aranovich, 2008, 2010; Skublov et al., 2011a, b, 2012, 2016; Berezin et al., 2012, 2013; Mel'nik, 2015; Travin, 2015; Imayama et al., 2017; Yu et al., 2017, 2019a, b).

Meso- and Neoarchean (2.88–2.82 Ga and ≥2.72 Ga) eclogites occur as remnant mineral assemblages preserved in intensely disintegrated amphibolites embedded in a TTG matrix which has been interpreted as the tectonic mélange in the Gridino area or as the eclogite-TTG mélange in the Kuru-Vaara and Salma areas (Fig. 1.2b; Volodichev et al., 2004; Slabunov et al., 2006a, b; Mints et al., 2010b; 2015; Konilov et al., 2004, 2005, 2011; Shchipansky et al., 2012a; Balagansky et al., 2015). Meso- and Neoarchean (2.82–2.8 Ga, 2.78–2.74 Ga and 2.72 Ga) medium-pressure (MP) granulites have also been reported from mélange zones. Minor 2.7 Ga S-type collisional leucogranites are also noteworthy; in addition, 2.67 Ga late- and postkinematic granites are common.

There are several models proposed for the tectonic evolution of the Belomorian province in the Meso- and Neoarchean. According to (Bibikova et al, 1999, 2004; Shchipansky et al., 2004, 2012a, b; Slabunov, 2008; Slabunov et al., 2006a, b, 2019; Hölttä et al., 2008, 2012, 2014), main stages of the Archean crustal evolution of the Belomorian province are as follows:

- *ca.* 2.9 Ga – initiation of subduction and the formation of the Seryak ophiolite-like sequence;
- *ca.* 2.88–2.82 Ga – the first subduction-accretion event recorded by island-arc volcanics of the Keret greenstone belt, fore-arc meta-graywacke of the Chupa paragneiss belt and the Salma eclogites;
- 2.81–2.78 Ga – the second subduction-accretion event marked by island-arc volcanics and supra-subduction ophiolite in the Iringora area, and metagraywackes and granulites in the Norozero area;
- 2.75 Ga – the third subduction event marked by island-arc volcanics in the Chelozero area;
- 2.73–2.72 Ga – the fourth subduction-accretion event marked by island-arc volcanics, granulites and the Gridino older eclogites (Balagansky et al., 2019 and this guidebook);
- *ca.* 2.7–2.66 Ga – collisional event marked by collisional S-granites, kyanite-type metamorphic rocks, molassa-type rocks, subalkaline granitoids and leucogabbro.

Another tectonic model (Mints et al., 2010b, 2015; Mints, Eriksson, 2016; Dokukina, Mints, 2019) suggests a leading role of subductional, accretionary and collisional processes during the growth of the Belomorian continental crust at 2.9–2.78 Ga and its reworking due to an impingement of mantle plumes at 2.78–2.74 Ga. Paleoproterozoic basic dikes in the Gridino area (Stepanov, Stepanova, 2005; Stepanova, Stepanov, 2010) have been re-interpreted as being Archean in age (Dokukina, Konilov, 2011; Dokukina et al., 2014) and their emplacement are thought to be related to subduction of a mid-ocean slow-spreading ridge beneath the Kola continental plate (Mints et al., 2010b; Konilov et al., 2011; Mints et al., 2014; Dokukina, Mints, 2019). According to this model, the Meso- and Neoarchean eclogite-facies overprint that occurred in these dikes is ascribed to the Archean collision; plume-related metamorphic changes are also suggested. The Archean age of the dikes is strongly disputable and needs more convincing evidence.

In the Early Paleoproterozoic (2.5–2.34 Ga) the Belomorian continental crust was subjected to a thermal influence by a mantle superplume impingement. Located beneath the eastern Fennoscandian Shield, this superplume was responsible for the formation of NW-trending rift-belts (Fig. 1.3) parallel to major Archean tectonic boundaries (Daly at al., 2006; Lahtinen et al., 2008; Stepanova et al., 2010, 2014; Kulikov et al., 2010, 2017; Egorova, 2017). Abundant small, commonly coronitic gabbroid intrusions and dikes (Fig. 1.3), as well as potassic granites were intruded under conditions of oblique crustal extension (Stepanov, 1981; Balagansky et al., 1998; Krivolutskaya et al., 2010; Stepanova et al., 2010; Slabunov et al., 2011; Kulikov et al., 2017). Specific plutonic rocks of this period are 2.44–2.39 Ga lherzolite-gabbronorite (Bibikova et al., 2004; Krivolutskaya et al., 2010; Stepanova, Stepanov, 2010; Slabunov et al., 2011; Volodichev et al., 2012), 2.44 Ga enderbite and charnockite (Korsakova et al., 2011) and rare gabbro-anorthosite of 2.5 Ga (Skublov et al., 2016; Stepanova et al., 2017).

The continental crust of the entire Fennoscandian Shield began to breakdown at 2.1–2.0 Ga ago as evidenced, first of all, by the rift-type ophiolite of Jormua (Peltonen, Kontinen, 2004), as well as by numerous Belomorian Fe-tholeiitic dikes (Fig.1.3) of that age (Stepanova et al., 2014). The Kola Ocean was opened at *ca.* 2.0 Ga along the boundary between the Belomorian and Kola provinces and its closure led to the Lapland-Kola collisional orogeny (Berthelsen, Marker, 1986; Daly et al., 2001, 2006; Balagansky, 2002; Lahtinen et al., 2008; Lahtinen, Huhma, 2019). The juvenile continental crust that composes the core of the Lapland-Kola collisional orogen (first of all, the Lapland granulite belt and the Umba granulite terrane) was formed during NE- or SW-directed subduction of the Lapland-Kola oceanic crust at 1.98–1.94 Ga in the Kola region and approximately 20–30 Ma later in northern parts of Finland and Norway (Daly et al., 2001, 2006; Mints et al., 2007; Mudruk et al., 2013; Lahtinen, Huhma, 2019). The latest studies that used a large body of geophysical data suggest a SW-directed subduction (Mudruk et al., 2013; Lahtinen, Huhma, 2019). Tuisku and Makkonen (1999) reported on a metamorphic rock that was formed under *P–T* conditions transitional between amphibolite- to eclogite facies (11–12 kbar and 670 °C) at 1.90–1.88 Ga. This rock developed from an olivine cumulate in a gabbroid intrusion in the Tanaelv collisional mélange that intervenes between the Archean Belomorian rocks and the overlying Paleoproterozoic Lapland granulite belt (Daly et al., 2001). Its igneous protolith can hardly be coeval to that of extended layers of the Meso- to Neoarchean Belomorian amphibolites containing remnants of eclogite-facies assemblages because these amphibolites originated from basalts of oceanic affinity (Slabunov, 2008; Shchipansky et al., 2012a, b; Mints et al., 2010b, 2014, 2015). The peak of the collision and high-P amphibolite- to granulite-facies metamorphism occurred in the Belomorian province and the Russian part of the overlying Lapland granulite belt at 1.925 Ga (Volodichev, 1990; Glebovitsky, 2005; Daly et al., 2006) and 20–30 Ma later in Finnish Lapland (Lahtinen, Huhma, 2019). Paleoproterozoic gabbroid intrusions and dikes were metamorphosed, and coronitic textures were largely developed (Fedorov, 1896; Stepanov, 1981; Larikova, 2000; Egorova, 2017).

For the first time, Paleoproterozoic eclogite-facies overprint expressed by patches of eclogite-facies mineral assemblages in the igneous matrix was discovered in Paleoproterozoic mafic dikes (Volodichev, 1990; Volodichev et al., 2004). Later the Paleoproterozoic eclogitic assemblages were reported both from Paleoproterozoic basic and gabbro-anorthosite dikes and massifs (Travin, Kozlova, 2005, 2009; Kozlovsky, Aranovich, 2008, 2010; Berezin et al., 2012, 2013; Volodichev et al., 2012; Travin, 2015; Skublov et al., 2016) and from Archean amphibolites (Skublov et al., 2010, 2011a,b; 2012; Herwartz et al., 2012; Mel'nik et al., 2013; Imayama et al., 2017; Yu et al., 2017, 2019a, b). It should be pointed out that these amphibolites are the same rocks in which relics of Archean eclogite were described. Furthermore, ultra-high pressure (UHP) eclogite-facies mineral assemblages were found in some meta-mafic rocks (Morgunova, Perchuk, 2012, Perchuk, Morgunova, 2014). At last, diamond-bearing eclogites that univocally evidence UHP metamorphism have been recently established in the Kuru-Vaara area but an Archean age is argued for these UHP rocks (Shchipansky et al., 2019 and this guidebook).

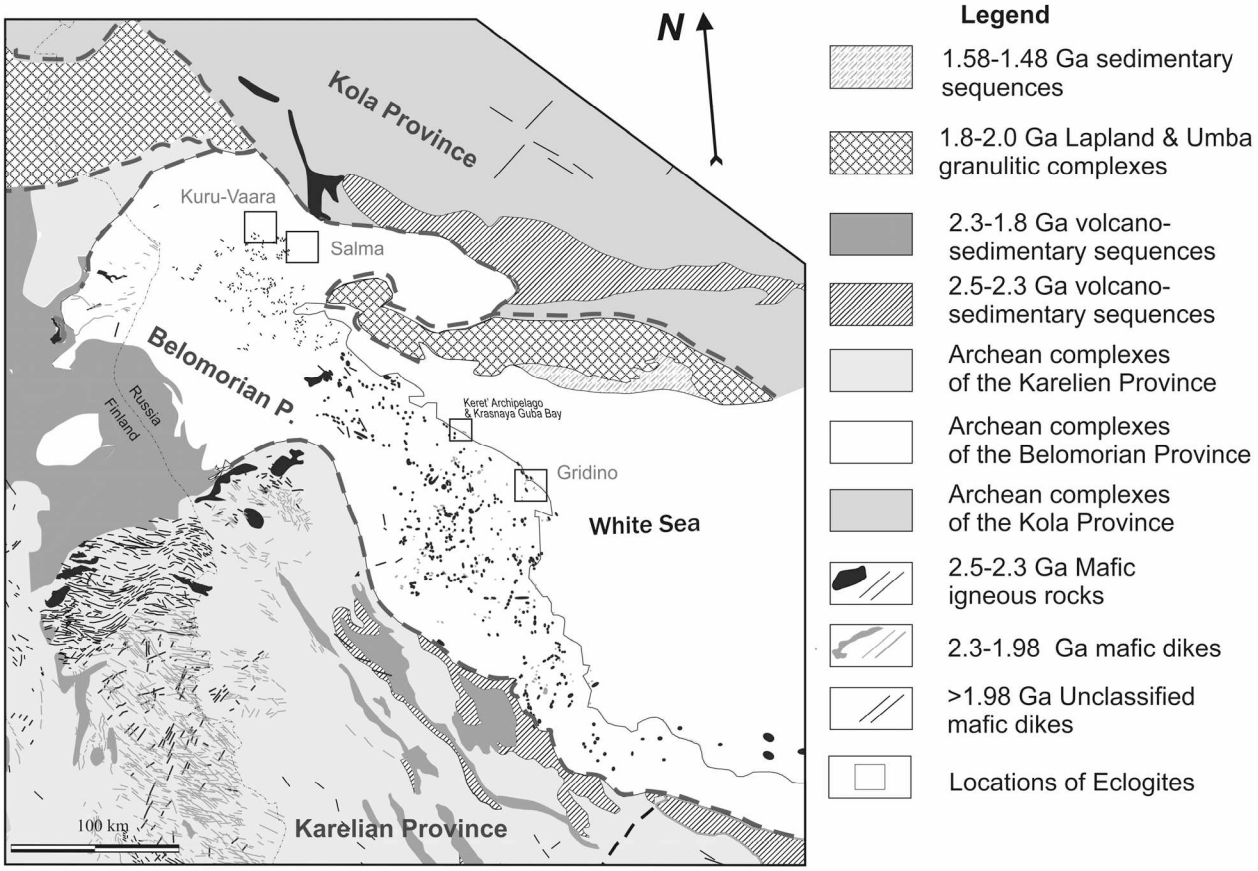

Fig. 1.3. Geological sketch map of the eastern Fennoscandian Shield showing the distribution of Paleoproterozoic mafic rocks (modified after Stepanova et al., 2014) and the location of eclogites in the Belomorian province

The Paleoproterozoic eclogite-facies overprint occurred at *ca*. 1.90 Ga as evidenced by 1.90–1.87 Ga zircon rims containing rare inclusions of omphacite, garnet and kyanite (Imayama et al., 2017; Yu et al., 2017, 2019a, b). These unambiguous Paleoproterozoic eclogites are considered as the younger eclogites in the Gridino area (Balagansky et al., 2019 and this guidebook). All dates obtained for the Paleoproterozoic eclogites fall in the period of the Lapland-Kola collision which started at 1.925 Ga in the Kola part of the Lapland-Kola orogen (Daly et al., 2006) and terminated at 1.88 Ga in the Finnish Lapland part (Lahtinen, Huhma, 2019). During this period, a collage of nappes was developed and resulted in thrusting Belomorian rocks onto the Karelian Craton in the southwestern Belomorian province and, thus, in exhumating its deep crustal levels. The exhumation is consistent with a spatial distribution of U-Pb titanite and rutile ages throughout the Belomorian province: the titanite ages decrease from 1.94 Ga to 1.82 Ga and the rutile ages from 1.81 Ga to 1.74 Ga southwestwards (Bibikova et al., 2001; Nesterova et al., 2011). In turn, the Lapland granulite belt, the Umba granulite terrane and the Tersk terrane were thrust onto the northern and northeastern Belomorian province. Thus, the Lapland-Kola collision resulted in the formation of the Belomorian crustal tectonic stacking so giving rise to the high-P metamorphism. It is the Lapland-Kola collisional orogeny that is considered to be responsible for the Paleoproterozoic eclogite-facies overprint (Balagansky et al., 2015; Lahtinen, Huhma, 2019).

An alternative tectonic model has been recently argued for the evolution of the Belomorian province in the Late Paleoproterozoic (Mints et al., 2015; Mints, Eriksson, 2016). The foundation stone of this model is the Lapland–Mid-Russia–South Baltia intracontinental orogen that originated and evolved due to an influence of mantle plumes. This geodynamic concept excludes the formation of eclogite at that time.

So, the Belomorian province drastically differs from other Archean tectonic units of the Fennoscandian shield in its tectono-metamorphic history (cf. Slabunov et al., 2006a, b). First, the Belomorian rocks underwent regional high-*P* (kyanite-type) amphibolite-facies and granulite-facies metamorphic events in the both Archean and Paleoproterozoic (Volodichev, 1977, 1990; Glebovitsky at al., 1986, 1996; Slabunov et al., 2016, 2017). Second, ultra-high-temperature metamorphic rocks have been reported from several localities of the Belomorian province (Azimov et al., 2017). Finally, vestigial UHP

mineral assemblages in the eclogitic remnants (Morgunova, Perchuk, 2012; Perchuk, Morgunova, 2014; Shchipansky et al., 2019 and this guidebook), and phengite-bearing zoisitites (Volodichev et al., 2014; Slabunov et al., 2015) have been also documented. It is obvious that the Belomorian eclogites are of the prime interest for Early Precambrian geodynamics. It comes as no surprise that their provenance and age remain much disputable. According to the review given above there are three points of view on the age of the Belomorian eclogites:

1. Archean and Paleoproterozoic eclogites (Volodichev et al., 2004, 2012; Slabunov et al., 2011; Balagansky et al., 2015; Li et al., 2015; Babarina et al., 2017; Maksimov, 2019);
2. solely Mesoarchean eclogites (Konilov et al., 2004; 2011; Mints et al., 2010a, b; 2015; Dokukina, Konilov, 2011; Dokukina et al., 2014; Shchipansky et al., 2012a, b; Dokukina, Mints, 2019; Mints, Dokukina, 2019);
3. solely Paleoproterozoic eclogite (Kozlovsky, Aranovich, 2008, 2010; Skublov et al., 2010, 2011a, 2012, 2016; Berezin et al., 2012, 2013; Morgunova, Perchuk, 2012, Mel'nik et al., 2013; Perchuk, Morgunova, 2014; Travin, 2015; Imayama et al., 2017; Li et al., 2017; Yu et al., 2017, 2019a, b; Brown, Johnson, 2018).

The planned geological excursions provide a good opportunity for the reader to exanimate these contradicting points of view immediately on perfect outcrops on islands of the White Sea, on the benches of the Kuru-Vaara quarry and in the walls of road pits in the Salma area.

Good luck, the reader!

Acknowledgements

The Ministry of Science and Higher Education of the Russian Federation is thanked for financial support of the conference. Mr. Alexander Yu. Orlov and Mz. Irina V. Kalinko (managements of the Kol'sky Pegmatit enterprise and the Kuru-Vaara quarry, respectively) are highly appreciated for the permission for visiting the Kuru-Vaara quarry. Xiaoli Li (Peking University) and Sergey G. Skublov (Institute of Precambrian Geology and Geochronology of the RAS) are thanked for the information on the location of eclogite samples studied by them. The guidebook has been partly prepared in the framework of research projects of the Karelian Research Center of the RAS (#A18-118020290085), the Kola Science Center of the RAS (#0226-2019-051) and Geological Institute of the RAS (#AAAA-A17-117030610104-2).

THE GRIDINO AREA

ARCHEAN AND PALEOPROTEROZOIC ECLOGITES AND ZOISITITES IN THE GRIDINO AREA

Balagansky, V.V.[1], *Maksimov, O.A.*[2], *Gorbunov, I.A.*[1], *Kartushinskaya, T.V.*[1], *Mudruk, S.V.*[1], *Sidorov, M Yu.*[1], *Sibelev, O.S.*[2], *Volodichev O.I.*[2], *Stepanova A.V.*[2], *Stepanov V.S.*[2], *Slabunov, A.I.*[2]

[1] Geological Institute, Kola Science Center, Russian Academy of Sciences, Apatity, Russia
[2] Institute of Geology, Karelian Research Center, Russian Academy of Sciences, Petrozavodsk, Russia

The goal of this field excursion is to show Archean and Paleoproterozoic eclogites including eclogitized Paleoproterozoic coronitic gabbroids, Archean zoisitites and their structural position in a Neoarchean mélange of migmatized TTG gneisses and mafic rocks in the central part of the Belomorian Province where Early Precambrian Belomorian eclogites were described in detail for the first time (Volodichev et al., 2004). This province resulted from the superposition of the Meso- to Neoarchean Belomorian accretionary-collisional orogeny (Slabunov et al., 2006a, b) and the Paleoproterozoic Lapland-Kola collisional orogeny (Daly et al., 2006), and deformational and metamorphic events of these two orogenies have been preserved in a mélange rock record.

The Early Precambrian rocks exposed in the Gridino area display two features crucial for an understanding of the structural position and age of the Belomorian eclogites. First, the Gridino area has a three-member NW-trending linear structure (Volodichev et al., 2004). The central member is a 6–7 km wide zone which has a complicated structure and irregular boundaries. Its matrix consists of TTG gneisses that developed mainly from tonalite, plagiogranite, enderbite and diorite protoliths. The TTG gneisses contain arcuate (waved) and folded sheet-like composite bodies in which deformed lenses and both angular and rounded boudins and fragments of garnet and garnet-clinopyroxene amphibolites and tholeiitic to ferrotholeiitic metagabbroids are hosted by similar TTG gneisses (Fig. 2.1). It is this zone that is interpreted as the tectonic mélange intervening between tonalitic TTG gneisses in the northeast and amphibolites, paragneisses and tonalitic TTG gneisses in the southwest (Fig. 2.1). For the first time, relics of intensely retrogressed eclogites were discovered just in the mafic metamorphic rocks of the mélange and were regarded as Archean (Volodichev et al., 2004). Second, Archean metamorphic and deformational events resulted in strong general reworking of TTG gneisses and amphibolites and the formation of the mélange, whereas the Paleoproterozoic reworking was local. Paleoproterozoic mafic dikes cross-cut the mélange and other Archean structures, show weak strain and compose a practically undeformed swarm (Fig. 2.1; Babarina, Sibelev, 2015 and references therein). Some of the Paleoproterozoic dikes experienced a local eclogite-facies overprint (Volodichev et al., 2004, 2011; Travin, Kozlova, 2005, 2009; Dokukina, Konilov, 2011). An idea that the emplacement of these dikes occurred in the Archean (Dokukina et al., 2014) needs more convincing evidence. A Paleoproterozoic eclogite-facies metamorphism (Skublov et al., 2011a, 2012; Yu et al., 2017, 2019a, b) was also established in the same boudin in which the Archean retrogressed eclogite was described. This boudin is referred to as the reference eclogite boudin and is the most critical object of the excursion in the Gridino area.

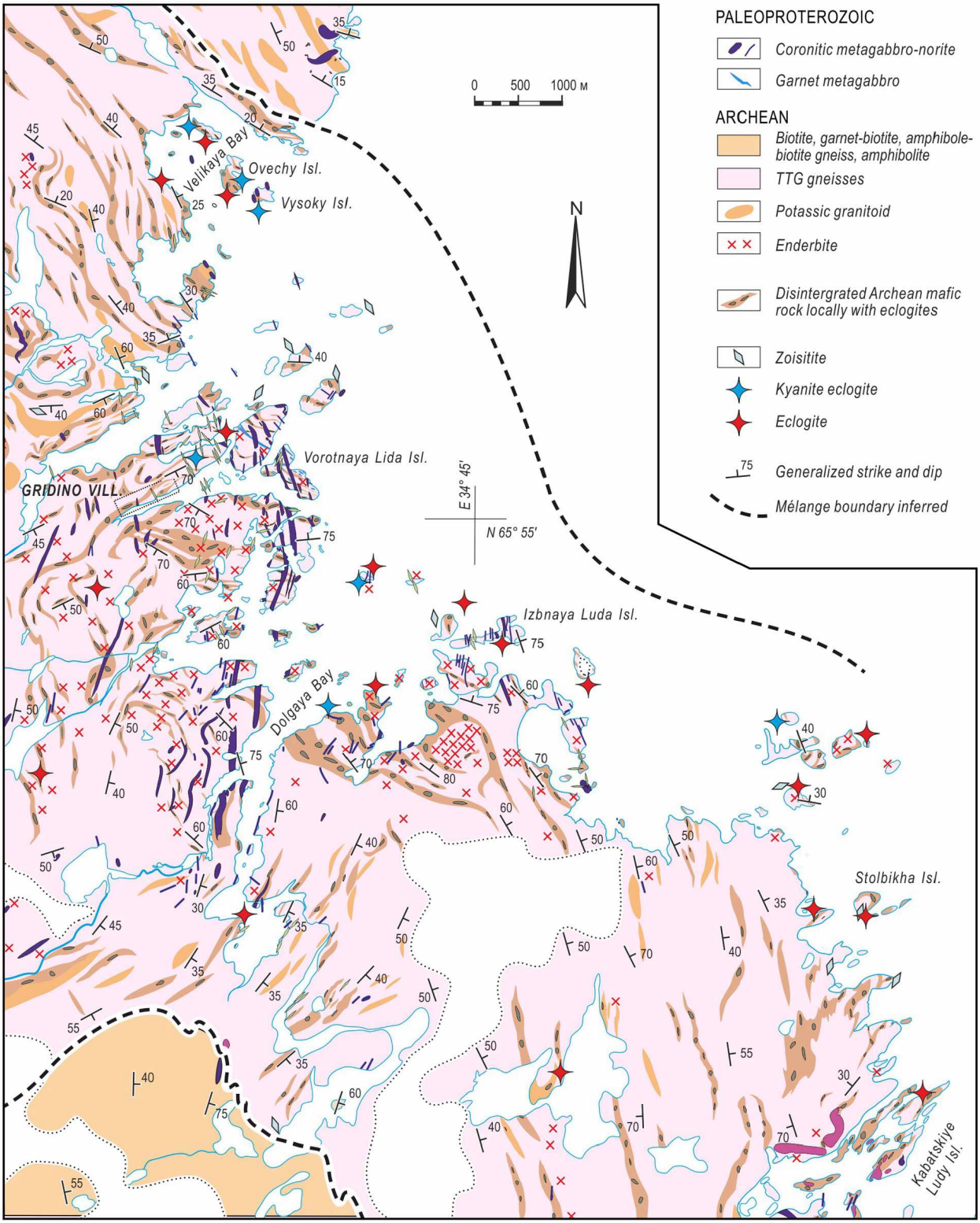

Fig. 2.1. Schematic geological map of the Gridino area compiled by O.S. Sibelev based on his own materials (Sibelev, 2012) and data by researchers from the Institute of Geology of the KarRS RAS (Petrozavodsk), and the Geological Institute of the RAS (Moscow)

Stolbikha Island

Stop 1. The reference eclogite boudin is located in Stolbikha Island (Fig. 2.1). This island is composed mainly of migmatized tonalitic and hornblende varieties of TTG gneisses which contain several strongly folded and boudinated amphibolite bodies and their ubiquitous smaller fragments, as well as pyroxenite and zoisitite enclaves (Fig. 2.2). Penetrative planar fabrics show an open dome and basin pattern and dip shallowly mainly in northwest, north and northeast directions (Fig. 2.2, inlet). Penetrative stretching lineations possess two preferred orientations: the dominant one plunges gently to the northeast and the subordinate one to the northwest (Fig. 2.2, inlet). The excursion objects are situated in the southern and southwestern parts of the island (Figs. 2.2 and 2.3). Here, mylonitized TTG gneisses display dominant shallow dips to the northeast, subordinate shallow dips to the southwest, and gentle stretching lineations plunging mainly northwestwards (Fig. 2.3, inlet). These deformational structural forms are cross-cut by a 2.70 Ga granitoid (Volodichev et al., 2004) and have resulted from an Archean thrusting during the Belomorian accretionary-collisional orogeny (Slabunov et al., 2006a, b). According to (Travin, 2015), the gentle shearing occurred in the Gridino area in the Paleoproterozoic. TTG gneisses and amphibolites that host the reference eclogite boudin are characterized by dome and basin pattern readable on a map and documented by an oval-like scattering pattern of planar fabric poles on a stereographic plot (Fig. 2.4). The attitude of planar fabrics in the reference eclogite boudin is close to those of some planar fabrics in the surrounding amphibolite and TTG gneiss and discordant to those of others.

Stops 1a–e (reference eclogite boudin). The exposed part of the reference eclogite boudin (about 9 × 16 m) has a rounded contour due to intense shearing together with the TTG host (Fig. 2.5). It is similar to a bean grain whose long axis appears to plunge shallowly (20–30°) south-southeastwards. The central part is composed of banded strongly retrogressed (completely symplectitic) eclogites (Figs. 2.5 and 2.6a). The eclogite banding dips gently south-southeastwards (Fig. 2.5, inlet). The banding is folded by recumbent tight to isoclinal folds and is refolded by upright open folds (Fig. 2.6b–c). Hinge lines of all these folds are (sub)parallel to each other and to mineral and aggregate lineations and plunge shallowly south-southeastwards (Fig. 2.5, inlet). Asymmetrical tight to isoclinal folds and lineations of similar orientations occur in the western and southwestern parts of Stolbikha Island (Figs. 2.2 and 2.3), which suggests that the banded retrogressed eclogites and TTG gneisses have the shared deformational history. The banding is gently bent near the boudin contacts where banded, folded, and retrogressed eclogites are sheared and changed into amphibolites and the banding disappears. The sheared amphibolites are migmatized in the northernmost margin (Fig. 2.6d) and are cross-cut by a later coarse-grained pegmatoid granite (Fig. 2.6e). Thus, the central part of the boudin has preserved older structural forms and banding that had been formed before the pre-2.70 Ga penetrative shearing and mylonitization. The latest undeformed pegmatite vein cross-cuts the entire boudin (Figs. 2.5 and 2.6a) and was dated at 1875 ± 30 Ma (Skublov et al., 2011a).

Stops 1a-c are located in the southern part of the boudin composed of banded folded retrogressed eclogites (Fig. 2.6a). The banding is formed by alternating melanocratic and leucocratic retrogressed eclogites chemically similar to each other (Volodichev et al., 2004). A melanocratic variety from Stop 1a (Fig. 2.5; sample V-3-2) is typical and contains coarse lamellar to globular symplectites of clinopyroxene Di_8 with plagioclase Pl_{24}[1]. Garnet forms large compositionally homogeneous grains and bears inclusions of quartz, rutile and zoisite. Edenitic hornblende occurs as large crystals in the *Cpx–Pl* symplectitic groundmass and rare inclusions in garnet. The component compositions of clinopyroxene, plagioclase, garnet and hornblende are shown in Fig. 2.7. Another melanocratic variety (Stop 1b, sample V-3-1, Fig. 2.5) contains symplectites of clinopyroxene Di_9 with plagioclase Pl_{43-49} in which large, relatively homogeneous garnet grains and anomalous plagioclase (bytownite with 85 % anorthite) occur. In addition, there are finer symplectites of clinopyroxene (6 % jadeite) and plagioclase (32–42 % anorthite) in this varieties. Microphotographs of melanocratic and leucocratic types of retrogressed eclogites from Stop 1c (Fig. 2.5) are presented in Fig. 2.8a–b. Leucocratic varieties display a well developed foliation (Fig. 2.8a), whereas melanocratic ones posses a rather massive texture (Fig. 2.8b). Dark color of the melanocratic variety is due to the elevated or high content of hornblende that replaced clinopyroxene in *Cpx-Pl* symplectites almost completely and formed larger anhedral grains containing relics of vermicular plagioclase (Fig. 2.8c).

[1] Mineral abbreviations are after Kretz (1983); Amp, amphibole; subscript index denotes the *Jd* content in *Omp* and *Di*, and the *An* content in *Pl*; superscript and subscript indices denote the *Prp* and *Grs* contents in *Grt*, respectively.

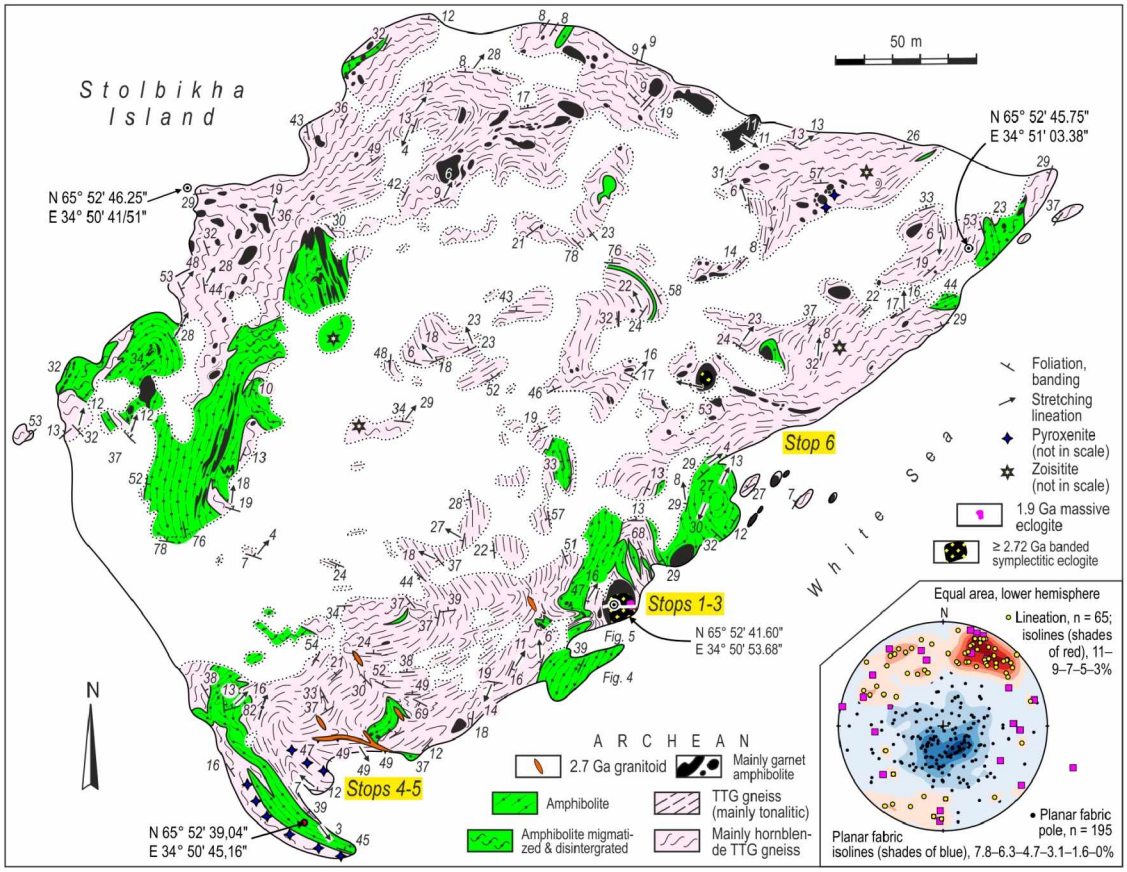

Fig. 2.2. Geological map of Stolbikha Island (compiled by O.S. Sibelev, S.V. Mudruk and I.A. Gorbunov based on their own materials and data by I.I. Babarina (Moscow), V.V. Balagansky and T.V. Kartushinskaya (Apatity), and O.A. Maksimov (Petrozavodsk). Hereafter, software "Openstereo 0.1.2 devel" by C.H. Grohmann and G.A.C. Campanha was used for producing the stereoplots

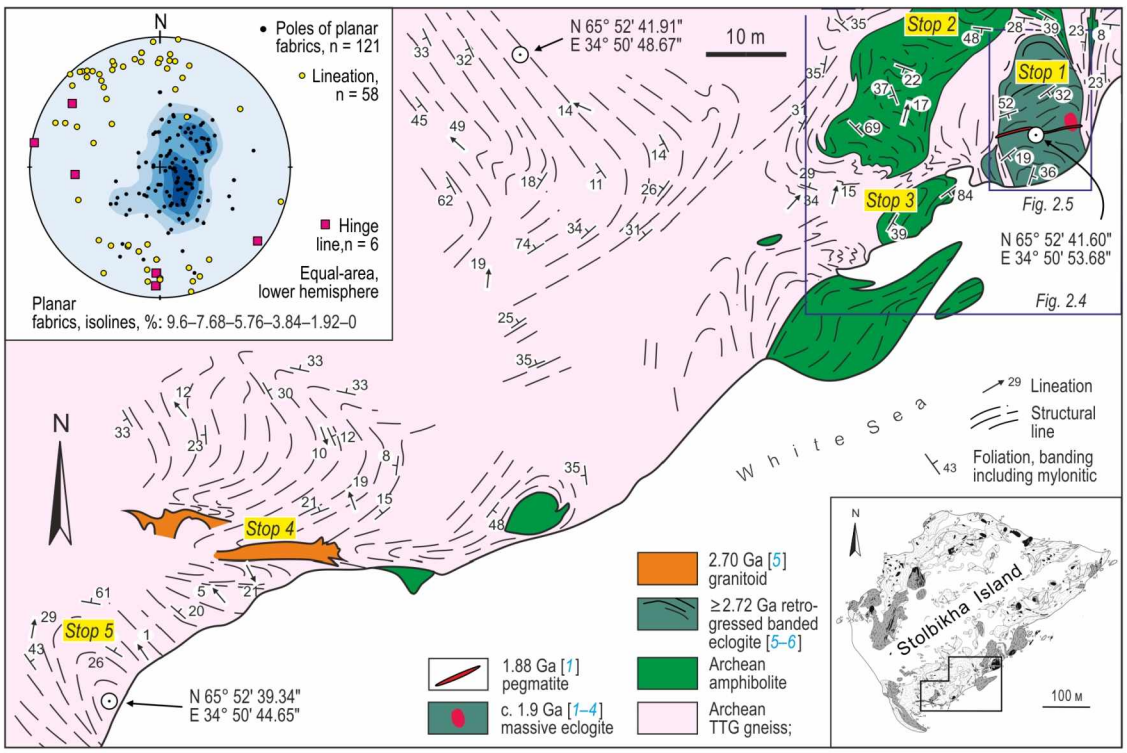

Fig. 2.3. Geological map of the southwestern part of Stolbikha Island (compiled by S.V. Mudruk, I.A. Gorbunov and T.V. Kartushinskaya)

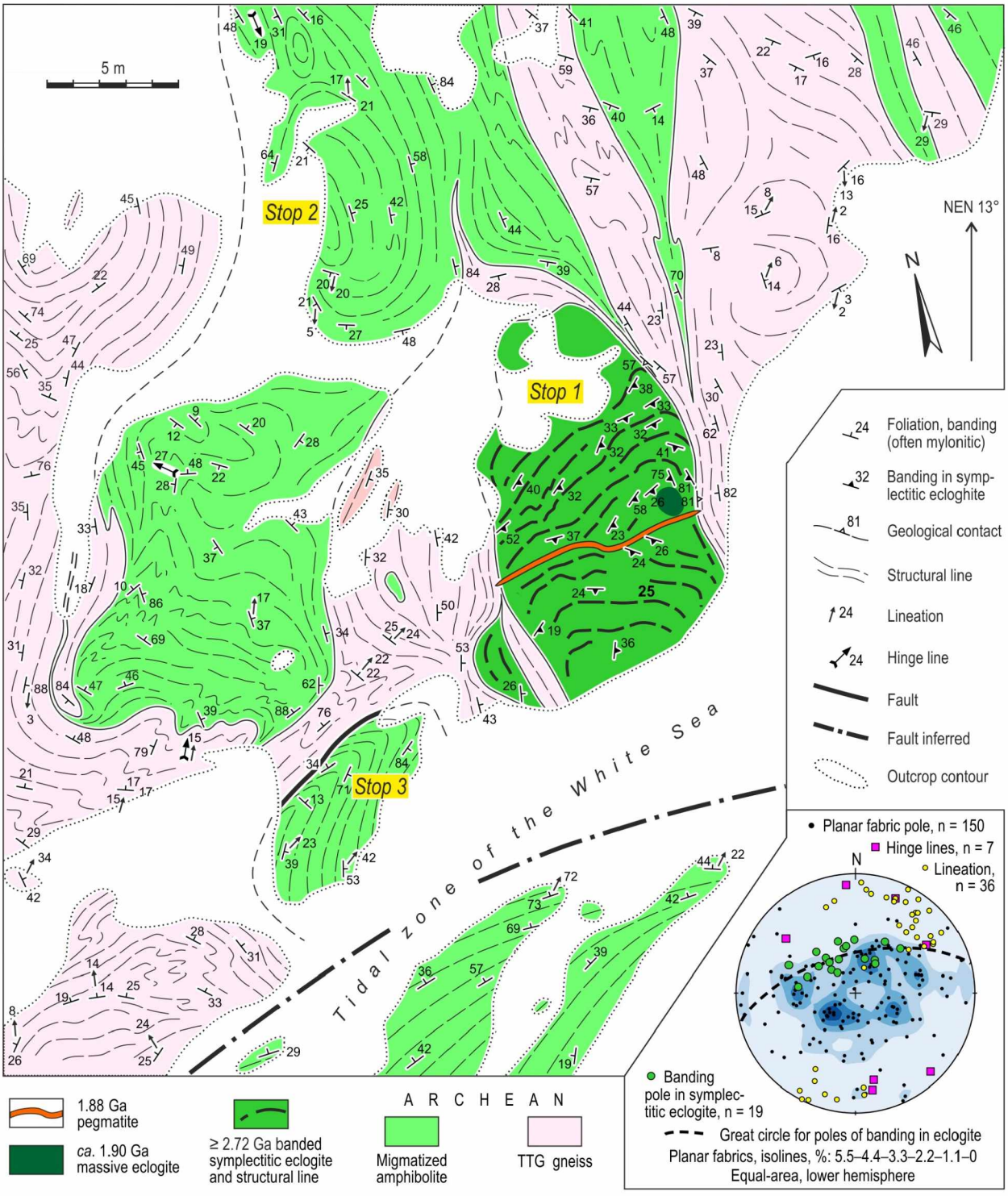

Fig. 2.4. Geological map of the amphibolite–TTG gneiss matrix hosting the reference eclogite boudin (compiled by V.V. Balagansky, 2016)

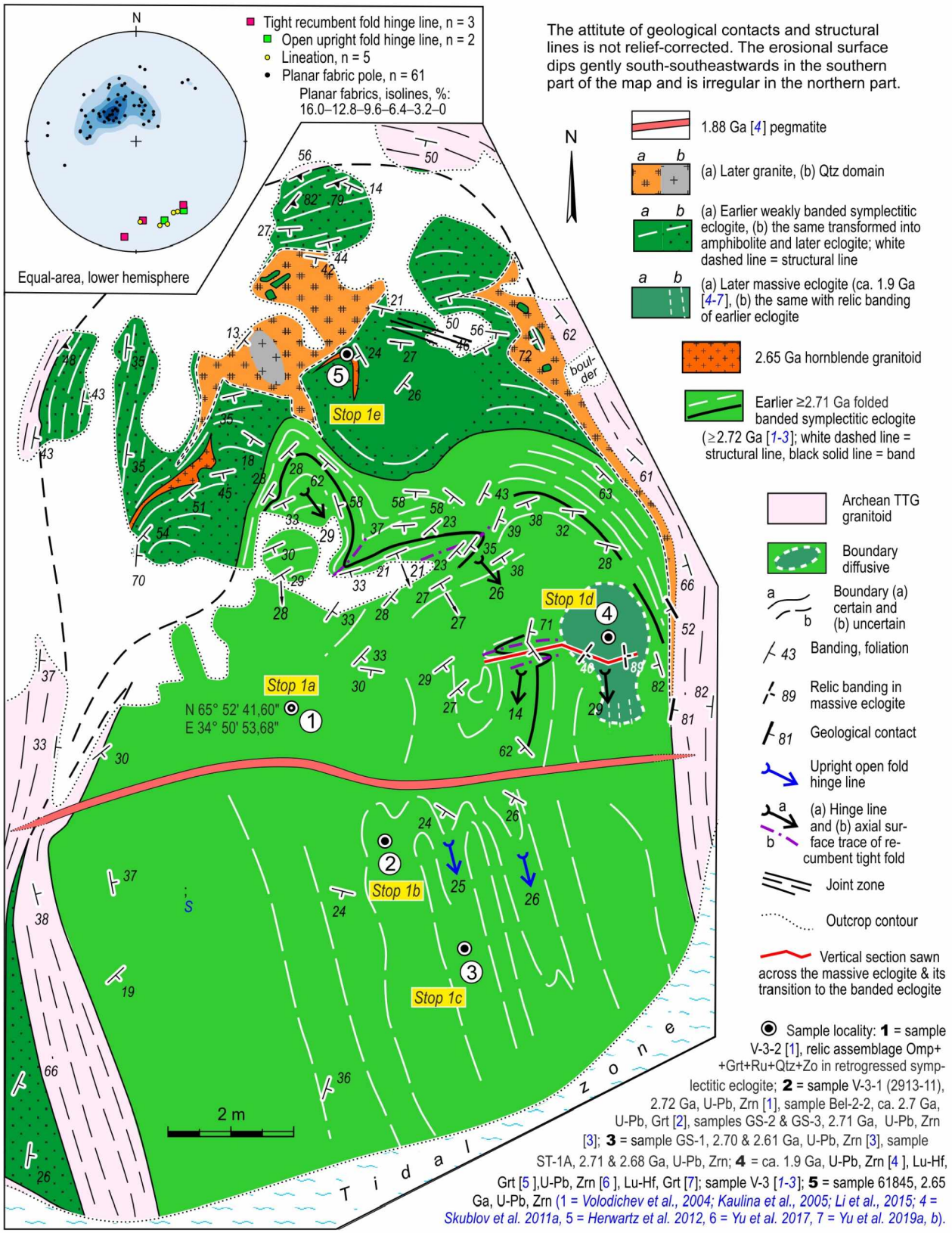

Fig. 2.5. Geological map of the reference eclogite boudin (compiled by V.V. Balagansky, 2018)

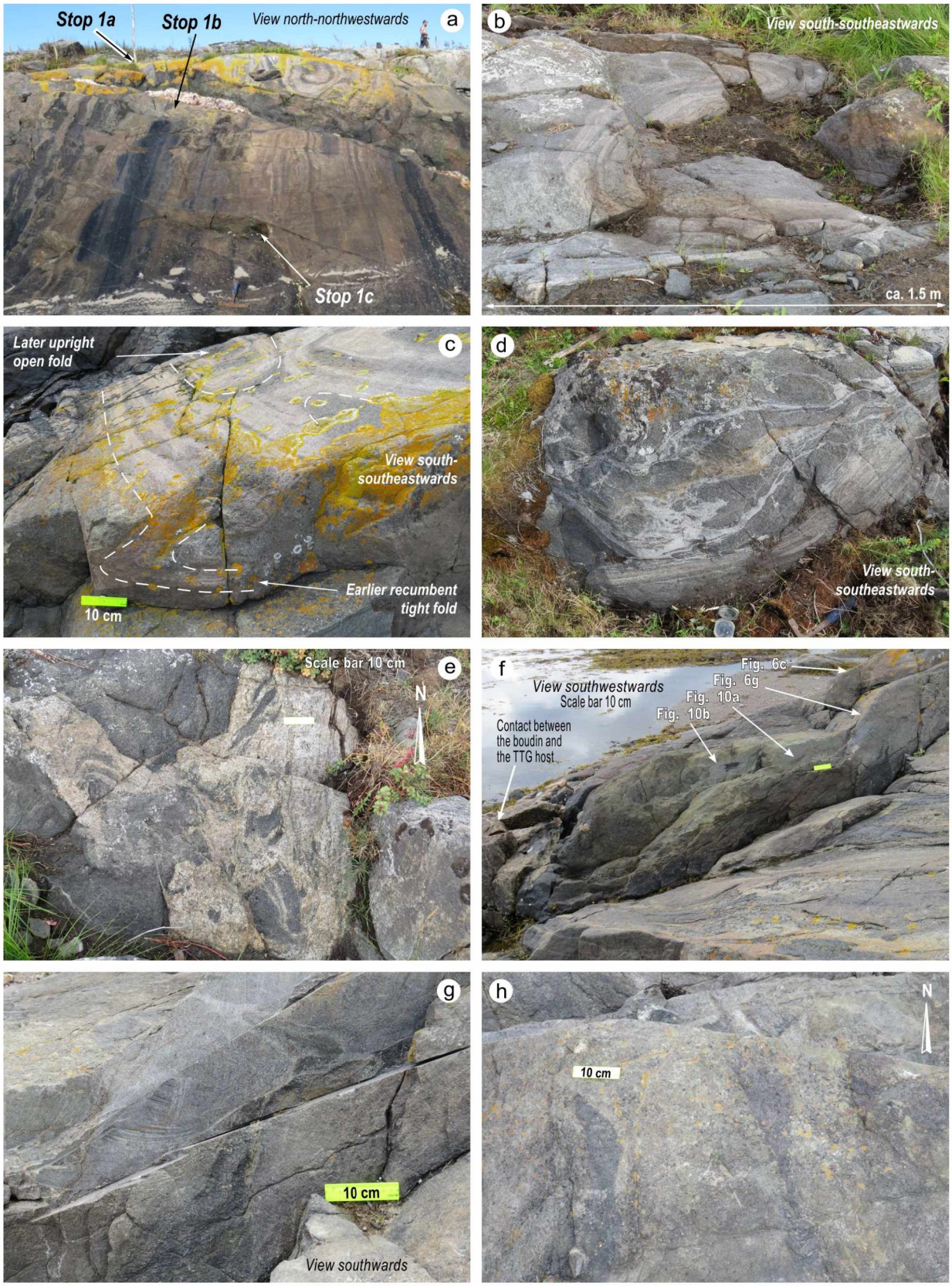

Fig. 2.6. (a) General appearance of the banded retrogressed eclogite; (b-c) tight to isoclinal folds deforming the banding in the retrogressed eclogite; (d) migmatized amphibolite after the retrogressed eclogite; (e) potassic pegmatoid granite intruded an amphibolite after the retrogressed eclogite. (f) General appearance of a patch of the specific grey-green massive eclogite. (g) Transitional zone between the grey-green massive eclogite (left) and banded retrogressed eclogite folded by a recumbent tight fold (right). (h) Relic fragments of an amphibolized banded retrogressed eclogite in the grey-green massive eclogite

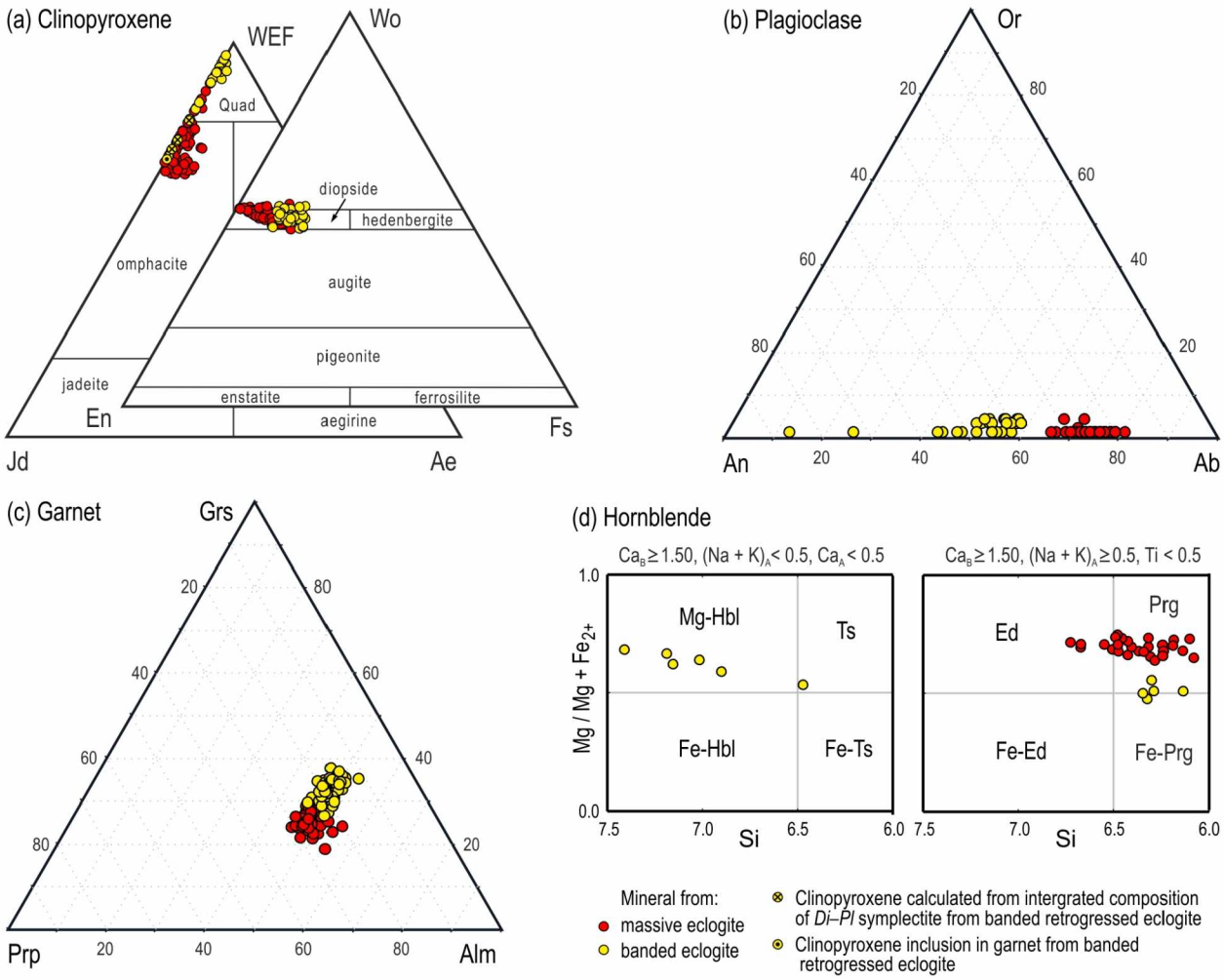

Fig. 2.7. Plots demonstrating the component composition of (a) clinopyroxene, (b) plagioclase, and (c) garnet; (d) nomenclature diagrams for hornblende

Stop 1a is a domain in which a primary eclogitic assemblage *Omp+Grt+Ru+Qtz+Zo* has been preserved. So far, omphacite has been found as the only inclusion in a garnet grain and contains 28 % jadeite (Fig. 2.8d), whereas quartz, rutile and zoisite inclusions are common in garnet. The jadeite content determined from integrated chemical compositions of *Cpx-Pl* symplectites varies from 19 to 25 % (Figs. 2.7a and 2.8e–g) and can be considered as minimal in a primary omphacite replaced by the symplectites (Boland, van Roermind, 1983; Anderson, Moeher, 2007). The primary assemblage *Omp+Grt+Ru+Qtz+Zo* was formed approximately at T = 750 °C (*Grt–Cpx* geothermometer by Powell, 1985) and P = 14 kbar (isopleth technique based on the *Jd* content in clinopyroxene by Holland, 1980). The formation of *Cpx–Pl* symplectites and its main assemblage *Grt+Cpx+Hbl+Bt+Pl+Qtz* resulted in the practically complete obliteration of the primary eclogitic mineralogy. This metamorphic event occurred at T = 750–900 °C and P = 11–14 kbar (computer program TWQ; Berman, 1988, 1991; Berman, Aranovich, 1996; Fig. 2.8) and these *P–T* parameters fall in the high-*P* granulite-facies field adjacent to the eclogite-facies field.

Stop 1b is a domain from which banded regressed eclogite V-3-1 was taken for dating (Fig. 2.5). Zircon from this rock is represented by almost equal, multifaceted, colorless and zoning-free grains characteristic of granulite and eclogite (Bibikova, 1989; Corfu et al., 2003). This yielded U-Pb SIMS age of 2721 ± 8 Ma interpreted as an age of eclogite-facies metamorphism (Volodichev et al., 2004). Garnet from sample Bel-2-2 collected from the same retrogressed eclogite gave a U-Pb TIMS age of *ca.* 2.7 Ga (Kaulina et al., 2005). According to data in (Mezger et al., 1989), the isotope composition of U and Pb in the dated garnet is not consistent with that of rutile and titanite, inclusions of which could have been in garnet, and this age of 2.7 Ga is suggested to be related to the crystallization of garnet during eclogite-facies metamorphism. Later Li et al. (2015) dated the same retrogressed eclogite again on zircon from

samples GS-2 and GS-3 (Fig. 2.5) by the U-Pb LA-ICP-MS method. Metamorphic zircons were almost identical to those dated by Volodichev et al. (2004), and their fir-tree zoning and REE pattern proved similar to those of zircons from high-*P* granulite and eclogite. These zircons yielded Archean dates of 2707 ± 31 Ma, 2655 ± 46 Ma and 2649 ± 31 Ma. The oldest one was equal within analytical uncertainties to the age of 2721 ± 8 Ma (Volodichev et al., 2004) and was thought to be related to eclogite-facies metamorphism. However, no inclusions of omphacite were found in all these metamorphic zircons. A date of 2761 ± 73 Ma from older cores in zircons was referred to an igneous protolith of eclogite.

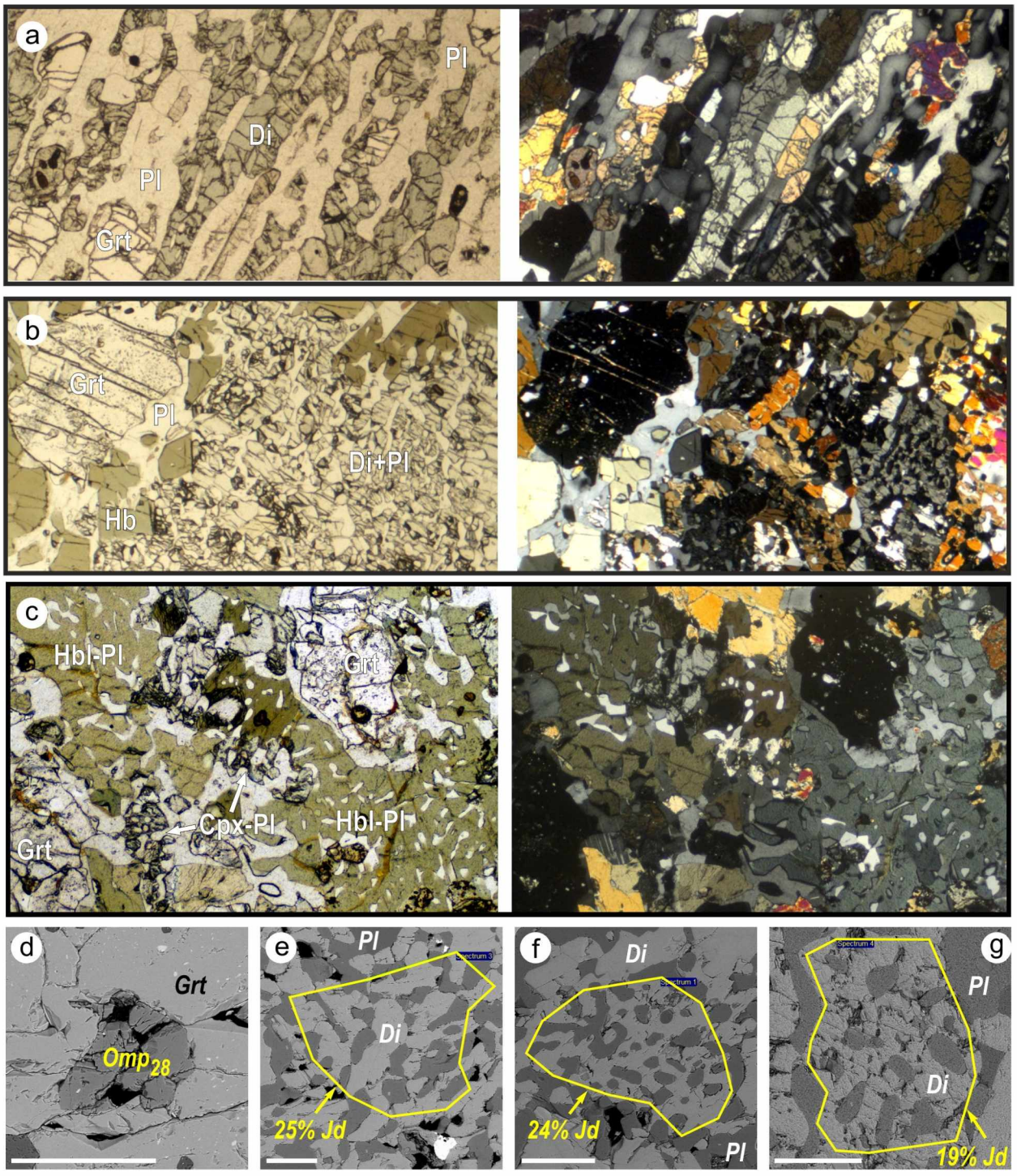

Fig. 2.8. Microphotographs of (a) melanocratic, (b) leucocratic, and (c) intensely amphibolized melanocratic varieties of the banded retrogressed eclogites (sample ST-1A) in transmitted (left) and transmitted cross-polarized (right) light (photo width *ca.* 2.1 mm). BSE images of (d) omphacite inclusion in garnet (sample V-3-2) and (e–g) domains of *Cpx-Pl* symplectites with the jadeite content determined from their integrated chemical compositions (samples V-3-2 and ST-1A); scale bar 175 μm for (d) and 200 μm for (e–g)

Stop 1c demonstrates another retrogressed eclogite dated by the Chinese researchers (Li et al., 2015). Metamorphic zircons from sample GS-1 were practically indistinguishable from those from samples GS-2 and GS-3 and gave two dates of 2607 ± 44 Ma and 2698 ± 28 Ma. Like the aforementioned metamorphic zircons, the crystallization of the 2698 Ma zircon was referred to eclogite-facies metamorphism though inclusions of unambiguous mineral indicators of eclogite-facies metamorphism were not found in zircon.

We have studied a melanocratic variety of sample ST-1A gathered from the same retrogressed eclogite (Fig. 2.9a–c). Zircons from this retrogressed eclogite are represented by rounded, (sub)isometric colorless multifaceted grains many of which posses a prominent fir-tree zoning observable in crystals dark- and light-colored in cathodoluminescence (CL). Some grains consist of a core and one or two rims, with both the cores and rims having the fir-tree zoning and different color in CL (Fig. 2.9d–e). In addition, the youngest rim is very thin and is composed of zircon that is white or almost white in CL. Two zircon generations have been dated by the U-Pb SIMS method. An older generation has yielded an age of 2705+/-24 and a younger generation 2683+/-34 Ma (Fig. 2.9f–g). All these zircons bear mineral inclusions characteristic of only amphibolite and granulite facies (the maximum content of the jadeite component in clinopyroxene inclusions is 12 %). They have similar $^{232}Th/^{238}U$ ratios and their average value is equal to 0.32. Similar values are believed to indicate the magmatic origin of zircon (Skublov et al., 2011a; Yu et al., 2019) but Th/U ratios must be treated with caution for distinquishing magmatic zircon from metamorphic and hydrothermal zircon (Harley, Kelly, 2007).

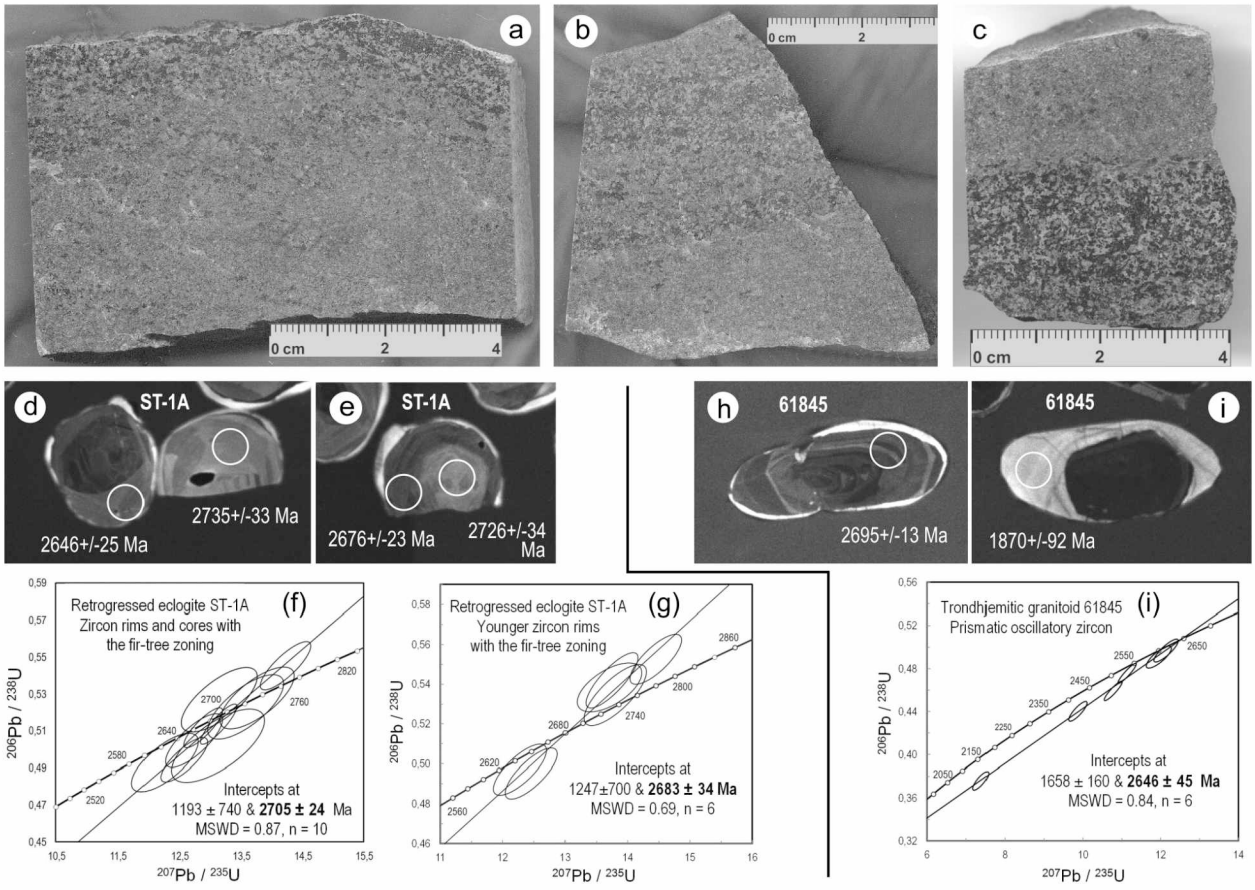

Fig. 2.9. Cathodoluminescence images of zircons from (a–b) a melanocratic variety of banded retrogressed eclogite ST-1A and (e–f) trondhjemitic granitoid 61845 (spot width *ca.* 30 μm; dates correspond to $^{206}Pb/^{207}Pb$ ages at the 68.3 % confidence level). (c–d and g) Concordia plots for zircons from the same rocks (hereafter, isotope data and ages were treated and calculated using Ludwig's computer programs SQUID 1.02 and Isoplot/Ex 4.15; and Isoplot/Ex 4.15; data-point error ellipses are 68.3 % conf.; age determinations are given at 95.4 % confidence level, i.e. 2σ)

In eclogites most zircons formed shortly after the eclogite-facies metamorphism peak at granulite- to amphibolite-facies conditions, and inclusions of eclogite-facies minerals are rare in zircons (Kohn, Kelly, 2018 and references therein). Therefore, eclogites that experienced an intense retrogression and were practically completely changed into banded garnet-clinopyroxene-plagioclase rocks (retrogressed eclogites whose primary *Omp+Grt+Ru+Qtz+Zo* assemblage has been preserved only as inclusions in

garnet) should have been formed shortly before 2.72 Ga. This conclusion needs to be confirmed by a finding of omphacite inclusions in Archean zircons, a study which demands a much larger number of zircon crystals.

Stop 1d exposes a specific massive eclogite that composes a patch in the eastern part of the boudin (Fig. 2.5) and has a specific grey-green color on the weathered surface (Fig. 2.6f). This patch is crop out in a small W–E-trending vertical wall in which the relationships of the massive eclogite with the banded folded retrogressed eclogites in the west and intensely sheared amphibolites after eclogites in the east (Figs. 2.5 and 2.6f) have been studied. The boundary between these eclogites is locally diffusional and the gradual transition can be observed in an exposure (Fig. 2.6g). Large and small relic fragments of the intensely amphibolized banded retrogressed eclogites in the massive eclogite can be observed in exposures (Fig. 2.6h) and polished samples (Fig. 2.10a–b). Fig. 2.10c shows a massive eclogite that contains almost no signs of its development after the banded retrogressed eclogite in a specimen. In a number of polished specimens the gradual transition between massive and banded eclogites can been observed (Fig. 2.10d–e). A relic "faded" banding has been preserved in some massive eclogites due to a different degree of the replacement of these rocks by the massive eclogite (Fig. 2.10d).

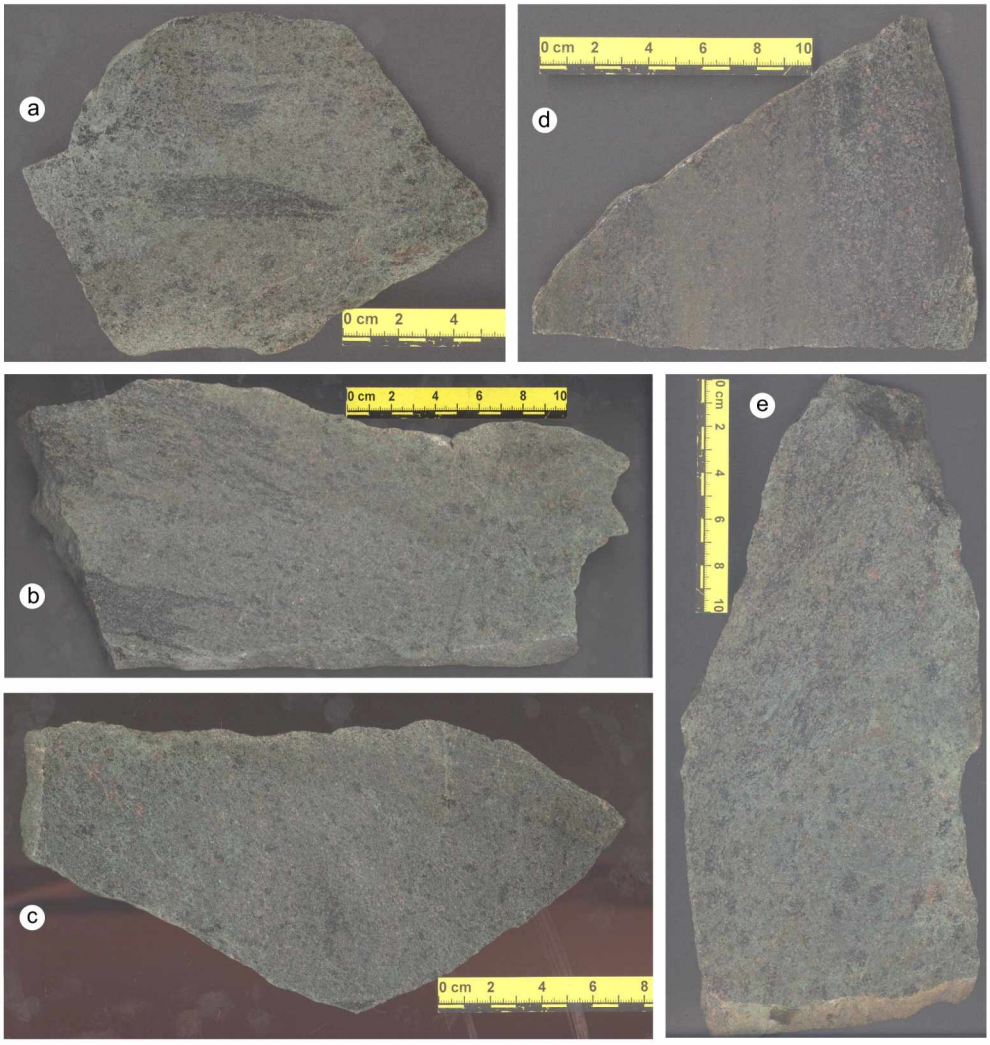

Fig. 2.10. Polished specimens from the massive eclogites: (a–b) relic fragments of amphibolized banded retrogressed eclogite with sharp boundaries, (c) massive eclogite without such fragments, (d–e) gradual transition between massive and banded varieties of eclogites

According to (Volodichev et al., 2004) and the authors' data, the most massive domains have an almost equigranular texture and consist of garnet and omphacite that compose >80 % of the domain volume and their contents are more or less similar (Fig. 2.11a–b). These minerals display no compositional zoning and are inclusion-free, and garnet from the massive eclogite differs prominently from that from the banded retrogressed eclogite (Fig. 2.11a–c). Figs. 2.11a and 2.11c also demonstrate the principal difference between

the massive and banded retrogressed eclogites. Omphacite cannot be compared because it has been found in the banded retrogressed eclogite as the only inclusion in garnet so far. Yu et al. (2017, 2019a, b) reported on garnet from massive eclogites that is zonal and contains mineral inclusions, with the most external zone containing a kyanite inclusion. Samples studied by these researchers seem to have been gathered from a massive eclogite that contains badly recognized relics of a banded retrogressed eclogite, and the zoning in garnet could be related to the replacement of the older banded eclogite by the younger massive eclogite. In thin sections the omphacite forms a weak foliation (Fig. 2.11b) unobservable in exposure.

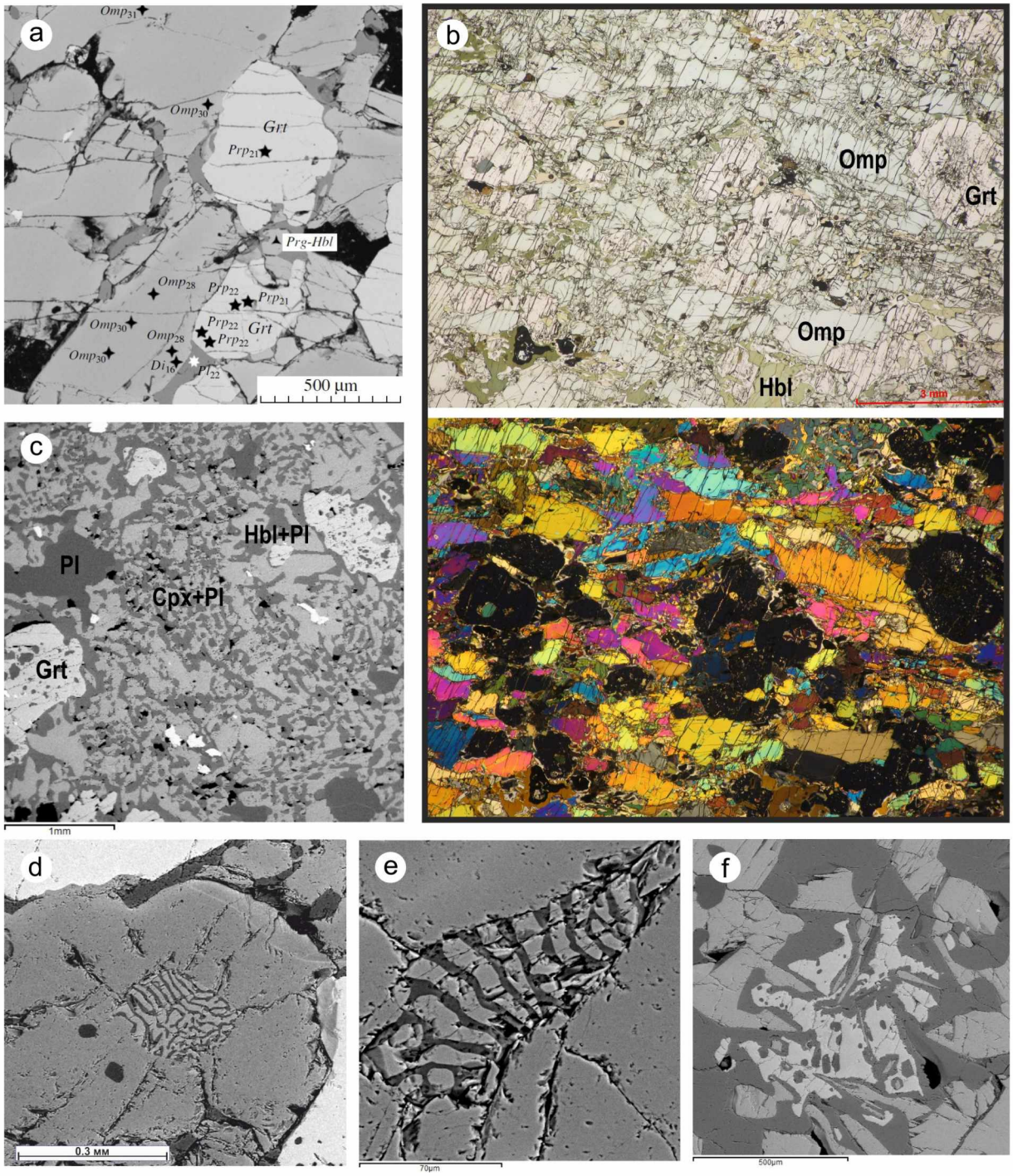

Fig. 2.11. Appearance of the massive eclogites: (a) BSE image of sample V-3 (Volodichev et al., 2004) and (b) microphotographs of sample GR9-5 in transmitted (top) and transmitted cross-polarized (bottom) light (photo width 12 mm), (c) BSE image of banded retrogressed eclogite V-3-2 given for comparison (photo width 3.5 mm). (d–e) BSE images of relic enclaves of *Cpx-Pl* symplectites in omphacite (photo widths 1,2 mm and 110 μm, respectively); note the lack of *Cpx-Pl* symplectites around the omphacite grain in (d). (e) BSE image of a relic garnet replaced by plagioclase, hornblende (both around garnet) and biotite (inside garnet) in an amphibolite after massive eclogite (photo width 1 mm; sample GR9-43)

The average amount of the jadeite component in clinopyroxene is *ca.* 30 % at the low content of the pyrope component in garnet (20–22 %) and the high content of the grossular component (28–31 %). The same average component compositions of clinopyroxene were reported in (Li et al., 2015; Yu et al., 2017). Secondary minerals are represented by hornblende (up to 5 %) and *Cpx-Pl* symplectite (<5 %), accessory minerals are quartz, rutile, ilmenite and zircon. The component compositions of clinopyroxene, plagioclase, garnet and hornblende are shown in Fig. 2.7. In discriminative plots garnets and plagioclases form different fields immediately adjacent to those of garnets and plagioclases from banded eclogites (Fig. 2.7b–c). Clinopyroxenes also form different fields; several clinopyroxenes from the massive eclogites, however, fall into the fields of clinopyroxenes from the banded eclogites (Fig. 2.7a). Hornblendes differ remarkably and are represented by pargasite and rarely edenitic hornblende in the massive eclogites and magnesian hornblende in the banded retrogressed eclogites (Fig. 2.7d). There is no exact information that could help in referring minerals (apart from clinopyroxene) reported in (Li et al., 2015; Yu et al., 2017, 2019) to massive or banded eclogites. Though many of these minerals have been taken from the massive eclogites, the major reason is the occurrence in them of relics of the banded retrogressed eclogites.

A specific feature of the massive eclogites is that omphacite contains enclaves of *Cpx-Pl* symplectites (Fig. 2.11d–e). It is noteworthy that the symplectites are absent around omphacite grains containing the enclaves. Together with relics of the banded retrogressed eclogites in the massive eclogites it indicates the development of the latter after the former. Another specific feature of these rocks is that garnet from the transition between massive eclogites and amphibolites developed after them is very corroded due to the development of plagioclase and hornblende around it and biotite within it (Fig. 2.11f).

Volodichev et al. (2004) calculated *P–T* conditions for the massive eclogites and determined *P* = 14.0–17.5 kbar and *T* = 740–865 °C (computer program TPF by V.I. Fonarev, A.A. Graphchikov and A.N. Konilov; Institute of Experimental Mineralogy of the Russian Academy of Sciences, Chernogolovka, Russia). These researchers interpreted the massive eclogites as protoliths for the banded retrogressed eclogites. Samples GR-9 and ST-2 (assemblage *Omp+Grt+Zo+Qtz+Ru*) collected from the most massive varieties have given *P* = 17–17 kbar and *T* = 700–800 °C (TWQ program). A cooling decompression led to *P* = 12–15 kbar and *T* = 750–850 °C (assemblage *Grt+Cpx+Hbl+Pl+Qtz*). The latest retrogression resulted in the formation of an assemblage *Grt+Hbl+Bt+Pl+Qtz* at *P* = 8–11 kbar and *T* = 600–650 °C.

Skublov et al. (2011a) dated zircons from the massive eclogites by the U-Pb SIMS method. Zircons consist of older cores and one or two rims. The cores are dark-colored in CL and show no zoning. The REE concentrations and Th/U ratios of the cores are similar to those of zircons from igneous basic rocks or are transitional between values from the basic rocks to eclogites. The rims are light-grey- or grey-colored in CL and have the mosaic structure; their geochemistry and Th/U ratios are typical for zircons from eclogites. The cores yielded a Concordia age of 2702 ± 25 Ma, and the rims a lower intercept age of 1878 ± 18 Ma. The former date was referred to a protolith and the latter to a Paleoproterozoic eclogite-facies metamorphism. A Lu-Hf dating of garnet from the same massive eclogite gave ages of 1937 ± 8 Ma and 1892 ± 10 Ma which were also interpreted as being related to eclogite-facies metamorphism (Herwartz et al., 2012).

Yu et al. (2017) analyzed zircons from the massive eclogites using the U-Pb LA-ICP-MS technique. They studied subhedral-euhedral, elongate, colorless crystals displaying clear cores and rims in CL. The cores are dark in CL, irregular or elliptical, whereas the rims are medium-grey and bright in CL and structureless. The REE abundances and Th/U ratios in the cores and rims are close to those from (Skublov et al., 2011a). An upper intercept age of 2745 ± 32 Ma was obtained for the cores. One type of homogeneous concordant and subconcordant rims yielded a weighted mean $^{207}Pb/^{206}Pb$ age of 1904 ± 4 Ma, whereas another type that bears inclusions of garnet and omphacite gave a weighted mean $^{207}Pb/^{206}Pb$ age of 1909 ± 11 Ma. Later Yu et al. (2019a) reported Lu-Hf garnet dates of *ca.* 1.96–1.92 Ga from the reference boudin and an eclogite from other boudin in Stolbikha Island and concluded that these dates along with the 1.91 Ga eclogite-facies zircon constrain the prograde stage of the eclogite-facies metamorphism in the Gridino area. According to these researchers, the peak of this metamorphism occurred at *P* >18 kbar and *T* = 725–730 °C, then a cooling decompression resulted in *P–T* conditions of high-*P* granulite facies following a clockwise *P–T* path (thermodynamics modeling based on quantitative compositional mapping results and an iterative thermodynamic model along with the program GrtMod). Li et al. (2015) reported similar *P–T* parameters and a *P–T* path based on data that appear to have been obtained from both the banded and massive eclogites.

Stop 1e is located in the northern part of the reference boudin (Fig. 2.5). Here, amphibolites are slightly disintegrated and their fragments are cemented by a trondhjemitic granitoid (Fig. 2.12a) which is partly cilicificated (up to 95.83 mass %). Hornblende composes relatively large grains with irregular contours and contains vermicular plagioclase forming specific symplectite-like aggregates. These aggregates are identical to those in melanocratic varieties of the banded retrogressed eclogites in which hornblende replaced clinopyroxene in *Cpx-Pl* symplectites (cf. Fig. 2.8c). This fact and field observations suggest that the amphibolites represent intensely and completely amphibolized banded eclogites, and the trondhjemitic granitoid was one of causes of amphibolization. This granitoid contains prismatic zircon crystals which display an oscillatory zoning (Fig. 2.9h) characteristic of TTG rocks. Some crystals contain older cores dark in CL and are surrounded by thin rims white- and light-grey-colored in CL (Fig. 2.9h–i). The oscillatory zircons have yielded an upper intercept age of 2646 ± 45 Ma (Fig. 2.9j) and the thickest rim has been dated at 1870 ± 92 Ma (1σ; Fig. 2.9i).

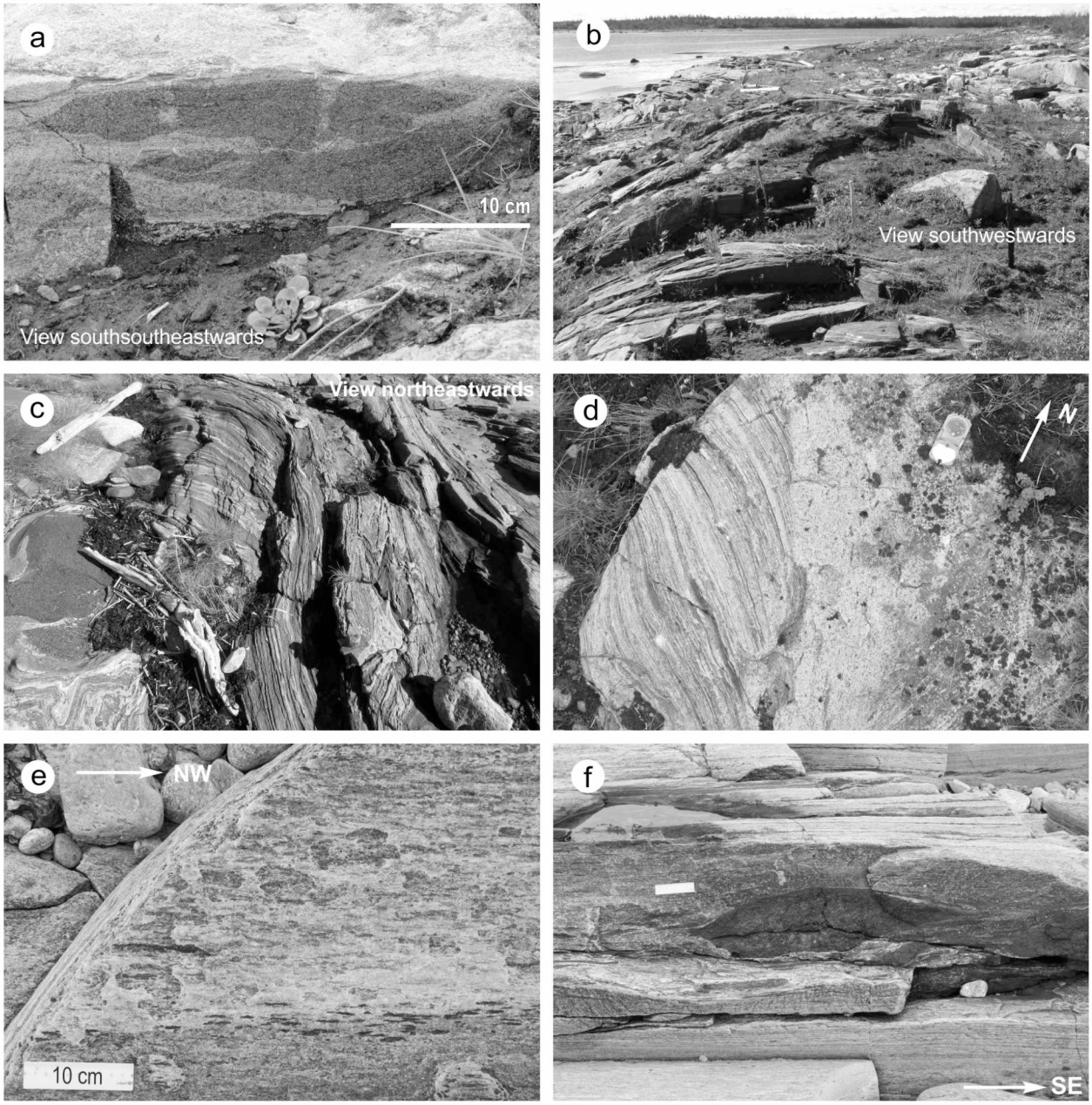

Fig. 2.12. (a) 2.65 Ga trondhjemitic granitoid cutting an amphibolite after the banded retrogressed eclogite. (b) Gentle dome formed by a large lens-like boudin of an amphibolite and forming an oval-like structure on a map. (c) Intensely mylonitized and sheared amphibolite. (d) Trondhjemitic dike truncating a thin layered pile composed of mylonitized and sheared amphibolite and TTG gneiss. (e) Stretching lineation in mylonitized and sheared TTG gneiss. (f) Enclave of mafic rocks in mylonitized and sheared TTG gneiss indicating top-to-the-south-east shear sense. For more explanation see the text

Summary of data from Stop 1. The reference eclogite boudin consists of older banded folded retrogressed eclogites and a patch of younger massive eclogites that replaced the older eclogites in the eastern margin of the boudin. Geochronology indicates that the older eclogite-facies metamorphism whose relic omphacite-bearing assemblage has been preserved only as inclusions in garnet seems to have occurred shortly before 2.72 Ga. The younger massive eclogites are related to a Paleoproterozoic eclogite-facies overprint at *ca.* 1.9 Ga. The Archean eclogites experienced isoclinal folding and very intense retrogression, whereas the Paleoproterozoic eclogites are practically deformation-free and underwent weak retrogression. Herwartz et al. (2011) reported on relics of two eclogite-facies metamorphic events in a single sample, Stop 1 provides a geological record of two eclogite-facies metamorphic events in a single exposure.

Stop 2 demonstrates an example of a rounded and lens-like shape of amphibolite boudins hosted by TTG gneisses (Fig. 2.12b). Due to a different extent of the erosion, the boudins form a dome-and-basin pattern on the map. In particular, structural lines produced by intersections of planar fabrics in sheared and mylonitized margins of boudins with the surface form ovals on the map (Fig. 2.4). These lens-like boudins resulted from gentle shearing in simple shear regime (Stop 5) before 2.70 Ga (Stop 4). The morphology of the reference eclogite boudin was formed by the same shearing. In contrast to the reference boudin, the central part of the amphibolite boudin shown in (Fig. 2.12b), is not exposed.

Stop 3 is an example of intensely sheared and mylonitized amphibolite (Fig. 2.12c) and TTG gneiss that host the amphibolite boudin in Stop 2 and the reference eclogite boudin in Stop 1. Note that stretching lineations and hinge lines are (sub)parallel to each other and posses the shallow attitude.

Stop 4 provides evidence that the shearing and mylonitization that resulted in the formation of lens-like shape of basic rock boudins including the reference eclogite boudin occurred in the Archean. Here, very intensely mylonitized amphibolites and TTG gneisses forming a thin layered pile are truncated by a trondhjemite dike (Fig. 2.12d). Prismatic, moderately elongated, well faceted and transparent zircon crystals have an upper intercept age of 2701 ± 8 Ga (U-Pb TIMS; Volodichev et al., 2004). Note that gentle penetrative stretching lineations are characteristic of these deformed rocks (Fig. 2.3, inlet).

Stop 5 shows a series of perfect coastal exposures in which intensely mylonitized TTG gneisses and amphibolite and pyroxenite enclaves can be observed. The TTG gneisses display subhorizontal stretching lineations formed by linear quartz-feldspar aggregates and microrods of amphibolites (Fig. 2.12e). In outcrops whose erosion surfaces are parallel to the stretching lineation and perpendicular to the mylonitic planar fabrics the amphibolite and pyroxenite enclaves show monoclinic symmetry characteristic for structural forms that are produced in simple shear regime and can be used as kinematic indicators (Hanmer, Passchier, 1991). Being interpreted as σ-structures, the enclaves are thought to indicate top-to-the-southeast sense of shear (Fig. 2.12f).

Summary data on Stops 1–5. The mylonitized amphibolites and TTG gneisses that are crop out in the southwestern part of Stolbikha Island and host the reference eclogite boudin experienced shearing and mylonitization before 2.70 Ga. It is deformational processes that are responsible for the lens-like shape of amphibolite boudins including the reference eclogite boudin, as well as the dome-and-basin pattern of several domains of this area. The banded retrogressed eclogites composing the internal part of the boudin possess planar fabrics, tight to isoclinal folds and later open upright folds whose orientation is similar to that in the amphibolite-TTG host.

Stop 6. Here, Yu et al (2017) have studied a small amphibolite boudin containing relics of eclogite (Fig. 2.13a). An eclogite-facies assemblage from sample Gd10 consists of garnet (35–40 %), omphacite (40–45 %), hornblende (5 %), *Di-Pl* symplectite (5 %), quartz, ilmenite and rutile (5 %). Petrography of eclogite Gd10 is shown in Fig. 2.13b, c. Cores of subhedral garnet porphyroblasts (up to 1.5 mm) contain inclusions of diopside, hornblende, epidote and plagioclase which are considered as a pre-eclogite assemblage. In addition, garnet hosts quartz and rutile inclusions. A characteristic feature of margins of the garnet porphyroblasts is kyanite, a typical high-*P* mineral (Fig. 2.13d). The component composition of garnet is Alm_{44-50}, Prp_{25-31}, Grs_{23-29}, and Sps_{1-2} but some crystals display a slight decrease in pyrope and a slight increase in grossular in the outermost zones. Omphacite (31 % jadeite) exhibits no compositional zoning. A *P–T* pseudosection for sample Gd10 was calculated in the system NCFMASHTO with H_2O in excess, and the *P–T* path is given in Fig. 2.14. The pre-eclogite assemblage was formed at P = 10–11 kbar and T = 650–670 °C, the peak *P–T* conditions corresponded to 20–21 kbar at 720–740 °C and the decompression led to P = *ca.* 13 kbar and T = *ca.* 730–750 °C. These data indicate a clockwise *P–T* path of metamorphic evolution.

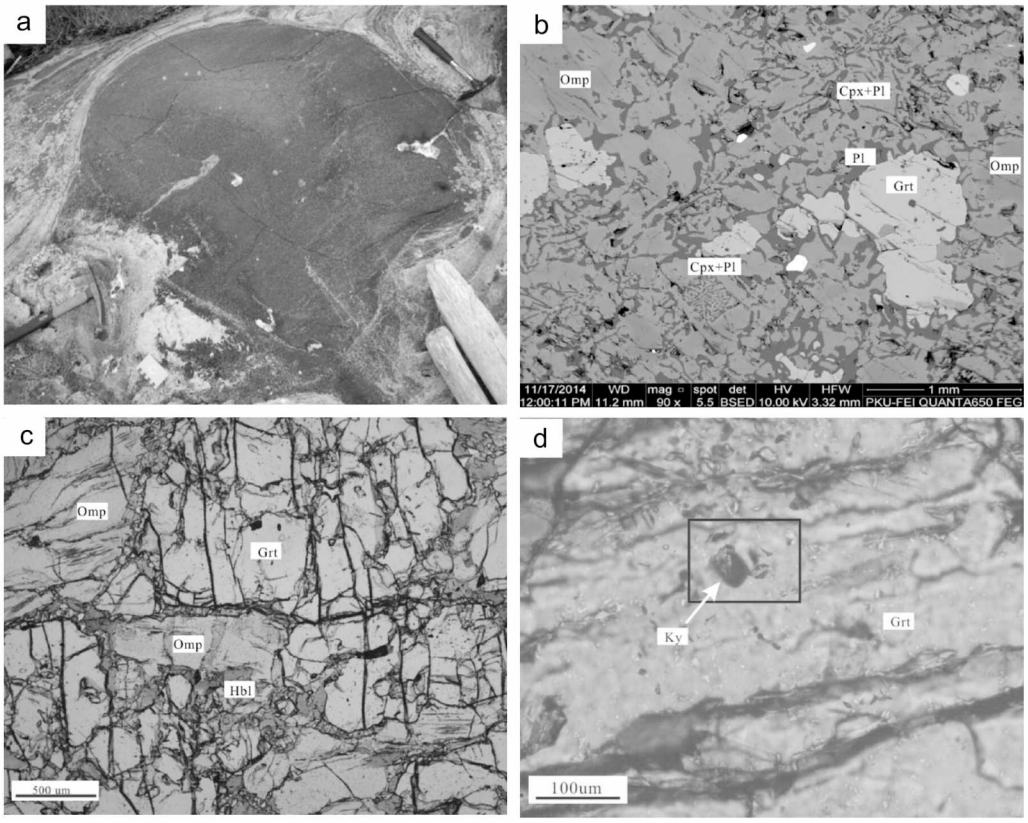

Fig. 2.13. (a) General appearance of boudin Gd10. (b) Petrographic features of retrogressed eclogite Gd10 (BSE image). (c) Garnet-omphacite assemblage in retrogressed eclogite Gd10. (d) Inclusion of kyanite in the most outer zone in a garnet porphyroblast. All photos from (Yu et al., 2019a)

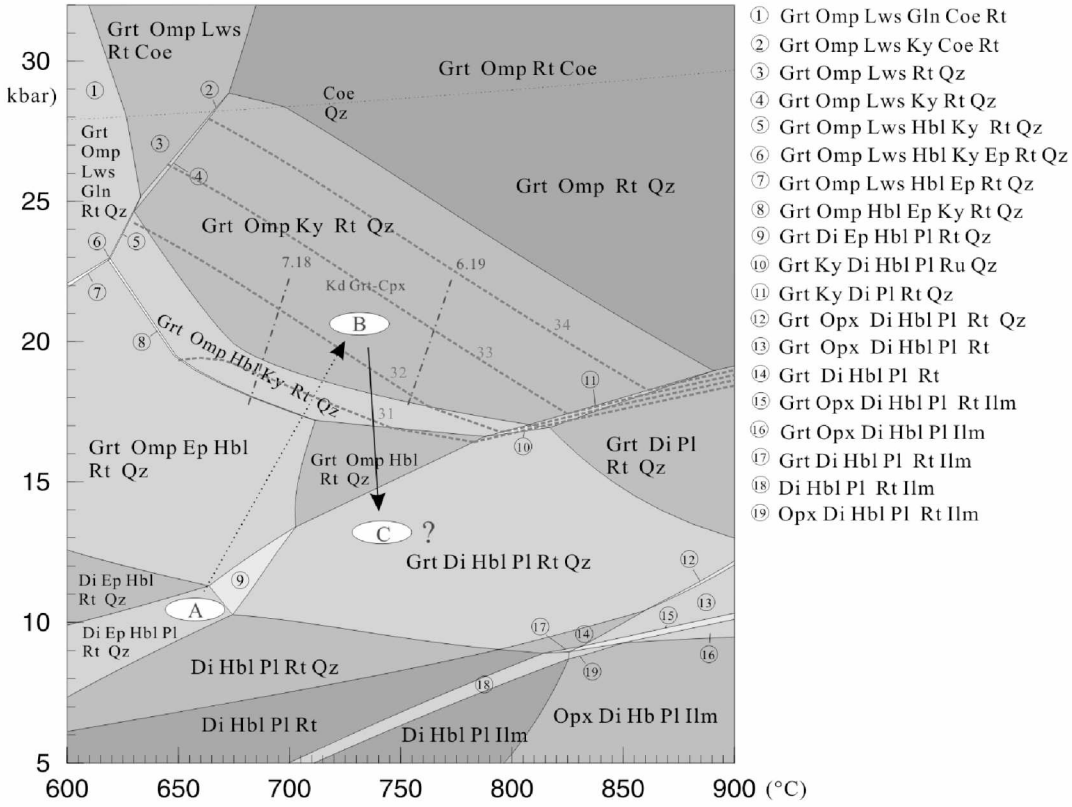

Fig. 2.14. *P–T* pseudosection for sample Gd10 calculated in the system NCFMASHTO with H_2O in excess, and inferred *P–T* path for the metamorphic evolution of the Gridino-type eclogite; green lines = isopleths of J_0 ((Na)M2 in clinopyroxene) (Yu et al., 2017)

Zircons from sample Gd10 have a core-rim zoning in CL. Small and fractured cores gave no meaningful age data due to lead loss. A weighted mean $^{207}Pb/^{206}Pb$ age of 1899 ± 5 Ma (U-Pb SIMS) was obtained for 17 zircon rims, and a weighted mean $^{207}Pb/^{206}Pb$ age of 1897 ± 10 Ma (U-Pb, LA-ICP-MS) for another 18 zircon rims. Th/U ratios vary from 0.002 to 0.026. Inclusions of omphacite and garnet have been found in the rims, which unambiguously indicate that this eclogite-facies metamorphic event occurred at 1.90 Ga.

Izbnaya Luda Island

Izbnaya Luda Island exposes three different structural domains that contain a geological record of both the Archean and Paleoproterozoic evolutionary history of the eclogite-bearing amphibolite and TTG gneiss matrix of the Gridino area (Travin et al., 2005). The most principal difference of this island from Stolbikha Island is that a nearly complete range of Paleoproterozoic mafic and ultramafic dikes is crop out in all of the three domains (Stepanov, Stepanova, 2005; Stepanova, Stepanov, 2010). These dikes are perfect benchmarks that permit distinguishing between Archean and Paleoproterozoic orogenic events including eclogite-facies metamorphic episodes (Babarina, Sibelev, 2015). The Eastern Domain (Fig. 2.15) actually is a vertical N-S trending shear zone with shallow stretching lineations (Fig. 2.15) which is suggested to have been formed in the Paleoproterozoic (Travin et al., 2005). The Central Domain has preserved a rather complete Archean history (Dokukina et al., 2014; Babarina, Sibelev, 2015) including the Archean eclogite-facies metamorphism (Volodichev et al., 2004) and the Paleoproterozoic eclogite-facies metamorphic overprint recorded here by a Paleoproterozoic gabbronorite dike (Travin, Kozlova, 2005, 2009; Dokukina, Konilov, 2011). A specific feature of the Central Domain is a series of pseudotachylite veinlets (Travin et al., 2005; Dokukina, Dokukin, 2015). The structure of the Western Domain is heterogeneous: TTG gneisses were repeatedly deformed into folds in its south western part and were sheared in subvertical NW-SE trending shear zones in its northeastern part (Fig. 2.15).

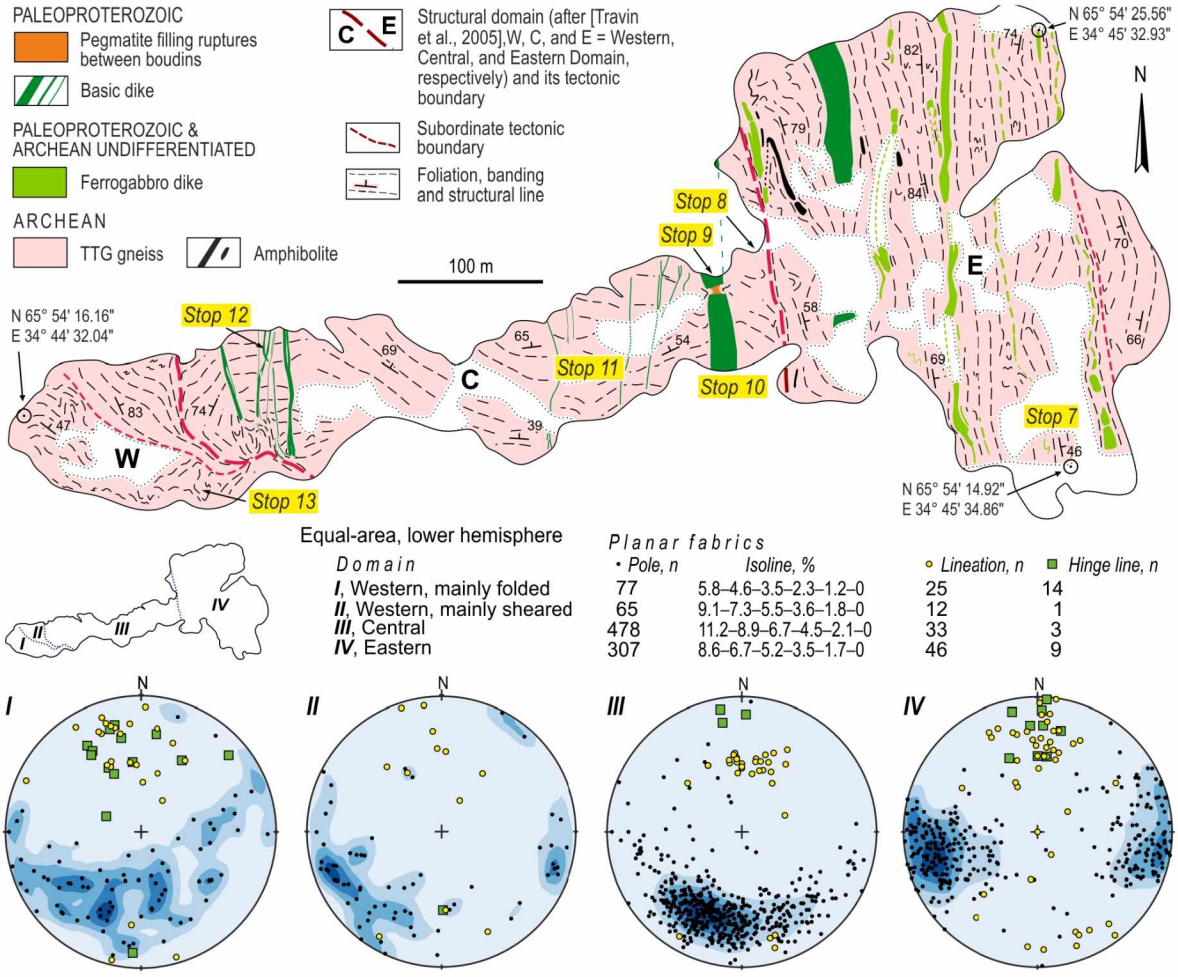

Fig. 2.15. Geological map of Izbnaya Luda Island. Compiled by I.A. Gorbunov, S.V. Mudruk, T.V. Kartushinskaya and V.V. Balagansky

The island is separated by the high tide in two islands; in addition, Stop 7 can be visited only at the lowest tide. That is why the order of visiting Stops may be changed in dependence on the lowest tide time.

Stop 7 demonstrates a mafic dike that cross-cuts migmatized Archean TTG gneisses, is boudinated and is folded by two adjacent tight to isoclinal asymmetrical folds related to shearing in the Eastern Domain (Fig. 2.16a). The morphology of these folds and other kinematic indicators combined with subhorizontal stretching lineations and subvertical shear planes indicate the sinistral sense of shear. The hinge of one of these folds is rounded and produced a lower pressure domain during folding like that in a boudin neck during boudinating. This domain is filled with a pegmatoid leucosome that splits into several veins parallel to the axial surface as a whole (Fig. 2.16b). The leucosome consists of quartz (50–55 %), plagioclase (35–40 %), biotite (1–3 %) and hornblende (1–2 %). Accessory minerals are garnet, epidote, titanite, pyrite and zircon. Zircon forms euhedral, prismatic crystals showing cores and up to four rims in CL images (Fig. 2.16c–f). The outermost rim is responsible for the euhedral shape of zircon, is white- and light-grey colored in CL, has a slight euhedral zoning and is interpreted as magmatic zircon that grew during the formation of the leucosome under amphibolite-facies conditions. Thirty two low-U rims of this type have given a Concordia age of 1941 ± 17 Ma (U-Pb, SIMS). Thus, the shearing, amphibolite-facies metamorphism and migmatization had occurred shortly before the Paleoproterozoic eclogite-facies overprint.

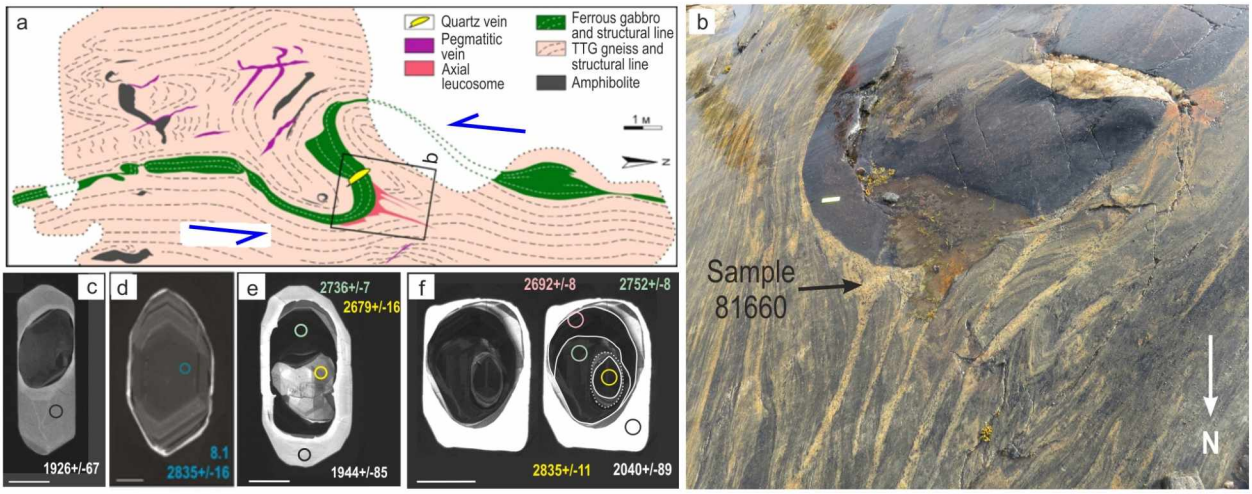

Fig. 2.16. (a) Mafic dike folded by tight to isoclinal folds which were produced by intense shearing in the Eastern Domain. (b) Rounded hinge of a fold generated a lower pressure domain in the TTG host (locus of the formation of a pegmatoid leucosome linked with a axial leucosome). (c–f) BSE images of zircon from leucosome 81660

The overwhelming majority of cores is composed of corroded elongated crystals some of them have preserved their primary euhedral morphology (Fig. 2.16d). All zircons display an oscillatory zoning (often thin) typical for TTG gneisses (Corfu et al., 2003) and are interpreted to have been inherited from the country TTG gneisses. Thirteen cores have yielded a Concordia age of 2831 ± 8 Ma (U-Pb, SIMS) which is considered as the crystallization age for the igneous TTG protolith (Kartushinskaya et al., 2018). A tentative dating of intermediate rims (Fig. 2.16e–f) permits suggesting their crystallization at 2.76–2.74 Ga and 2.71–2.68 Ga. Note that these dates are consistent with those from Stop 1. In addition, several older cores have given ages of 2.90–2.93 and 3.14 Ga and are interpreted as inherited by TTG melts from an older crust.

Stop 8 exposes the transitional narrow zone between the Eastern and Central Domain (Fig. 2.17). Here, this transition is well exposed, which is very rare for tectonic boundaries. The intensely sheared rocks of the Eastern Domain posses the regular N-S strike and subhorizontal stretching lineations, while the TTG rocks of the Central Domain strike northwestwards and are bent near the tectonic boudary suggesting the sinistral shear sense. It is one of two shear zones that is believed by Travin (2015) to have resulted to the Paleoproterozoic eclogite-facies overprint recorded in a Paleoproterozoic olivine-bearing gabbronorite dike (Stop 9).

Stop 9. Here, a coronitic olivine-bearing gabbronorite dike is crop out, cuts Archean TTG gneisses, displays narrow chilled margins and is a typical example of the Paleoproterozoic lherzolite–gabbronorite complex widespread throughout the Belomorian province (Stepanov, Stepanova, 2005; Stepanova, Stepanov, 2010). This dike is boudinated and the fracture spacing represents an irregular rectangular quadrangle (*ca.* 12 × 6 m; Fig. 2.17). The central part of the fracture spacing is filled with a pegmatitic

leucocratic granite whose origin is related to a rapid decompression after the break-up of the dike and the following melting of its TTG host. The pegmatitic granite contains numerous fragments of TTG gneisses and intensely amphibolized gabbronorites. The western, narrower part of the fracture spacing is filled with the country TTG gneisses folded by an isoclinal fold which resulted from the invasion of these rocks into a lower pressure area between the two boudins. The eastern, wider part is filled with the same gneisses folded by several tight to isoclinal folds of the same origin (Fig. 2.17).

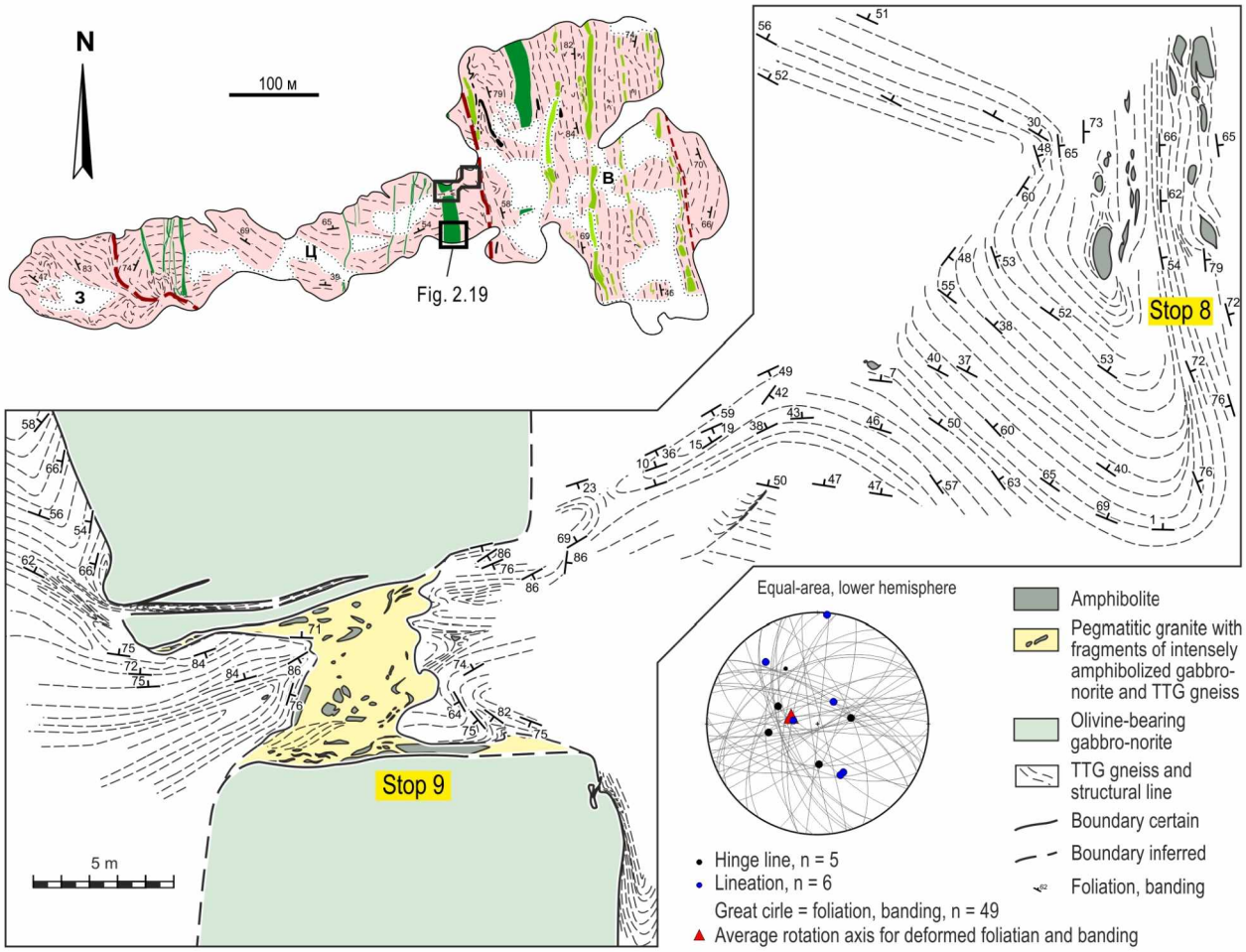

Fig. 2.17. Geological map of the northern part of the olivine-bearing gabbronorite dike in Izbnaya Luda Island (compiled by S.V. Mudruk and T.V. Kartushinskaya)

Petrography and metamorphic evolution of the gabbronorite dike are described in (Dokukina, Konilov, 2011). Igneous minerals have been preserved in the central part of the dyke and are represented by olivine, augite, pigeonite, orthopyroxene, chromite, and plagioclase, with olivine being commonly observed as inclusions in clinopyroxene. Coronas of orthopyroxene with omphacite intervene between igneous plagioclase and clinopyroxene (Fig. 2.18a, b). Orthopyroxene (Fig. 2.18c) and pyroxenes exhibit exsolution structures formed by inverted pigeonite and augite (Fig. 2.18d). The dike was crystallized at $T = ca.$ 1030 °C and $P = ca.$ 5 kbar.

Eclogitization started with the formation of a garnet corona with inclusions of kyanite, plagioclase, clinopyroxene, and quartz (Fig. 2.18e) between the igneous pyroxene and plagioclase. Then the coronitic garnet with kyanite inclusions completely replaced the igneous plagioclase. The garnet composition is homogeneous as a whole but rims are moderately enriched in iron. The matrix consists of *Opx-Cpx-Pl* symplectites characteristic of intensely retrogressed eclogites. Rare omphacite relicts (36 % jadeite) have been preserved in the symplectites; in addition, this omphacite together with kyanite and quartz has been preserved as inclusions in garnet (Fig. 2.18e). Together with data from other dikes, omphacite can be divided into two types: (1) free of inclusions and (2) with oriented quartz needles. The content of the jadeite component is 20 % in the omphacite with quartz needles, while that in the needle-free omphacite is 30 %. The pressure reached at the peak of the eclogite-facies metamorphism is estimated at 16–17.5 kbar, and these values are minimal.

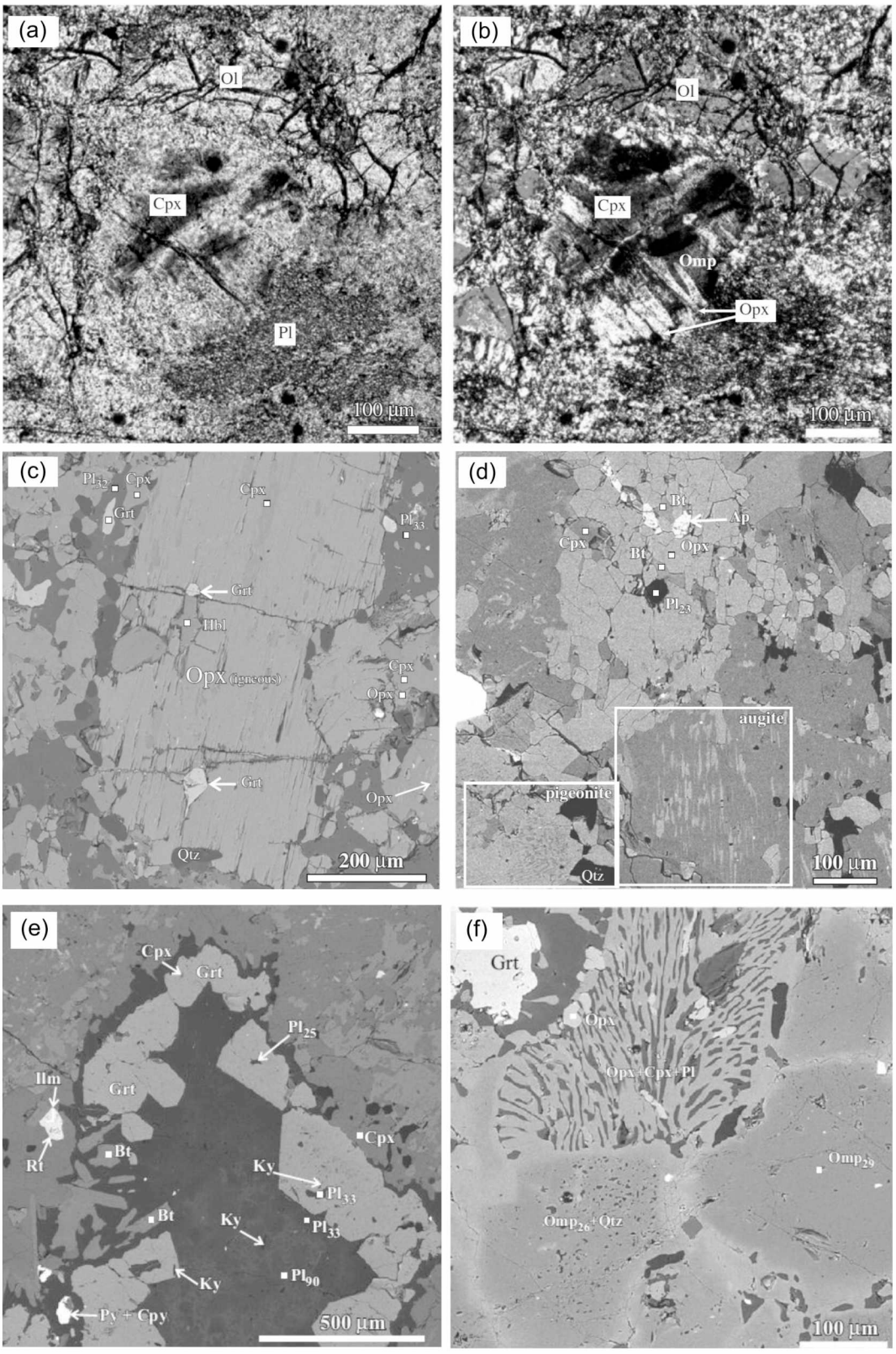

Fig. 2.18. Petrographic peculiarities of the olivine-bearing gabbronorite dike in Izbnaya Luda Island (a–e) and a basic dike in Vorotnaya Luda Island (f); after (Dokukina, Konilov, 2011).

(a & b) Plane-polarized light (a) and transmitted cross-polarized light (b) images of olivine; note a prograde *Omp-Opx* corona around igneous clinopyroxene (b). (c) Igneous orthopyroxene in a metamorphic garnet-clinopyroxene-plagioclase-quartz matrix. (d) Relicts of igneous pyroxene: postmagmatic exsolution texture of pigeonite (orthopyroxene host with clinopyroxene lamellae) and augite (clinopyroxene host with orthopyroxene lamellae). (e) Garnet corona with kyanite at the plagioclase-pyroxene boundary and relics of igneous plagioclase in a metamorphic plagioclase aggregate. (f) Inclusion-free omphacite and omphacite with quartz rods and *Opx-Cpx-Pl* symplectite in omphacite (eclogite patch)

During the following granulite-facies overprint orthopyroxene replaced part of the *Cpx-Pl* symplectites and formed a corona around garnet (Fig. 2.18f). Locally, the orthopyroxene formed part of granoblastic orthopyroxene-clinopyroxene domains. Furthermore, the gabbronorites were completely changed into a *Grt+Opx+Cpx* granulite in a zone (*ca.* 5 m width) at the western margin of dike. Estimates of *P–T* parameters for the granulite-facies stage are 10–13 kbar and 750–800 °C.

Amphibolite-facies retrogression led to amphibolization of both igneous and metamorphic components of the dike along the outermost narrow (*ca.* 10 cm) marginal zones. In addition, garnet developed at the boundary between the amphibolized margins of the dike and the TTG host. The gabbronorites were also amphibolized along later fractures and felsic pegmatite and carbonate veins. This amphibolization occurred at P = *ca.* 8.0–9.5 kbar and T = 530–660 °C kbar (Sibelev et al., 2004; Volodichev et al., 2004).

V.V. Travin (Travin, Kozlova, 2005, 2009; Travin, 2015) has interpreted the fracture spacing between two boudins of the gabbronorite dike as a W-E trending ductile shear zone. Observations that the primary igneous textures are obliterated in gabbronorites near the fracture spacing, a garnet-clinopyroxene assemblage is dominant in these rocks and the N-S trending dike is located just *ca.* 25 m from the Eastern Domain (Fig. 2.17), which is a large shear zone, permit this researcher to conclude that the eclogite-facies overprint recorded in the gabbronorite dike is related to these two Paleoproterozoic shear zones.

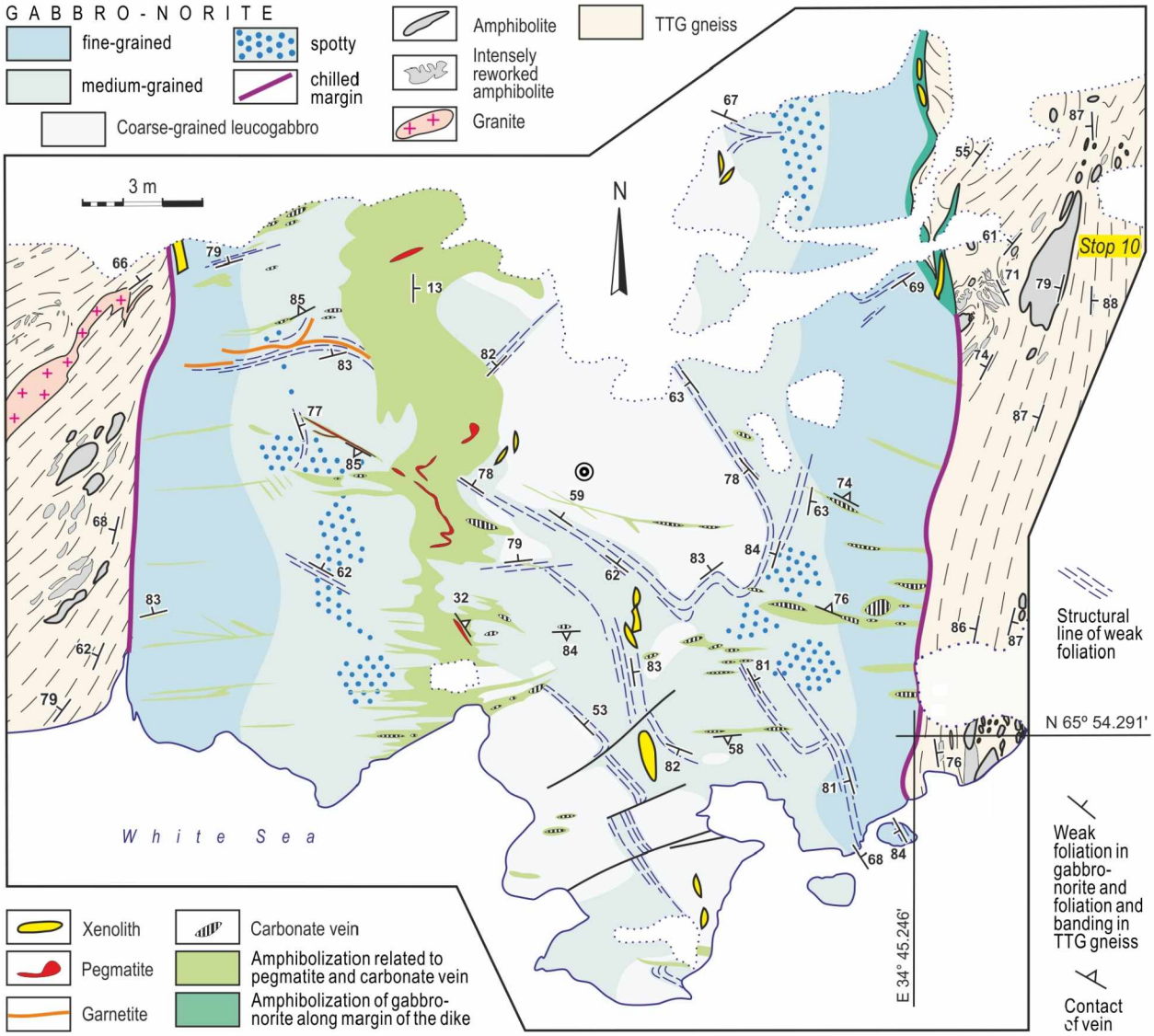

Fig. 2.19. Geological map of the southern part of the olivine-bearing gabbronorite dike in Izbnaya Luda Island (compiled by O.S. Sibelev)

According to (Dokukina et al., 2012) a granitic leucosome cross-cuts the gabbronorite dike in the inter-boudin space. Relationships between this granitic leucosome and the pegmatitic leucocratic granite are unknown. The leucosome contains prismatic and long prismatic zircon crystals displaying cores and thin rims which are dark-colored and light-colored in CL, respectively. The cores are characterized by a well developed oscillatory zoning. Four zircon crystals yielded an upper intercept age of 2651 ± 2.4 Ma. Dokukina et al. (2012) have referred this date to the crystallization of the granitic leucosome, which thus suggests an Archean age of the gabbronorite dike. These authors have not touched an issue of probable inheritance of the dated zircon from the country Archean TTG gneisses.

Stop 10. A relic retrogressed eclogite has been found in an intensely deformed and migmatized amphibolite layer that occurs in TTG gneisses several meters from the eastern contact of the Paleoproterozoic gabbronorite dike (Volodichev et al., 2004). This eclogite is composed mainly of garnet and clinopyroxene and contains minor amounts of plagioclase, hornblende, quartz, and rare flakes of biotite. A characteristic accessory mineral is rutile. Garnet composes large porphyroblasts with abundant inclusions (mostly of quartz) in the clinopyroxene–hornblende–plagioclase matrix. The primary omphacite (31 % jadeite) is replaced by symplectites of omphacite (22 % jadeite) and plagioclase (18 % anorthite). The garnet displays a weak retrograde zoning: the content of the pyrope component is 28 % in the cores and 25–27 % at the margins. The garnet cores contain inclusions of omphacite (30 % jadeite), while the margins host inclusions of diopside (7 % jadeite) and plagioclase (21 % anorthite). A later amphibole is a Fe-rich pargasitic hornblende. The matrix and *Di-Pl* symplectites contain flakes of titanium-rich biotite (TiO_2 up to 4.75 mass %).

Stop 11. A specific feature of the TTG gneisses of the Central Domain is a set of numerous thin veins and veinlets of pseudotachylite (Travin et al., 2005). These veins are related to small sinistral fractures displaying a left-hand en-echelon pattern (Fig. 2.20a). As a rule, they are subvertical or dip steeply and moderately to the northwest and possess a dominant NE trending (Fig. 2.20b). They appear to have been connected with rapid brittle deformation of rocks in some domains, while the same rocks were subjected to simultaneous ductile deformation in adjacent domains. This conclusion is drawn from a gentle bending of a thin left part of a peraluminous granite vein whose thick central part is fractured and is cut by the pseudotachylite veins (Fig. 2.20a). The pseudotachylite veins are believed to have resulted from seismic deformation related to a subducting lithospheric plate in the Late Mesoarchean (Dokukina, Dokukin, 2015).

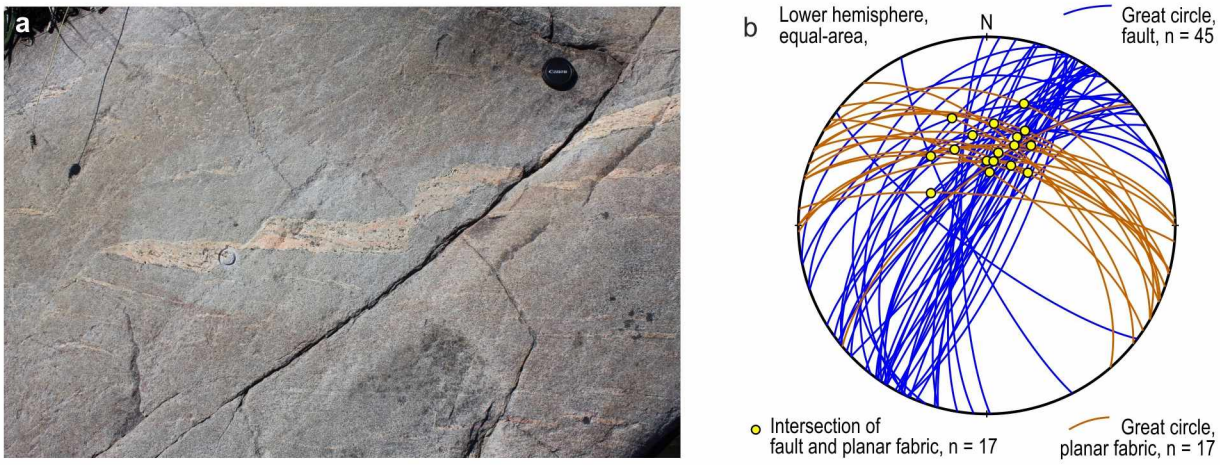

Fig. 2.20. (a) Set of pseudotachylite veinlets in the Central Domain and (b) their orientation

Stop 12. Peraluminous leucocratic granites are widespread in the Central Domain. They compose veins whose thickness vary from 1–2 cm to *ca.* 1 m, cut migmatized, foliated and folded Archean TTG gneisses and are folded by tight to isoclinal folds (Fig. 2.21a). The folded veins are cut by a gabbronorite dike and a younger basic dike, and peraluminous granite IZ13-1/5 was taken from a domain between these cross-cutting dikes free of Paleoproterozoic deformation (Figs. 2.15 and 2.21b). Zircon composes euhedral unzoned crystals (Fig, 21c–d) that have yielded a Concordia age of 2670 ± 8 Ma (U-Pb, SIMS; Fig. 2.21e). This date is thought to define the time of the magmatic crystallization of the granite. Anyhow, it evidences that the TTG gneisses and amphibolites experienced deformational and metamorphic reworking before 2.67 Ga.

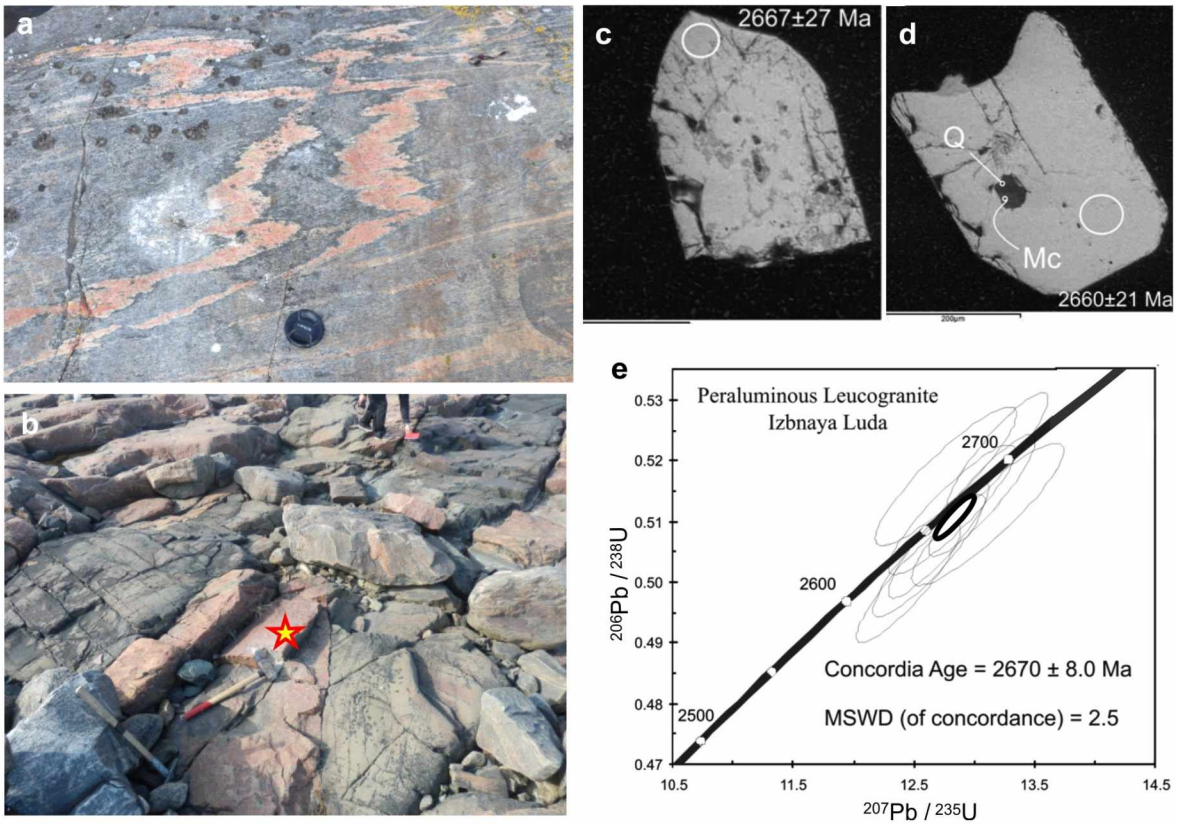

Fig. 2.21. (a) Folded peraluminous leucogranite veins cross-cutting migmatized, foliated and folded TTG gneisses in the Central Domain. (b) Location of sample IZ13-1-5 taken from rocks free of Paleoproterozoic deformation (this is marked by the star and is situated between two undeformed Paleoproterozoic dikes). (c–d) BSE images of dated zircon crystals. (e) Concordia plot for zircon from sample IZ13-1-5

Stop 13. Peraluminous leucocratic granites are also widespread in the Western Domain. They also compose veins of the same thickness and truncate migmatized and sheared TTG gneisses folded by isoclinal folds. In turn, these granites are folded first by tight to isoclinal folds (similar to recumbent) and then by open upright folds (Fig. 2.22a). It is important that these two folding phases were separated by the emplacement of a Palaeoproterozoic (?) dike that truncates the tight to isoclinal folds in the granite and is folded together with them by the upright open folds. In CL images, zircon grains from granite sample 81657 exhibit oscillatory-zoned cores, oscillatory-zoned rims (all dark-colored) and thin outer white-colored rims (Fig. 2.22b–e). The cores have given a Concordia age of 2716 ± 7 Ma (Fig. 2.22f) and the dark in CL rims a Concordia age of 2657 ± 23 Ma (Fig. 2.22g). The outermost white in CL and low-U rims (Fig. 2.22b–e) have a Concordia age of 1875 ± 21 Ma (MSWD = 0.99, n = 3; U-Pb, SIMS). The cores are suggested to be inherited, the oscillatory-zoned rims to be referred to the magmatic crystallization, and the outermost unzoned rims to be related to a Paleoproterozoic metamorphic overprint.

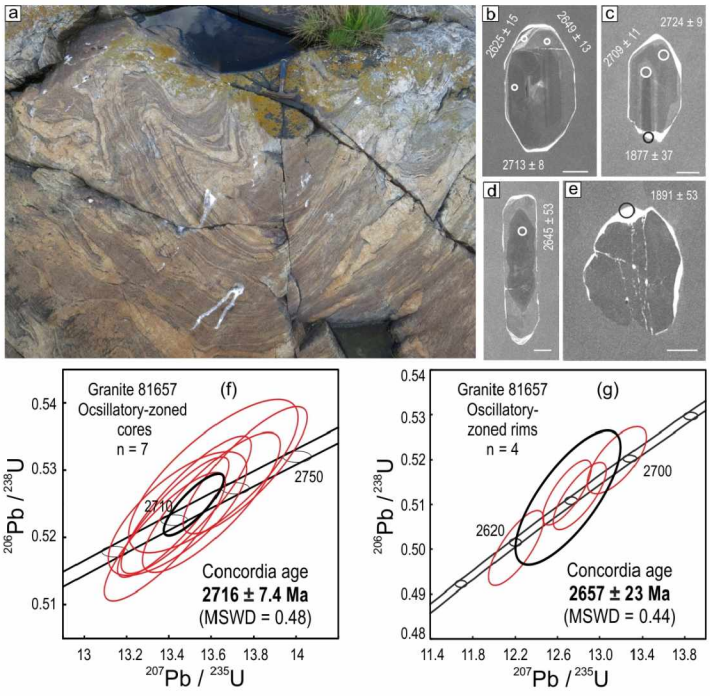

Fig. 2.22. (a) Folded potassic granite veins cross-cutting migmatized, foliated and folded TTG gneisses of the Western Domain. (b–e) BSE images of dated zircon crystals. (f–d) Concordia plots for zircon from sample 81657

Tsoizititovy Island

Stop 14. Zoisitites are common in the Gridino area from Nikonov Island in the south (south of Stolbikha Island, where Archean eclogites have been found for the first time and described (Volodichev et al., 2004; 2014) to Point Kirbey in the north. Zoisitites are thus always associated with eclogites (Fig. 2.23). Like eclogites, they have been subjected to a varying degree to multiple retrograde metamorphism and have been changed epidosites with or without relics of zoisite. However, protolith minerals, basic plagioclase ± diopside, occasionally occur in zoisitites and their epidotized varieties.

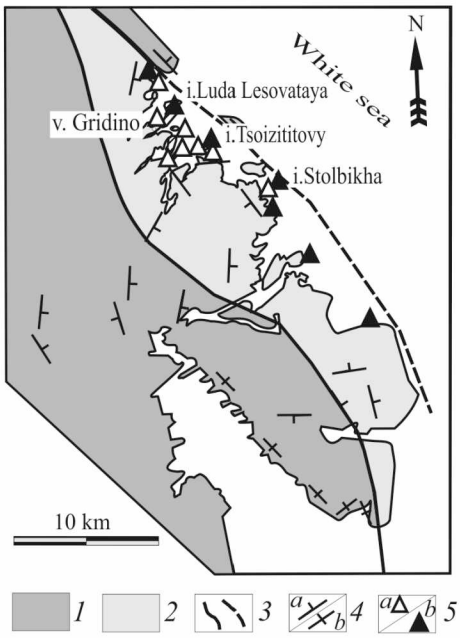

Fig. 2.23. Schematic geological map of the Gridino area with main locations of zoisitites.

1 – rocks of the Belomorian complex (gneiss, amphibolite, tonalite); 2 – Gridino eclogite-bearing complex; 3 – tectonic boundaries; 4 – gneissic banding dip (a – 10–70 deg; b – *ca.* 90 deg); 5 – main locations of eclogites (a) and zoisitites (b)

The zoisitites, found and studied at three localities on Stolbikha Island, Luda Lesovata Island and an island located to west of Izbnaya Luda Island and named Tsoizititovy Island because of the highest zoisitite xenolith concentration in TTG gneiss and the maximum size of the xenoliths (Fig. 2.24).

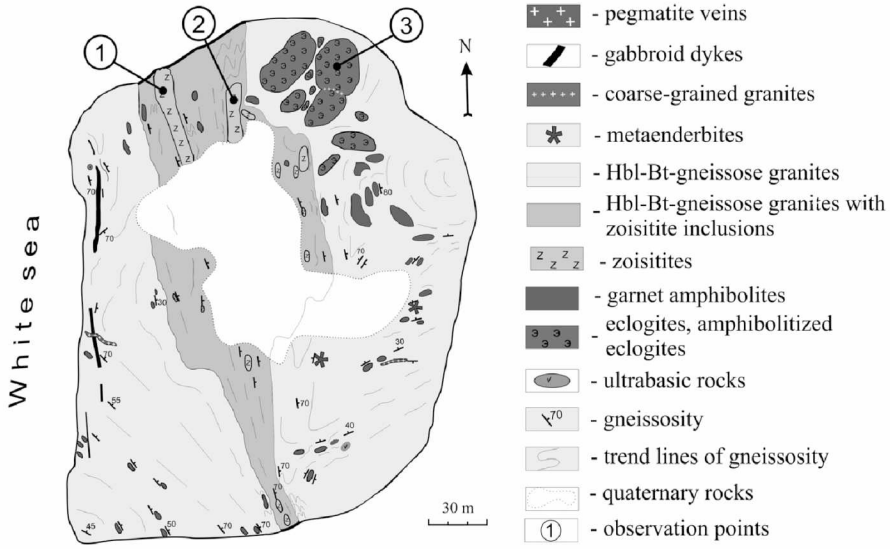

Fig. 2.24. Geological scheme of Tsoizititovy Island (Slabunov et al., 2015)

There is a cluster of oval-shaped highly altered eclogite bodies, varying in size from 4 × 4 m to 40 × 10 m, in the northeastern part of Tsoizititovy Island (Fig. 2.24). These retrogressed eclogites contain relic omphacite with 22 % jadeite (Volidichev et al., 2004, sample V-7-2). Enclaves of more fine-grained garnet amphibolite occur farther southwards, while enclaves of N-S-trending coarse-grained zoisitites (up to 60 × 10 m) are common farther westwards. Zoisitite enclaves, occurring in the southern and central parts of the island, vary in size from 3 to 5 m.

The zoisitite bodies consist of fine to medium prismatic white, locally green zoisite crystals. Green zoisitites contain elevated concentrations of TiO_2 (1.57–3.63 mass %) and some trace elements such as Cr, V, Cu, Nb (Tab. 2.1). In quartz-bearing zoisitites the quartz concentration is variable and quartz composes thin veins in some varieties. Other zoisitites contain aggregates composed of plagioclase and occasionally diopside. The results of petrologic studies have shown that plagioclase-bearing zoisitites are most informative for identifying their possible protolith and revealing metamorphic characteristics at the prograde and retrograde stages of metamorphic evolution.

Table 2.1. Chemical composition of zoisitites from Tsoizititovy Island

	1	2	3	4
Sample No	GR10-6/1	GR10-6/2	2919-1	258
# Mg	3.84	7.29	8.12	23.27
SiO_2	45.50	43.52	50.00	44.10
TiO_2	1.57	0.43	0.37	0.52
Al_2O_3	26.51	28.64	25.95	28.27
Fe_2O_3	2.00	2.46	1.92	2.20
FeO	0.43	0.28	0.29	0.43
MnO	0.01	0.02	0.02	0.018
MgO	0.05	0.11	0.10	0.41
CaO	21.43	21.24	18.46	21.50
Na_2O	0.24	0.58	0.52	0.32
K_2O	0.04	0.23	0.13	0.14
H_2O	0.03	0.07	0.02	0.03
ппп	1.77	0.00	1.66	1.93
P_2O_5	0.15	0.06	0.06	0.03
Cr	564	88	72.30	154.35
Ni	80	7	7.10	6.69
Co	1	1	1.8	1.69
V	137	73	73.60	75.99
Rb	1	5	2.90	2.66
Ba	0	16	22.0	14.95
Sr	1132	1053	1266.8	1214.44
Nb	17.1	4.0	6.0	4.79
Zr	63	38	34.6	42.99
Y	19	6	7.40	7.43
Th	1.55	3.01	2.55	3.03
U	0.28	0.14	0.19	0.17
La	24.92	26.04	29.79	31.02
Ce	62.14	48.54	50.90	58.37
Pr	7.72	4.71	4.96	5.80
Nd	34.92	18.46	16.28	22.95
Sm	7.36	2.75	2.24	3.20
Eu	0.84	0.94	1.08	1.13
Gd	5.95	2.38	1.88	2.98
Tb	0.78	0.24	0.25	0.32
Dy	4.44	1.28	1.32	1.63
Ho	0.77	0.22	0.26	0.28
Er	2.24	0.66	0.67	0.82
Tm	0.26	0.08	0.10	0.10
Yb	2.04	0.59	0.66	0.76
Lu	0.24	0.07	0.10	0.10

Petrography and metamorphism. Plagioclase in plagioclase-bearing zoisitites belongs to three generations and displays a variety of compositions from bitownite (82–83 % An) to albite with three maxima: 77–79 % An, 63–65 % An and 0–10 % An consistent with its major generations. Plagioclase of the earliest generation (82–68 % An) forms mosaic aggregates of fine grains replaced by more fine-grained clusters of white mica of the muscovite-seladonite series (Fig. 2.25a). Some white mica flakes are composed of phengite with Si concentrations of 3.15–3.27 apfu, whereas the matrix consists of mica, which has no counterparts in the white mica nomenclature (Nomenclature..., 1998). At Si concentrations of 3.12–3.55 apfu they contain no Fe or Mg, but Ca (0.04–0.26 apfu) and Na (0.18–0.84 apfu) concentrations increase, while K concentration decreases gradually (0.92–0.37 apfu) (Fig. 2.26). The extreme member of this sequence (Na > K > 0.5 apfu) is a Na mica, paragonite with uncommonly high Si concentrations of 3.44–3.55 apfu. Another predominant constituent of the mica clusters may tentatively identified as "aluminoseladonitic muscovite".

Talc-chlorite is a rare accompanying mineral which forms fine scales in the mica matrix (Si = 3.80–3.99 apfu., F = 3.8–4.4 %).

The chemical composition of the rocks was determined in the Analytical Laboratory at the Institute of Geology, KarRC, RAS (analysts A.I. Polishchuk and V.L. Utitsyna). Rare and trace element concentrations were estimated by the ISP method on XSeries 2 ICP-MS (Thermo Scientific, USA) using the standard SGD-AA sample in the Institute of Geology, KarRC, RAS (analyst A.S. Paramonov). In tables #Mg was calculated as $MgO/(FeO + 0.8998Fe_2O_3 + MgO) \times 100$ (molecular concentrations).

The plagioclase-mica aggregates bear newly-formed zoisite crystals varying in size and shape. Some of the crystals contain plagioclase inclusions (67–68 % An, Fig. 2.25b) occasionally associated with phengite (Si = 3.18–3.19 apfu). In a crystal bearing a plagioclase inclusion, its central part is composed of $Zo_{0.12}$[2], whereas a margin consists of $Zo_{0.17}$ (Fig. 2.25b). A monomineral zoisitite occurs around the plagioclase-mica aggregates which are made up by zoisite (97–98 %), quartz and muscovitized plagioclase. The zoisite crystals, up to 3–4 mm in size, vary in shape from xenomorphic to idiomorphic

[2] Underscrypt denotes $X_{Ps}=Fe^{+3}/(Fe^{+3}+Al-2)$ (Deer et al., 1986).

and display a growth zoning: the center is composed of $Zo_{0.12}$, and the margins consist of $Zo_{0.17}$ (Fig. 2.25c). Large zoisite crystals often contain inclusions of fine subidiomorphic Zo crystals, 150–300 μm in size. Average Fe^{+3} concentrations in these inclusions and the zoisite host are about the same, but $Zo_{0.10\text{-}0.12}$ is observed in both cases. Inclusions of minerals of the clinozoisite-epidote group are scarce.

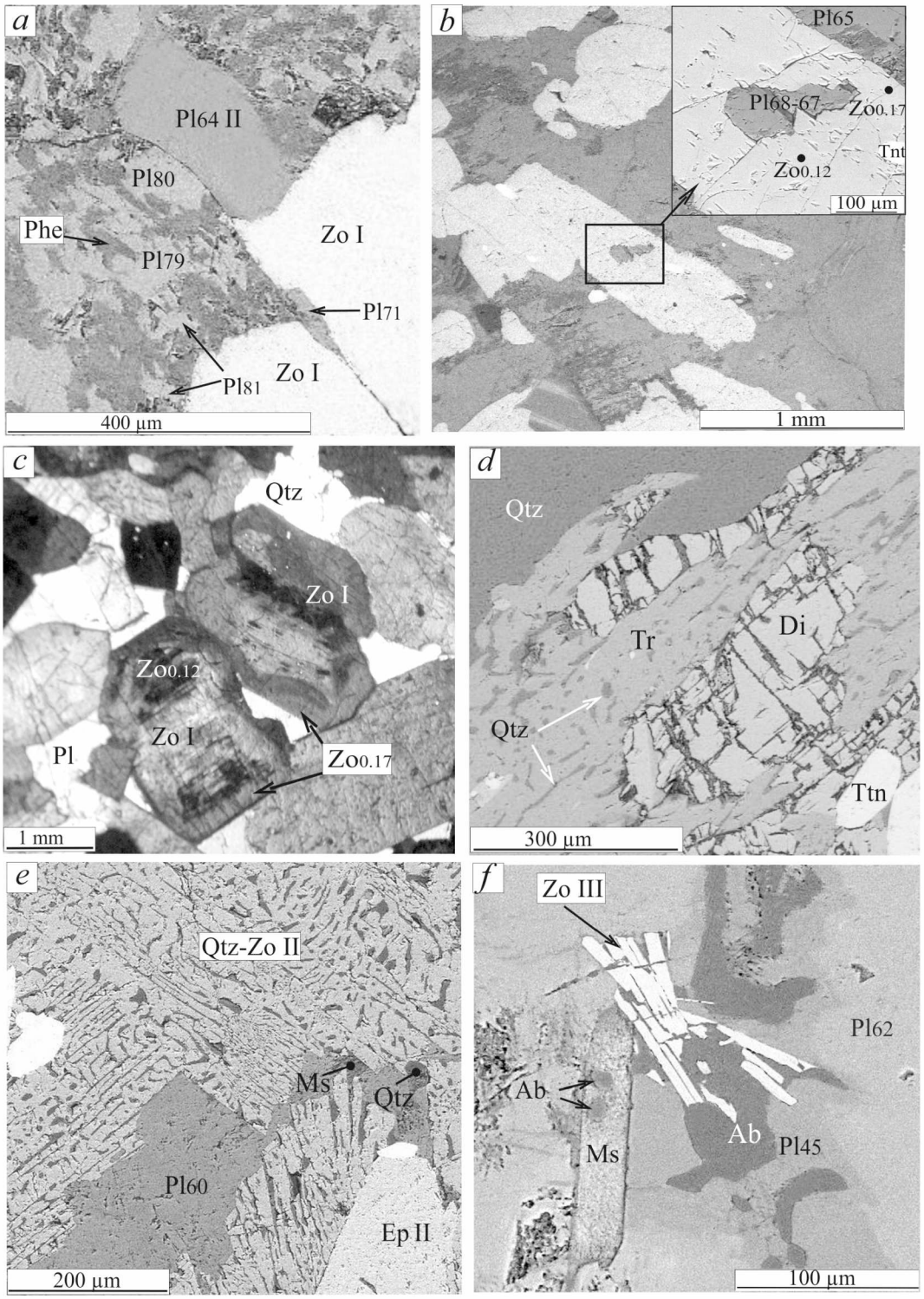

Fig. 2.25. Micrographs of a zoisitized anorthosite: (a) relict zone of a Pl-protolith replaced by more fine-grained white mica aggregates (+ phengite) which were, in turn, partly replaced by later Zo I and Pl II (thin section 1603-2a, BSE image); (b) zoisite with $Pl_{68\text{-}67}$ inclusions (thin section 1603-2b, BSE image); (c) idiomorphic and sub-idiomorphic zonal Zo I crystals (thin section 258-3, BSE image); (e) Qtz–Zo II symplectite (thin section 258-3, BSE image); (f) Zo III + Ms + Ab paragenesis of the second retrograde stage (thin section 1603-1, BSE image)

A green zoisitite is enriched in TiO_2 (up to 3 mass %) and contains two modifications of titanite: (i) fine (5–30 μm) inclusions in $Zo_{0.10\text{-}0.11}$ and (ii) clusters of coarser (up to 200–300 μm) grains occurring between inclusion-free $Zo_{0.14\text{-}0.16}$ crystals of the late generation.

Two textural groups of quartz-bearing zoisitites are distinguished: (i) a massive group with xenomorphic Zo grains and (ii) a group of suvidiomorphic elongated prismatic Zo crystals showing a preferred orientation in deformation zones. The zoisites of these groups are similar in composition. Their prograde zoning is poorly defined, but the marginal zones consist of of clinozoisite and epidote in some places.

The above data have led us to a conclusion that the increase of the Fe^{+3} concentration in the zoisite from 0.10 to 0.17 apfu occurred at the prograde stage of metamorphic evolution. The formation of the white mica and phengite with the increase of the Si abundance in the latter from 3.15 to 3.27 apfu (Fig. 2.26) that had taken place at the preceding stage seems to have also been prograde.

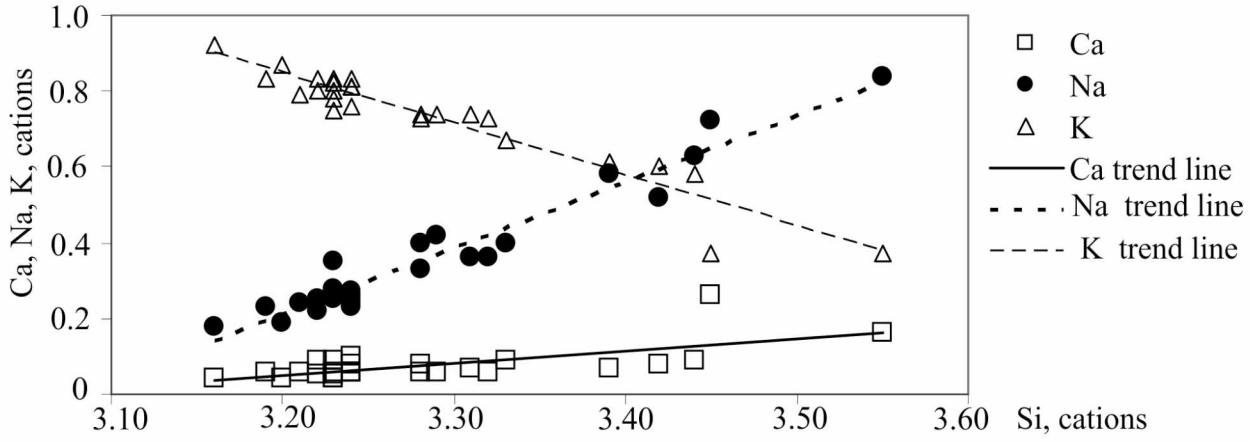

Fig. 2.26. Diagram showing the compositions of white mica of the muscovite-seladonite-series (except from phengite) formed after basic plagioclase prior to the zoisite crystallization

In the same plagioclase aggregates a later plagioclase (Pl II) has been established (up to 63–65 % An). This plagioclase is referred to as the Pl II generation and occurs as irregular grains up to several millimeters in size. Pl II was not subjected to micatization (Fig. 2.25a) and often contains shadow relict inclusions of altered plagioclase of the first generation.

Diopside is seldomly observed in fragments of altered protoliths. It commonly occurs as relics in crystals of tremolite, the dominant mineral of the matrix of the altered protoliths (Fig. 2.25d). Pl II (60–66 % An) is replaced by quartz-zoisite symplectites (Fig. 2.25e), whose zoisite is referred to as Zo II and has relatively stable composition (Fe^{+3} = 0.10 apfu). Epidote is a common mineral in this association (Fig. 2.25e). The relationship of epidote with the Qtz – Zo II symplectite suggests its formation at the latest stage of the same episode of metamorphic evolution: Pl II → Zo II (+ Tr) → Ep II.

The next stage of metamorphic evolution is well recorded in the same zoisite-plagioclase domains. This stage is indicated by a new zoisite generation referred to as Zo III which mainly composes druse-like or brush-like aggregates of fine, elongated, homogeneous twinned crystals locally ingrown into albite (Fig. 2.25f). The mineral assemblage of this stage is well determined as $Zo\ II_{0.08}$ + Ms + Ab (Fig. 2.25f).

So, zoisite was crystallized at two stages. At the first stage, the muscovite-seladonite series white mica replaced the protolithic plagioclase (≥ 82–83 % An); phengite and paragonite, high-*P* minerals, were also crystallized (assemblage Pl_{80} + K_2O + Na_2O + H_2O was replaced by a new one Pl_{65} + K-Na mica). The second stage overlapped partly with the first stage in time and was characterized by the crystallization of zoisite by means of reaction "relic Pl_{80} + newly-formed Pl_{65} + K-Na mica → Zo + Qtz + K_2O + Na_2O", which led finally to the formation of the monomineral zoisitic rock. The coherent compositional changes in phengite (increase of Si from 3.15 to 3.27 apfu) and zoisite (increase of Fe^{+3} from 0.10 to 0.17 apfu) suggest the prograde character of these metamorphic stages. Two retrograde metamorphic stages can also be established: (i) crystallization of the Qrt–Zo symplectite and (ii) assemblage Zo + Ms + Ab.

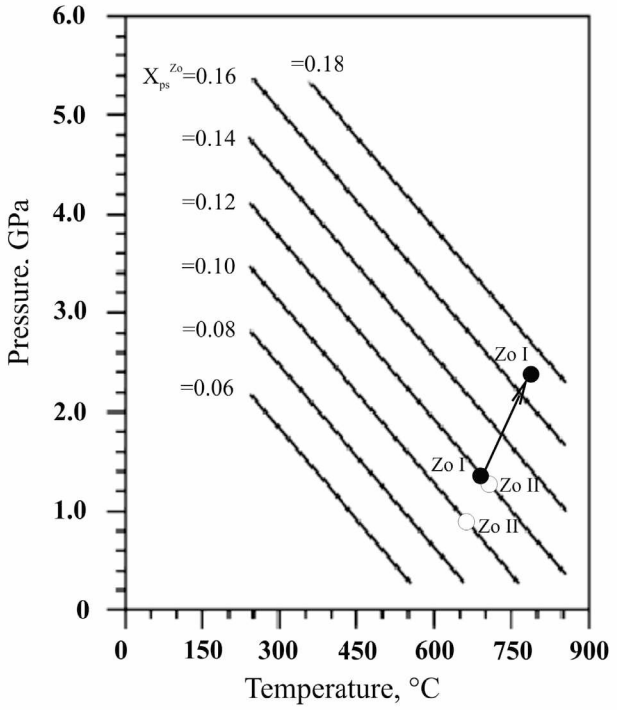

Fig. 2.27. *P-T* conditions of the zoisite formation at prograde and retrograde stages (estimated using a geothermobarometer, Brunsmann et al., 2002)

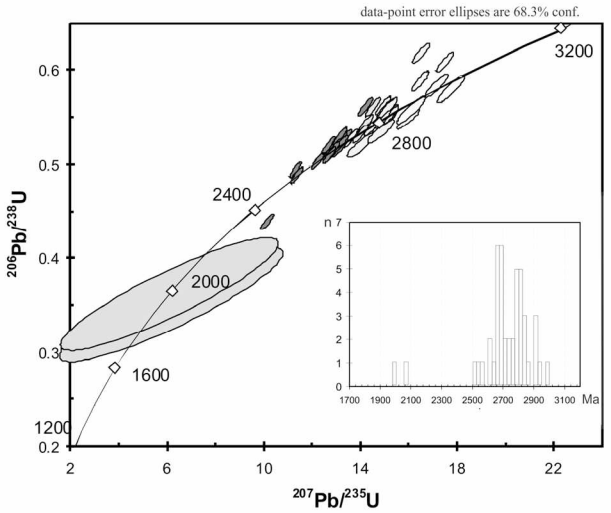

Fig. 2.28. Concordia diagram and histogram of $^{207}Pb/^{206}Pb$ ages for zircons from the zoisitites of the Gridino eclogite-bearing melange. The colours show various zircon generations

P-T conditions of the zoisitite formation were assessed using a geothermobarometer by Brunsmann et al. (2002). *T* = 600–800 °C was estimated from rutile and titanite (Zr geothermometers, Watson et al., 2006a, b). Judging from these temperatures and the increase of the Fe^{3+} content from 0.10 to 0.17 apfu in the zoisitite, pressures would have increased from 13 to 23.5 kbar (Fig. 2.27). If temperatures of the phengite formation have been the same, pressures would have been varied from 9 to 22 kbar (a geobarometer by Kamzolkin et al., 2015). Pressures of 9–13 kbar seem to have occurred at an initial stage of the retrograde white mica formation which was coeval with the zoisite crystallization. The crystallization of $Zo_{0.10}$ is assumed to have taken place at *T* = *ca.* 600 °C and *P* = *ca.* 13 kbar during the first retrograde stage and $Zo_{0.08}$ at *T* = *ca.* 570 °C and *P* = *ca.* 8 kbar during the second one.

Geochronology. A U-Pb dating of zircons from a large lenticular zoisitite body was performed by the LA-ICP-MS method at Beijing University, China (Volodichev et al., 2014; Slabunov et al., 2015). 45 concordant and subconcordant isotope ages were obtained from 26 zircon grains (Fig. 2.25). About 70 % of the ages were concordant. $^{207}Pb/^{206}Pb$ ages vary from 3000 to 1980 Ma and form two prominent maxima of 2820–2830 and 2720–2670 Ma (Fig. 2.28). As zircons of different isotope ages differ in morphology, geochemistry and mineral inclusions, up to six age groups of zircon can be identified which are assumed to reflect distinct geological processes.

Two zircon groups can be identified from their morphology and internal structure. The first group consists of idiomorphic to sub-idiomorphic zonal prismatic zircon crystals (length/width ratio, L/W = 3), and the second, subordinate one comprises rounded prismatic grains. One domain in a zircon grain yielded the oldest $^{207}Pb/^{206}Pb$ age of 2999 ± 16 Ma (1σ; Fig. 2.29a) and its geological meaning is unclear. The cores of zircon of the both groups gave an upper intercept age of 2904 ± 54 Ma (Fig. 2.29a, b). In some grains these cores are not clearly separated from later overgrowths, with both the cores and overgrowths being dark- and/or medium-grey-colored in CL (grains GR-2, GR-10, GR-24 and GR-26 in Fig. 2.29b). These overgrowths yielded ages of *ca.* 2.82 Ga and *ca.* 2.72 Ga (Fig. 2.29b). The latest overgrowths are thin and white- and light grey-colored in CL. The zircons host inclusions of albite, quartz, apatite, chlorite and calcite, suggesting that these zircons could have been crystallized in granitoid.

The third group of zircons consists dominantly of prismatic zonal crystals (L/W = 3–4) with poorly defined overgrowths (rounded pyramid faces). Rounded ellipsoidal unzonal crystals and their fragments are less common (Fig. 2.27b). A concordant age of 2815.9 ± 11 Ma was calculated for eight grains (Fig. 2.27a).

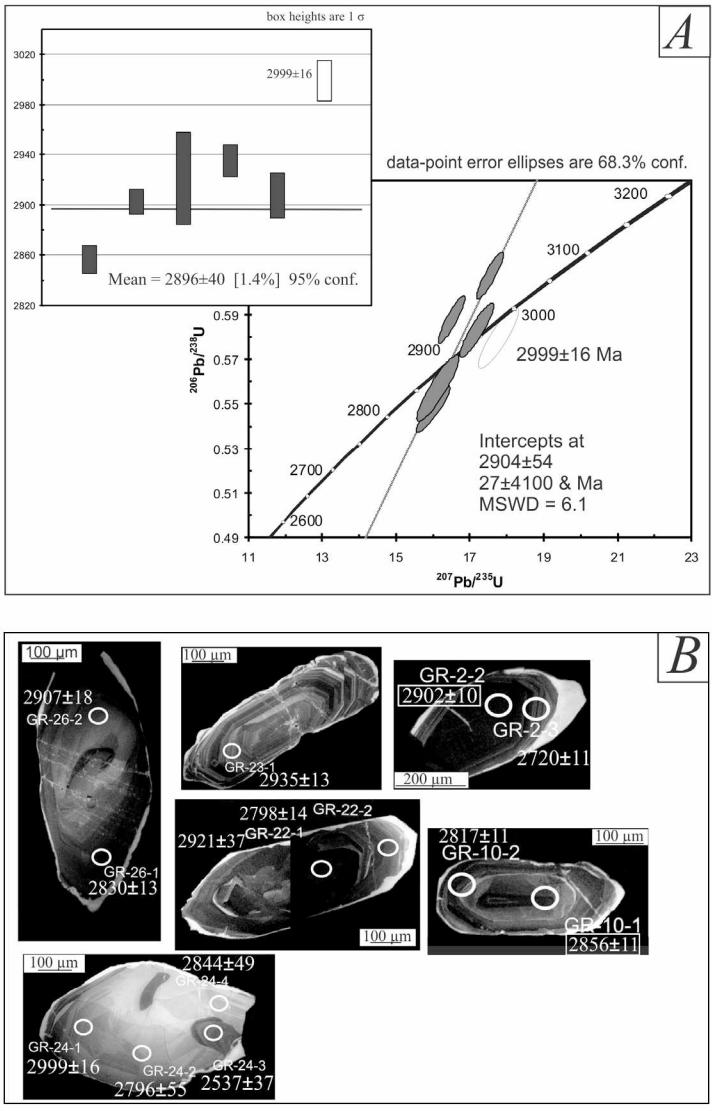

Fig. 2.29. Concordia diagram and histogram of $^{207}Pb/^{206}Pb$ ages (A) and cathodoluminescence (CL) images of zircons dated at ≥ 2.9 Ga.

The positions and numbers of data-points and $^{207}Pb/^{206}Pb$ age values are shown on zircon images (B)

These zircons exhibit the shape characteristic of both igneous and metamorphic zircons (Fig. 2.20b; grains GR-20 and GR-21, respectively). Mineral inclusions in these crystals (apart from the latest rims) comprise albite, apatite, biotite and chlorite, minerals common in granitoid.

An upper intercept age of 2745 ± 24 Ma was calculated for data-points from zircon grains GR-12 and GR-17 and was supported by a concordant age of 2746 ± 11 Ma obtained for data-point GR-12-2 (Fig. 2.31a, b). Grain GR-17 displays an almost perfect prismatic crystal (L/W = 2.5) with a poorly defined zoning, whereas grain GR-12 is a fragment of a crystal (Fig. 2.31b). The core of this crystal is dark-colored in CL and has a $^{207}Pb/^{206}Pb$ age of 2772 ± 11 Ma. It is surrounded by an overgrowth which is also dark-colored in CL and was dated at 2746 ± 11 Ma. The outermost rim is light-grey-colored in CL and has an age of 2065 ± 936 Ma (Fig. 2.31b). The older zircon cores contain epidote, biotite and chlorite inclusions which occur in fracture zones and could thus have been related to late metamorphic processes. The zircons that compose the cores and the first, dark-colored in CL overgrowths are characterized by relatively high LREE and HREE concentrations and display a gently sloping positive distribution pattern (Fig. 2.31C). These differ in concentrations of MREE from the youngest zircon overgrowths and are similar in concentrations of LREE and HREE. These zircons have the highest temperatures of their formation (810 and 900 °C; Volodichev et al., 2014). All of the characteristics of the zircons under consideration, combined with their morphology, suggest that these zircons have a magmatic origin.

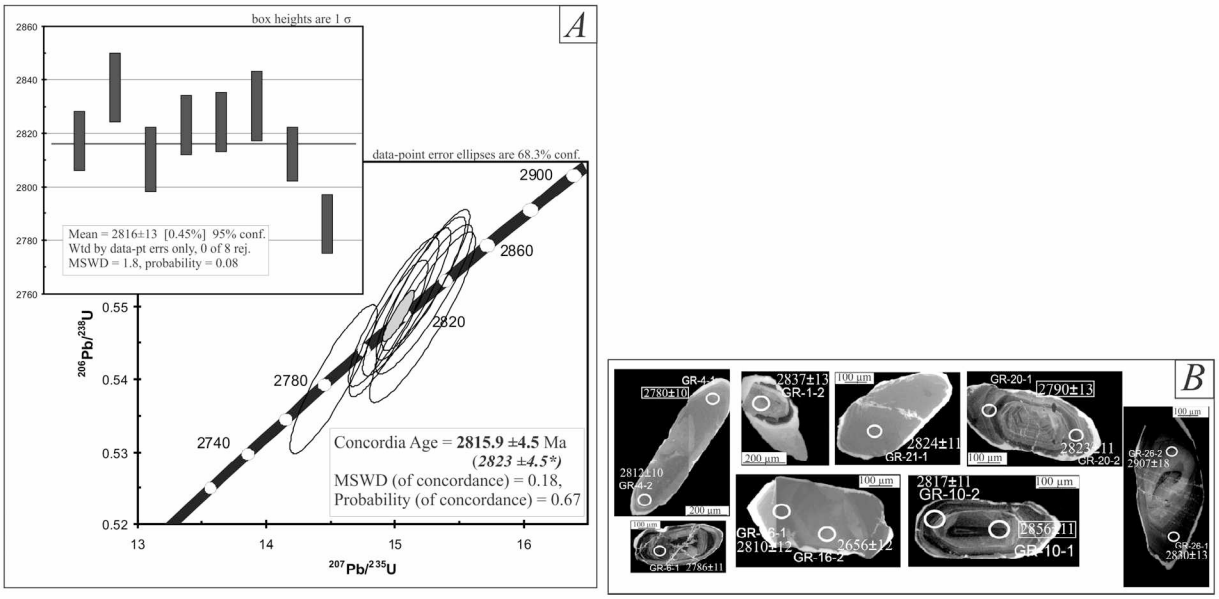

Fig. 2.30. Concordia diagram and histogram of $^{207}Pb/^{206}Pb$ ages (A) and CL-images of zircons dated at *ca.* 2820 Ma (B).

The positions and numbers of data-points and $^{207}Pb/^{206}Pb$ concordant ages are shown on zircon images (B). Discordant age dates are shown by a rectangle

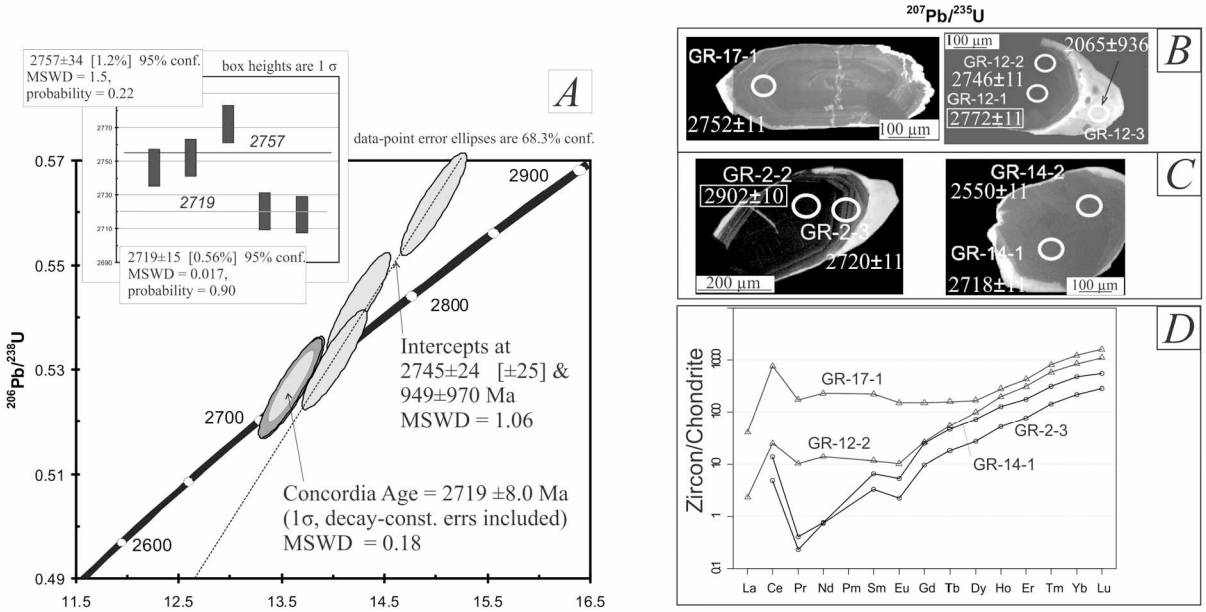

Fig. 2.31. Concordia diagram and histogram of $^{207}Pb/^{206}Pb$ ages (A), CL-images of zircons dated at 2745 (B) and 2719 (C) Ma and normalized (Nakamura, 1974) REE (D) concentrations in zircons dated at 2745 (grey lines) and 2719 (black lines) Ma.

The positions and numbers of data-points and $^{207}Pb/^{206}Pb$ concordant ages are shown on zircon images (B, C). Discordant age dates are shown by a rectangle

A Concordia age of 2719 ± 8 Ma (Fig. 2.31a) was determined for two concordant data-points, GR14-1 and GR-2-3 (Fig. 2.31c). Data-point GR-2-3 characterizes an oscillatory zoned and dark-colored in CL zircon that surrounds an older, almost black-colored in CL core, and is, in turn, surrounded by the outermost, white in CL rim. In contrast, data-point GR-14-1 features an almost homogeneous and grey-colored in CL zircon surrounded by the outermost rim identical to the aforementioned one. These two zircons are similar to the 2745 Ma zircons in the shape and internal structure and are thought to have an metamorphic origin. However, they considerably differ from them, in the geochemistry (Fig. 2.27d) and are referred to a separate age group. No mineral inclusions have been found in these zircons.

The next, younger age zircon group has a Concordia age of 2679 ± 10 Ma (Fig. 2.32a). It comprises eleven dated zircons that compose rounded and relatively homogeneous crystals and rims around older cores, with all of them being dark- or grey-colored in CL (Fig. 2.32b). They are similar to metamorphic varieties of zircon. They contain zoisite inclusions, which favors their metamorphic origin and suggests their crystallization simultaneously with one of zoisite generations.

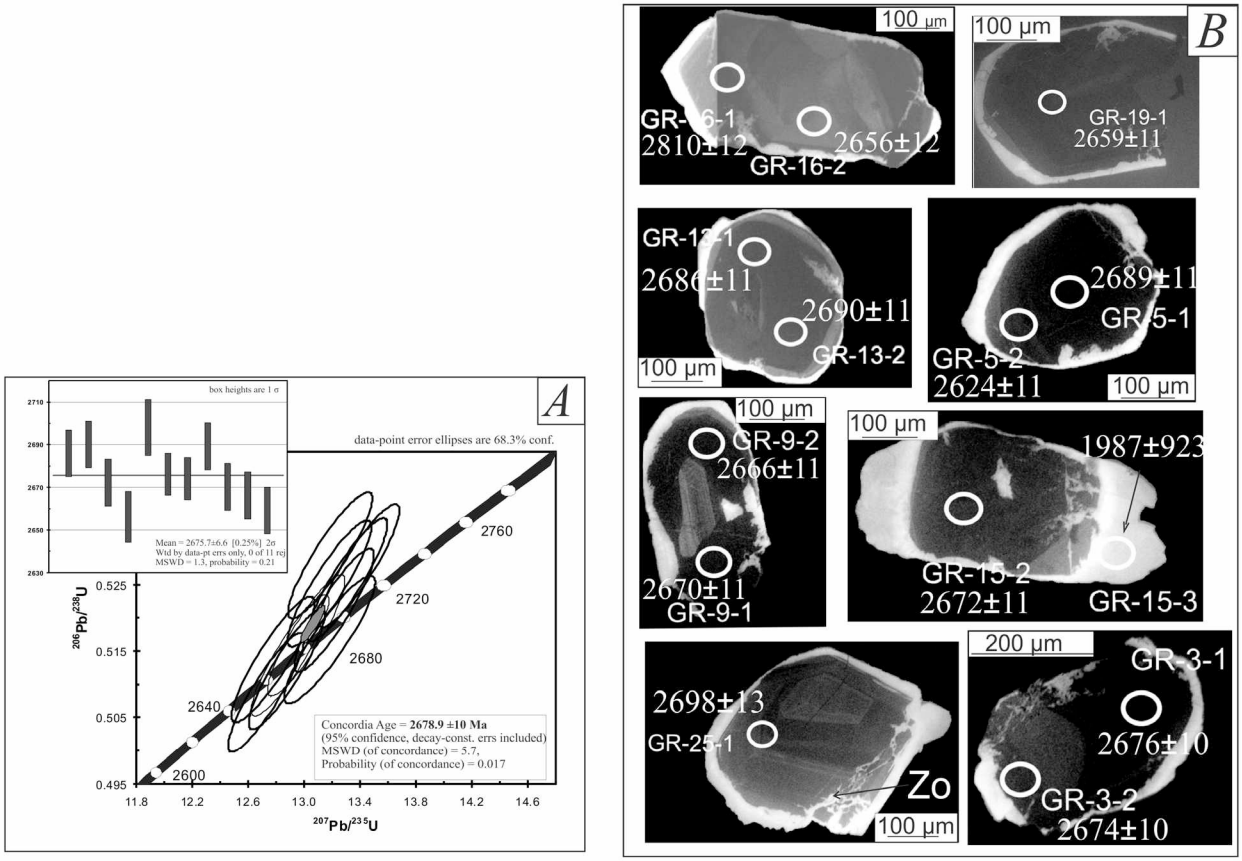

Fig. 2.32. Concordia diagram and histogram of $^{207}Pb/^{206}Pb$ ages (A) and CL-images of zircons with the concordant age of 2678.9 ± 10 Ma.

The positions and numbers of data-points and $^{207}Pb/^{206}Pb$ ages are shown on zircon images (B)

The youngest zircon group comprises the outermost zircon overgrowths around of practically all of the zircons described above. These overgrowths are, as a rule, thin, white- or light-colored in CL and zoning-free. The overgrowths contain epidote and sphene inclusions. They are thickest on tips of crystals where they display sub-idiomorphic shapes (Figs. 2.30b, 2.31b and 232b). It is noteworthy that zircon of this type does not compose separate crystals. Two overgrowths were dated and gave a Concordia age of 1960 ± 130 Ma (Fig. 2.28) i.e. these were crystallized during the Paleopropterozoic Lapland-Kola collisional orogeny. A large analytical uncertainty is due to the very low uranium content (0.63 and 0.65 ppm).

So, the zoisitites are interpreted to have developed from an anorthosite protolith. Like amphibolites that bear relic eclogites, these have been intensely disintegrated and strongly reworked within the Gridino eclogite-bearing mélange and represent its clastic component. The age of 2745 Ma is considered to be related to the formation of anorthosites. The anorthosites are supposed to have intruded into a continental granitoid crust as indicated by many inherited zircons that show features characteristic of TTG gneisses and were dated at *ca.* 3.00, 2.90 and 2.82 Ga. The formation of the early eclogite-facies assemblage that occurred at $P = ca.$ 20 kbar is assumed to have taken place at 2719 ± 8 Ma. This age coincides with dates of 2.71 and 2.72 Ga suggested for an Archean eclogite-facies metamorphism earlier (Volodichev et al., 2004; Li et al., 2015).

These age determinations all are consistent with those reported from many study areas in the Belomorian province. After all, all these numerous Archean magmatic, metamorphic and deformational

events and their succession can satisfactory be explained by the tectonics of lithospheric plates operated in the Belomorian province in the Meso- and Neoarchean (Volodichev, 1990; Glebovitsky et al., 1996; Bibikova et al., 1999; Slabunov, 2008). The occurrence of fragments of oceanic and continental crustal rocks in the Gridino eclogite-bearing mélange suggests that this mélange was formed at a continental subduction stage. Thus, a multidisciplinary study of the zoisitites has provided new insights into the formation of the Archean Belomorian accretionary-collisional orogen and permits identifying the continental subduction stage (Slabunov et al., 2015).

Short summary on Stops 1–14. Geochronological data available from structurally-constrained samples and published data on the metamorphic evolution of and ages from the TTG gneisses, amphibolites, granites and leucosomes (ages that can be unambiguously interpreted) permit to suggest a tentative succession of some major geological events in the Gridino area. This succession is given in Table 2.2.

Table 2.2. Tentative succession of some major geological events in the Gridino area

Stage	Geological event
	Post-eclogitic metamorphic overprint, 1.88 Ga
	Eclogite-facies metamorphism, *ca.* 1.90–1.91 Ga
D_4	Sinistral shearing in N-S &-NW-trending zones, folding, migmatization, 1.94 Ga
D_3	Shearing, upright open folds
	Basic dikes (~ 2.45 Ga)
D_2	Shearing, migmatization, tight to isoclinal recumbent folds
	Peraluminous leucocratic granite, 2.66–2.67 Ga
	Trondhjemitic granite, 2.70 Ga
	Granulite- to amphibolite-facies metamorphism, 2.68–2.72 Ga
	Eclogite-facies metamorphism, shortly (?) before 2.72 Ga
D_1	Shearing (top-to-SE shear sense), isoclinal folding, migmatization
	Igneous protolith of the TTG gneisses, 2.83 Ga

Vorotnaya Luda Island

Vorotnaya Luda Island (Fig. 2.1, 2.33). The island is located in the Gridino Dike Field (GDF) highly saturated with mafic dikes. Paleoproterozoic dikes in the GDF have cross-cutting relations to Gridino eclogite-bearing complex rocks (Stepanov, Stepanova, 2005; Slabunov et al., 2008; Volodichev et al, 2014; Babarina, Sibelev, 2015). Recent studies have shown that six groups of dikes, distinguished on the basis of geological, mineralogical-petrological and geochemical data, are exposed in the GDF. Three groups of mafic dikes, early Mg-tholeiites, olivine gabbronorites and late tholeiites, are exposed on Vorotnaya Luda Island.

Dikes of early Mg-tholeiites are the oldest in the GDF. They have been highly deformed in ductile flow regime and seldomly retain the primary dike morphology. Early Mg-tholeiites form a near-E-W-trending swarm and are traced from the western end to the central Vorotnaya Luda Island. The bodies are typically long, vary considerably in thickness (most bodies are not more than 1 m thick) and display sharp, cross-cutting contacts. Apophyses and anastomosing dikes are common, and fold-like forms occur from place to place. The rocks of early dikes have been highly altered and have largely lost the primary structural features and mineral composition. No magmatic minerals have been preserved in early Mg-tholeiites. As the association $Cpx_{9\text{-}13}$ + $Pl_{15\text{-}16}$ ± $Grt_{13\text{-}14}$[21-22] ± $Opx_{44\text{-}46}$ + Hbl is characteristic of the least deformed dikes, metamorphic *P–T* parameters of the rocks suggest a high-*P* granulite facies (*T* = 720–730 °C and *P* = 10–11 kbar). Relics of gabbroic and drusitic structures show that plagioclase was an essential constituent of primary rocks and that olivine was present. The chemical composition of early Mg-tholeiites is fairly persistent, as shown by representative analyses in Table 2.3, no 1. Metagabbro is classified as a tholeiite-series and normal-series rock with a mixed a Ti-Cr geochemical specialization, differentiated REE distribution and LREE enrichment.

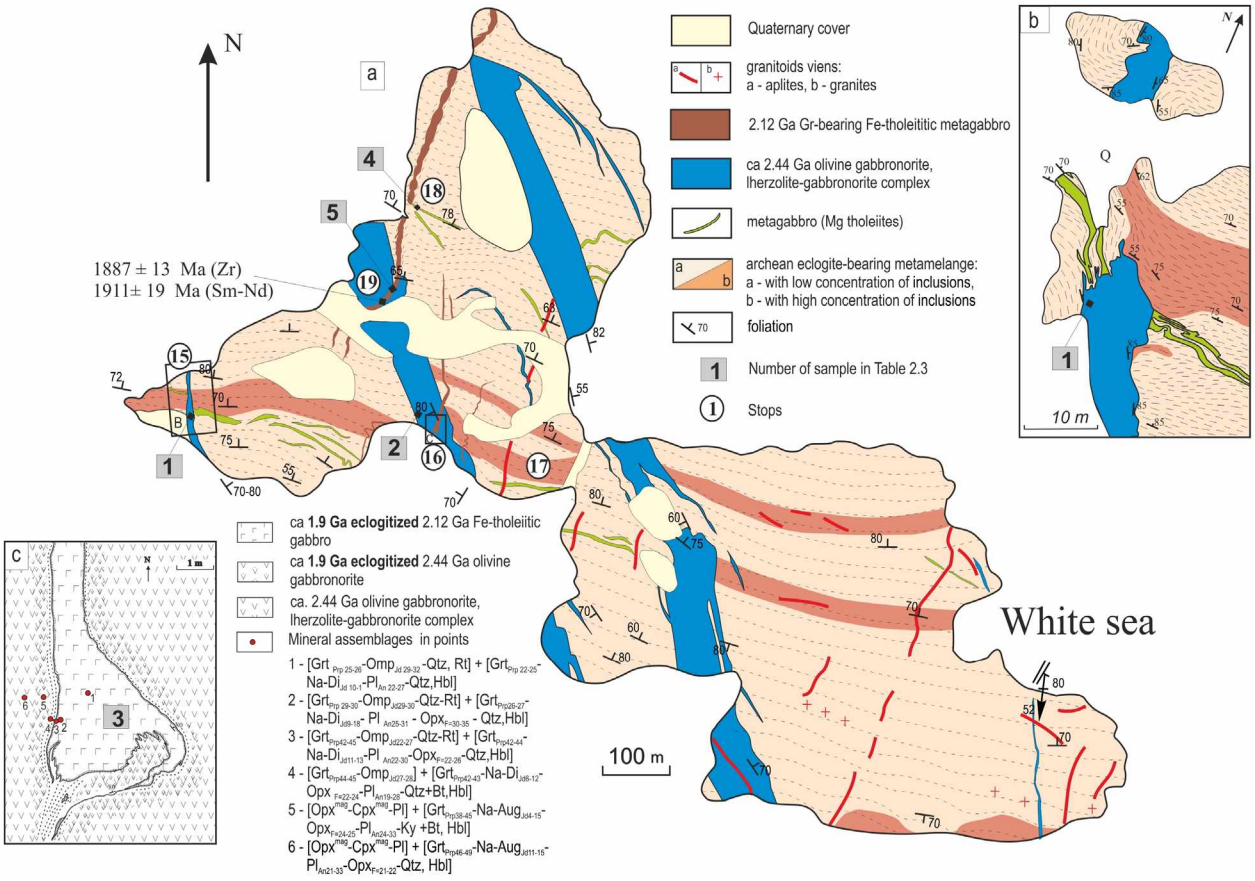

Fig. 2.33. (a) Geological scheme of Vorotnaja Luda Island; sketch-map of Stop 15 area (b); sketch-map of Stop 16 area (c) (Stepanova, Stepanov, 2005; Volodichev et al., 2005, 2014). Geochronological data (Zr – U-Pb ages of zircons (SHRIMP II), Sm-Nd – Sm-Nd minerals (Grt, CPx) isochron) after Berezin at el., 2012

Dikes of olivine gabbronorites are the most common dikes in the GDF. They belong to a lherzolite–gabbronorite complex (Stepanov, 1981) dated at *ca.* 2.4 Ga (Slabunov et al., 2011; Volodichev et al., 2012), and make up a NW-trending swarm. The dykes vary in thickness from a few centimeters to 100 m. One petrographic characteristic of the rocks is that the Opx-Cpx association is common in coronitic structures.

On Vorotnaya Luda Island three relatively large (over 50 m thick) dikes and a series of small dikes of olivine gabbronorites crop out, extend in a northwest direction across the entire island and continue outside. The dike contacts are steep, vertical to near-vertical and typically intrusive: they exhibit a cross-cutting pattern and well-defined chilled margins, numerous apophyses and host rock xenoliths. The internal structure of the dykes is simple, and differentiation is observed solely as minor variations in the chemical composition of the rocks and in the occurrence of small gabbro-pegmatite schlieren. The gabbronorites have largely preserved the primary mineral paragenesis, Opx + Cpx + Pl ± Ol, and magmatic hypidiomorphic-granular structures.

The original magmatic melt, presumably similar in composition to chilled dike rocks (Table 2.3), was crystallized in the stability field of the Ol–Pl association (P < 8 kbar). Opx–Cpx drusitic (coronitic) structures were developed later at higher pressures (P > 8 kbar). Their formation was triggered by a total bimetasomatic reaction between Ol and Pl in the rocks of the complex. A subsequent alteration of the structure and mineral composition of the gabbronorites is displayed locally in tectonic and contact zones. At this stage, the Grt–Cpx rims of coronitic structures were formed over a wide range of pressures and temperatures and, as indicated by the compositions of the minerals (Table 2.3), reached eclogite facies. The Grt–Cpx association with a high percentage of the jadeiti component in Cpx was identified in metamorphosed gabbronorites in places where the gabbronorites are cross-cut by younger dikes of coronitic gabbro. Amphibolization is usually the latest process common in the rocks of the complex. On Vorotnaya Luda Island, amphibolization seems to have occurred at two stages. The earlier stage, recognized in 2–3 cm thick marginal zones of the dikes, was close in time to the emplacement of the dikes. The gabbronorites are rich in Mg (#Mg = 0.7), Cr (> 900 ppm) and SiO_2 and show a differentiated REE distribution pattern.

Table 2.3. Paleoproterozoic gabbroids and eclogitized gabbroids from Vorotnaya Luda Island (1–5) and Gridino area (6–9)

No	1	2	3	4	5	6	7	8	9
Sample	*C-2407-41*	*C-2407-3*	*C-2407-20*	*B-204*	*C-2407-64*	*B-16/65*	*B-16/66*	*B-16/67*	*B-35*
SiO_2	50.44	51.02	50.50	49.25	48.83	48.10	49.40	48.70	48.08
TiO_2	1.08	0.60	0.73	0.96	0.99	0.57	0.62	0.53	1.27
Al_2O_3	10.39	10.56	11.60	14.15	14.66	8.82	10.10	12.00	14.90
Fe_2O_3	2.54	3.26	1.20	2.13	3.40	1.10	1.70	2.46	3.30
FeO	10.49	8.76	9.33	10.87	9.76	9.40	8.85	7.80	11.25
MnO	0.18	0.18	0.24	0.23	0.22	0.19	0.19	0.17	0.23
MgO	9.83	14.48	13.66	7.47	7.32	20.90	17.70	15.30	7.22
CaO	9.25	8.00	8.40	11.23	11.02	8.22	8.80	8.98	9.53
Na_2O	2.95	1.68	2.00	2.09	1.96	1.20	1.46	1.85	2.22
K_2O	0.79	0.51	0.61	0.08	0.03	0.32	0.35	0.44	0.40
P_2O_5	0.16	0.08	0.17	0.12	0.09	0.07	0.07	0.08	0.18
H_2O	0.15	0.17	0.16	0.16	0.05	0.07	0.02	0.31	0.13
Loi	1.43	0.75	1.04	1.23	1.14	0.93	0.76	1.00	1.09
Cr	404	1813	810	151	96	3913	–	1862	170
Ni	423	521	213	126	164	1627	–	850	217
Co	87	102	–	79	59	101	–	69	62
V	140	224	–	358	179	203	–	195	348
Rb	19	16	–	1.75	0	9	–	10	14
Cs	3.76	0	–	0.02	0.01	0.15	–	0.26	0.28
Ba	234	183	–	19.47	7	108	–	181	202
Sr	368	145	–	64.95	53	116	–	220	124
Ta	0.78	0.03	–	0.12	0.2	0.17	–	0.18	0.43
Nb	10.7	3	–	1.53	4.7	2.7	7	2.4	6.5
Hf	2.8	0	–	0.63	0.71	1.02	–	1.27	1.91
Zr	110	67	–	13.00	23	38	69	49	70
Y	17	13	–	19.80	21	12	28	15	34
Th	2.33	1.4	–	0.90	0.5	1	–	0.99	1.37
La	20.39	5.2	–	2.40	15.17	5.64	–	4.61	9
Ce	44.19	12	–	7.10	14.88	13.12	–	11.32	21.87
Pr	6.09	1.55	–	1.15	14.62	1.71	–	1.59	2.96
Nd	25.27	8	–	6.14	13.96	7.22	–	7.27	13.78
Sm	5.53	1.95	–	2.19	13.44	1.67	–	1.8	3.54
Eu	1.38	0.5	–	0.84	10.75	0.51	–	0.62	1.09
Gd	4.37	2.05	–	2.94	11.89	1.73	–	1.9	4.05
Tb	0.63	0.27	–	0.57	11.8	0.29	–	0.32	0.72
Dy	3.48	2.3	–	3.69	12.85	1.91	–	1.98	4.99
Ho	0.71	0.34	–	0.77	13.71	0.43	–	0.43	1.11
Er	1.85	1.25	–	2.33	14.93	1.21	–	1.2	3.35
Tm	0.27	0.14	–	0.33	15.2	0.17	–	0.18	0.52
Yb	1.69	1.18	–	2.25	15.2	1.14	–	1.1	3.27
Lu	0.25	0.15	–	0.32	15.17	0.18	–	0.16	0.49

Note: 1 – early Mg-tholeiites; 2, 3 – olivine gabbronorites; 4, 5 – tholeiitic dike; 6-8 – eclogitized gabbronorites; 9 – eclogitized Fe-tholeiitic gabbro; dash = not determined

Fe-tholeiite dikes form a NE-trending swarm and are younger than the olivine gabbronorites dikes. The dikes clearly cut across the country TTG gneisses, too. Banding and foliation in the TTG gneisses were completely obliterated in *ca*. 20–30 cm thick zones near the dike boundaries. In these zones new planar fabrics were developed that are concordant to the dike boundaries and are discordant to the older planar fabrics in the country TTG gneisses. The rocks of this dikes are chemically classified as tholeiites similar in the distribution pattern of incompatible elements to N-MORB. These dikes are similar in composition to the Fe-tholeiitic metagabbro dikes well-known in the Belomorian Province and dated at 2114 ± 16 Ma (Stepanova et al., 2003; Stepanova, Stepanov, 2010). The Fe-tholeiite dikes have not preserved igneous minerals and structures and consist of metamorphic garnet, clinopyroxene and plagioclase. Zircons from this metagabbro display a metamorphic origin and have been dated at 1887 ± 13 Ma (Berezin et at., 2012) and 1878 ± 15 Ma (O.I. Volodichev, unpublished data). These ages are close to a Sm-Nd age of 1911 ± 11 Ma from garnet and clinopyroxene from the metagabbro (Berezin et at., 2012).

Petrographically, metagabbro is represented by garnet-plagioclase-clinopyroxene (high-*P* granulite facies) and garnet-clinopyroxene (eclogite facies) rocks. In the latter a paragenesis Grt_{25-26} + Omp_{29-32} ±

Qtz ± Ru (Table 1.3, no 4, T = 750–790 °C and P = 14.8–15 kbar) and a retrograde metamorphic assemblage Grt^{21-23} + Cpx_{10} + Pl_{20} ± Hbl were established. Oriented quartz lamellae, usually interpreted as an indicator of UHP metamorphism, are characteristic of omphacites. In this case, however, lamellae in omphacites consist not only of quartz but also of amphibole, suggesting that they were produced by retrograde metamorphism as a result of the reaction Omp + H_2O → Amp + Qtz.

There are garnet- and clinopyroxene-omphacite-enriched zones at the margins of the dikes. Retrograde alteration in the zones are more intense, especially in the outermost marginal zone, where biotitization and amphibolization, associated with deformations, are common. The host rocks (Fig. 2.33c, points 5 and 6) are represented by gabbronorites with drusitic structures, which suggests a low degree of their eclogitization in this zone.

The chemical composition of these rocks is illustrated by representative analyses (Table 2.2, nos. 4 and 5). They typically contain low percentages of Ti and #Mg of 0.52–0.53. The Vorotnaya Luda coronitic gabbro is most similar to N-MORB in trace element distribution.

Stop 15. The western part of Vorotnaya Luda Island (Fig. 2.33a, b). This locality is characteristic of a geological relationship between an olivine melanogabbronorite dike and early Mg tholeiite dikes. The melanogabbronorite dike has chilled margins and cross-cutting contacts with the host rocks and cross-cuts symplectitic metagabbro dikes (Fig. 2.33b). The early Mg-tholeiite dikes differ in the orientation and mineral composition. The field observations are unambiguous: the gabbronorite dikes are younger than the metagabbro dikes.

On the way from Stop 15 to Stop 16 the group will see the morphology of metagabbro dikes, a melange complex with varying degrees of disintergration of amphibolites, including varieties with relics of eclogites, and intensity of multiple deformations and a dike showing a tholeiite composition. The morphology of the dike in the southern part differs markedly from that in the northern part, which is in good agreement with the composition of its host rocks. In gneissose granites the dike is rectilinear, and in the zone of disintergrated amphibolites it is deformed. Such a pattern is also characteristic of other dikes of this group.

Stop 16. The western part of Vorotnaya Luda Island (Fig. 2.33a) is located near the western contact of the olivine melanogabbronorite dike (Fig. 2.33c). The group will also see the cross-cutting pattern of the contact between a late tholeiite dike and an olivine gabbronorite dike (Fig. 2.33b, c).

Petrographically, tholeiite metagabbros are garnet–plagioclase-clinopyroxene (high pressure granulite facies) and garnet-clinopyroxene (eclogite facies) rocks. The latter consist of $Grt_{Prp25-26}$ and Omp(Jd_{29-32}) with quartz and rutile (Fig. 2.33c, point 1). The rocks have been subjected to moderate retrograde alterations that gave rise to both clinopyroxene-plagioclase symplectites and monocrystals of clinopyroxene with a reverse zoning from omphacite to diopside and intergranular aggregates of plagioclase. There are garnet- and clinopyroxene-omphacite-enriched zones at the margins of the tholeiitic dike (Fig. 2.33c, points 2–4). Retrograde alteration in the zones is more intense, especially in the ouermost zone, where biotitization and amphibolization, associated with deformations, are common. The host rocks (Fig. 2.33c, points 5 and 6) are represented by gabbronorites with drusitic textures, which suggests a low degree of their eclogitization in this zone.

Stop 17. The central part of Vorotnaya Luda Island (Fig. 2.33a). Here, the group will see the morphological characteristics of early Mg-tholeiite dikes and и their relationship with the host rocks of the Gridino eclogite-bearing complex.

Stop 18. The NW part of Vorotnaya Luda Island (Fig. 2.33a). The group will stop here to see a late tholeiite dike and its relationship with host rocks and early Mg-tholeiite dikes.

Stop 19. The NW part of Vorotnaya Luda Island (Fig. 2.33a). This intersection, together with those discussed earlier (Stop 16), shows clearly that the tholeiite dikes are younger than the gabbronorite dikes. A tholeiite dike, up to 2–3 m in thickness, has been traced for over 400 m in a northeast direction. It extends outside the island, and in its southern part the dike is deformed into a series of lens-shaped bodies spaced widely apart. So, the dike displays a pinch-and-swell structure in some places and separated swells (boudins) in other places.

Gridino village

Gridino village area (Figs. 2.1 B; 2.34). At the eastern end of Gridino, the Neoarchean eclogite-bearing mélange is cut by Paleoproterozoic gabbroid dikes and dike-like bodies, some of which are eclogitized (Slabunov et al., 2008, 2011; Volodichev et al., 2012).

Stop 20. The eastern end of Gridino village (Fig. 2.1). An eclogitized olivine gabbronorite dike on a mainland point (Fig. 2.34, Table 2.2). The central part of the dike is made up of coronitic (drusitic) eclogites – medium-grained rocks, whose mineral composition and structural and textural pattern of the protolith have been best preserved (Zone 1). These magmatic-metamorphic units consist of magmatic cumulus minerals, such as olivines, orthopyroxenes and clinopyroxenes, and completely metamorphosed intercumulus ingredients represented, together with thin omphacitic rims of ortho- and clinopyroxenes, by the eclogitic associations $Grt_{48-49} + Omp_{30-41}$, $Grt_{48-51} + Omp_{38-48} \pm Crn \pm Ky$ formed at temperatures of 765–930 °C and pressures of 15–19 kbar. In central parts of intercumulus space there are associations $Omp_{57} + Pl_{16-19} + Crn$ and $Pl_{40} + Ed + Spl, Spr$.

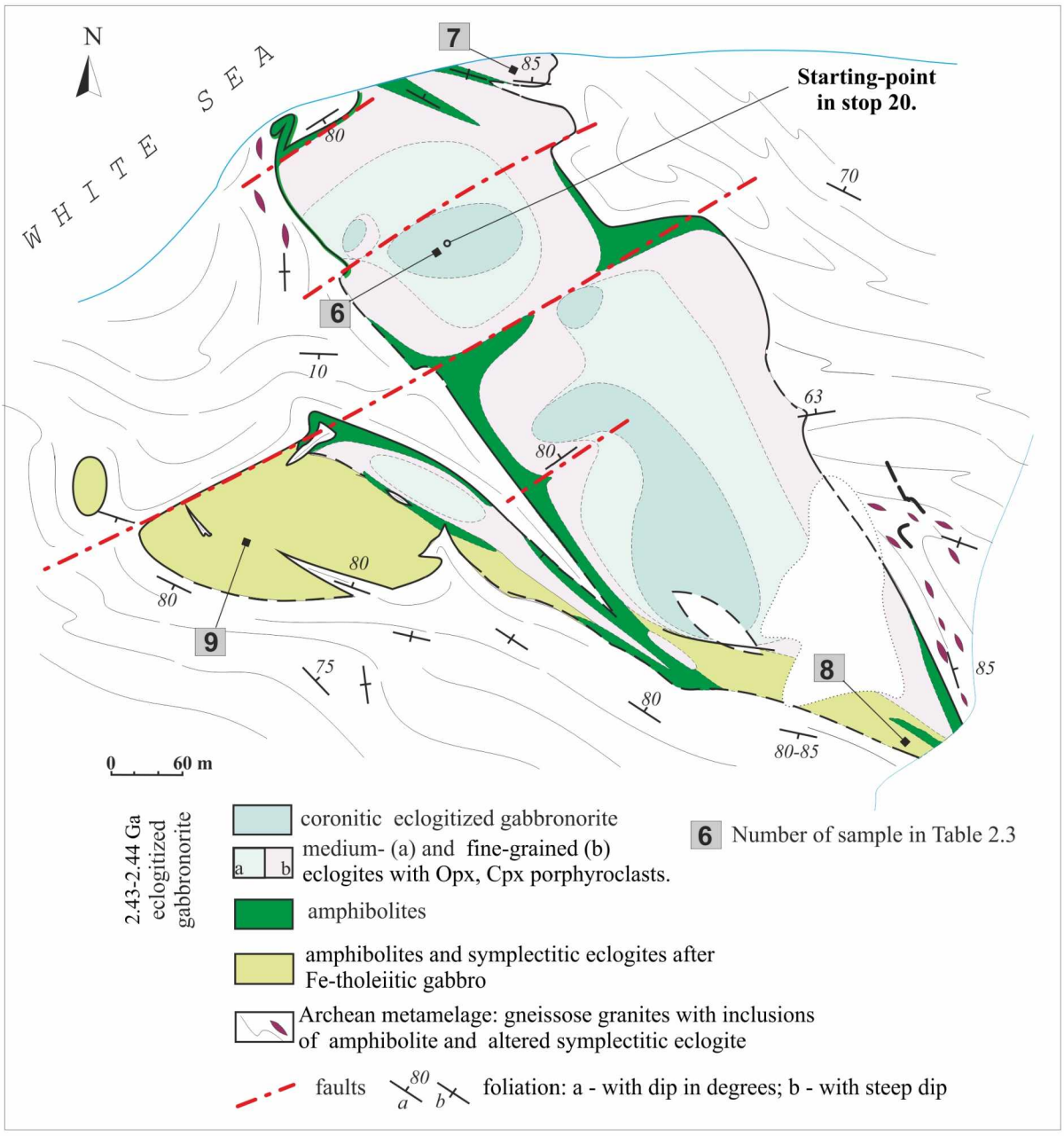

Fig. 2.34. Geological scheme of an eclogitized dike of the 2.4 Ga lherzolite-gabbronorite complex at the eastern end of Gridino (Volodichev et al., 2005, 2012, 2014)

Clinopyroxene in gabbronorite cumulus occurs as diopside (chrome-diopside with percentages of jadeite uncommon for magmatic rocks: 12 % in the grain center to 26 % on the grain margin). The clinopyroxene contains many orthopyroxene-enstatite ingrowths and abundant suboriented lamellar amphibole – edenitic hornblende ingrowths not observed in the rim of this crystal composed of omphacite

that contains up to 41 % Jd. A similar pattern has been formed in an altered orthopyroxene crystal, whose central, unaltered portion contains a lot of very small, suboriented spinel ingrowths and intergrowths with clinopyroxene, similar in composition to omphacite (19 % Jd). Developed after the orthopyroxene is diopside which contains17 % Jd, inclusions or relics of orthopyroxene and, like the crystal described above, abundant suboriented, elongate lenticules (lamellae), pargasitic hornblende which does not occur in the marginal omphacitic rim.

The above evidence suggests that as early as the subsolidus stage gabbronorites were crystallized at increasingly high pressures with involvement of fluids (amphibole lamellae). The magmatic crystallization was followed by a metamorphic stage (eclogitization).

An isotopic age of igneous zircons (Fig. 2.35) from this zone is 2389 ± 25 Ma (Slabunov et al., 2011; Volodichev et al., 2012). Here is a different point of view regarding the age of eclogitized dikes: K. Dokukina (Dokukina et al., 2012a, 2014) considers them as Archean, interpreting early zircon generations as igneous zircons related directly to the formation of gabbronorites, rather than zircons trapped from the host granite gneiss.

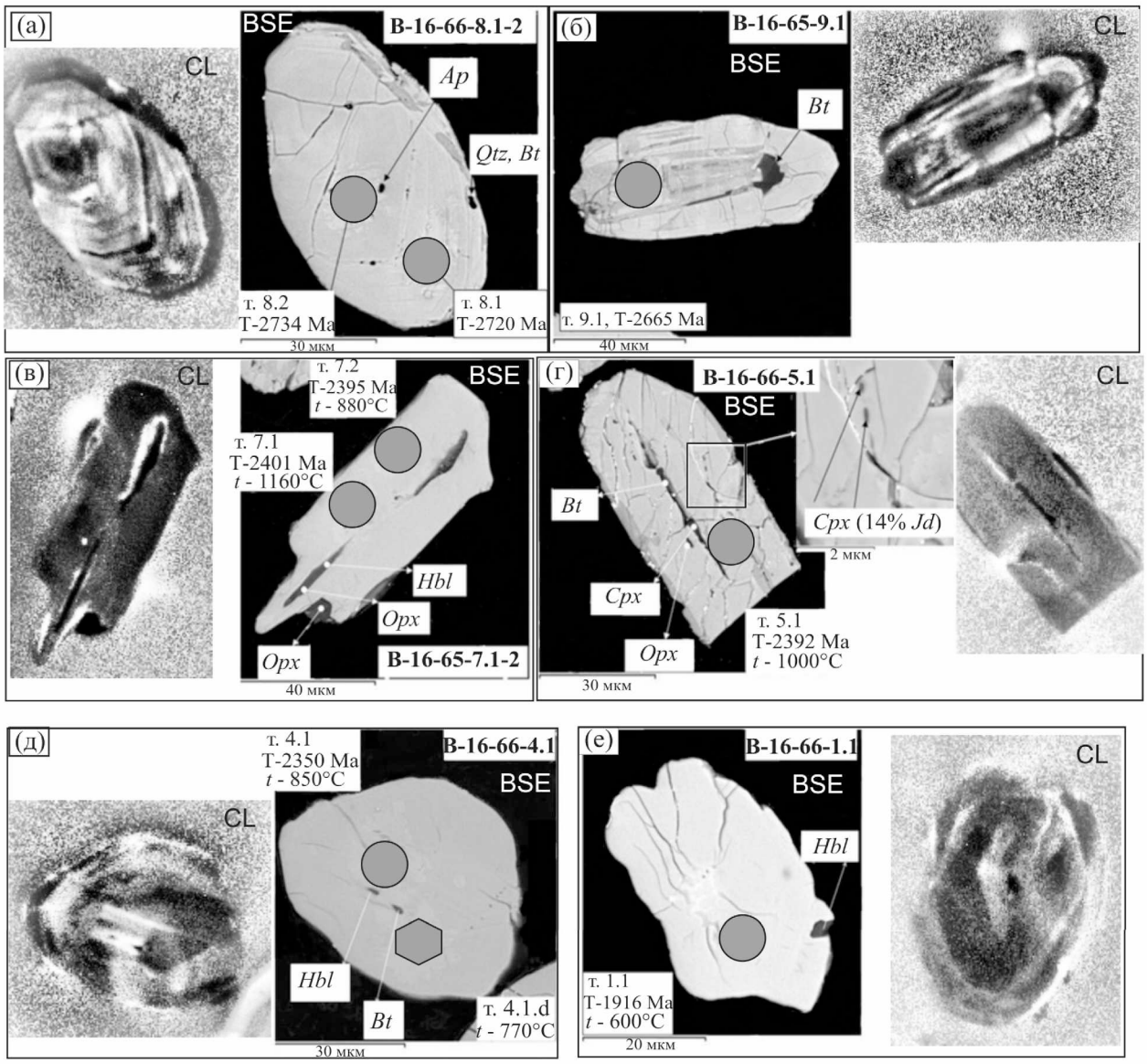

Fig. 2.35. Photographs of zircon crystals in cathodoluminescence (CL) and back-scattered electrons (BSE) with the symbols of mineral inclusions and the places of determination of isotopic ages and rare-earth and rare-element content and with the $^{207}Pb/^{206}Pb$ ages and temperatures of zircon formation:

a–b – Archaean short-prismatic (a) and prismatic (b) xenogenic zircons; c–d – Paleoproterozoic igneous zircons formed at late gabbronorite crystallization stages − 2389 ± 25 Ma (eclogitization probably began at the latest stages); e–f – metamorphic zircons: e – Paleoproterozoic zircon (2350 Ma), presumably an eclogitization stage (?); f – Paleoproterozoic zircon, amphibolite-facies stage (1911 ± 9.5 Ma)

The intermediate zone (2) consists of medium-grained "granulated" eclogites that have already become a largely metamorphic rock composed of garnet, orthopyroxene and omphacite. It contains varying quantities of unequally altered magmatic minerals such as orthopyroxenes and smaller amounts of clinopyroxenes in the form of omphacite-rimmed porphyroblasts that contain 19–22 % Jd, as do granulated mass omphacites. The associations Grt_{44-48} + Omp_{19-22} + Opx show that they were crystallized at temperatures of 715–785 °C and pressures of 12.5–14.0 kbar. Rounded zircons (Fig. 2.35), dated at 2350 Ma, seem to have been formed simultaneously with this paragenesis (Slabunov et al., 2011; Volodichev et al., 2012).

Retrograde alterations in eclogites are indicated by the formation of a regressive zonation in Cpx (21→18→7 % Jd) and in Grt, the formation of the paragenesis Hbl+Pl and, to a lesser degree, the formation of Cpx-Pl symplectites (Volodichev et al., 2008). In sample B-16-66, collected from this zone for a geochronological study, retrograde alterations in eclogites are marked by the occurrence of the associations Grt (44–48 % Prp, 13–18 % Grs) – Cpx (8–12 % Jd) – Hbl ± Opx, Grt (46–47 % Prp, 12–13 % Grs) − Hbl (T = 620–630 °C and P = 8–9 kbar consistent with high pressure amphibolite facies). The zircon age of this gabbronorite alteration stage is estimated at 1911 ± 9.5 Ma (Slabunov et al., 2011).

The marginal zone (3) (Fig. 2.34) is built up by fine-grained, equigranular eclogites with scarce, dominantly orthopyroxene, porphyroclasts. The rock consists of garnet (42–46 % Py), omphacite (18–24 % Jd) and orthopyroxene. Amphibole, which occurs as common, actinolitic and pargasitic hornblende, is present in varying quantities (up to 20–25 %).

The host rocks are represented by Archean amphibolite and biotite gneisses (some are Grt- and Cpx-bearing), repeatedly deformed and metamorphosed granitoids with fragments of amphibolites and intensely transformed Archean eclogites. The P-T metamorphic conditions of host rocks are consistent with amphibolite facies (T = 650–700 °C, P = 6.5–7.0 kbar).

Acknowledgements

We highly appreciate the Russian Foundation for Basic Research for a long-term financial support of our investigation of the Gridino eclogite without which it would have been hardly possible (grants ## 14-05-31137 mol_a and 16-05-01031). This communication has been partly prepared in the framework of research projects of the Kola Science Center of the RAS (#0226-2019-051) and the Karelian Research Center of the RAS (#A18-118020290085).

THE SALMA AND KURU-VAARA AREAS

ECLOGITE AND RELATED ROCK IN THE KOLA PART OF THE BELOMORIAN PROVINCE, FENNOSCANDIAN SHIELD, RUSSIA: WHEN AND HOW DID THEY FORM?

Shchipansky, A.A.[1], *Balagansky, V.V.*[2], *Sidorov, M.Yu.*[2]

[1] Geological Institute of RAS, Pyzhevsky per. 7, 119180, Moscow, Russian Federation
[2] Geological Institute of Kola Scientific Center of RAS, Fersman St., 14, 184209, Apatity, Russian Federation

The first report for a credible existence of HP mineral assemblages over the Kandalaksha Bay area in the Kola region has been published by Pentti Eskola in his classical monograph 'On the eclogite of Norway' (1921), where he wrote: "The rock could, therefore, very well, at some earlier stage, have been an eclogite in which the pyroxene was later converted into feldspar and hornblende, the rutile into titanite, and the garnet alone was preserved as a rutile. A feature in the composition of the garnet would even support this supposition: its lime content which is higher than that met in the average garnets of the amphibolites" (p. 108). It should be noted that he also separated this former eclogite from the 'drusite' (Fedorov, 1896) by using clear petrographic evidence: a lack of magmatic minerals in eclogite, and, conversely, their preservation in drusite, for which he proposed the term 'garnet norite'. Shortly after that, Nikolay Sudovikov (1936) discovered a truly Cpx-Grt assemblage preserved in garnet amphibolites near the Chuna River, about 60 km northwest of Kandalaksha Town. In the late 20th century several reports on eclogite findings in the Belomorian Belt were published by Soviet scholars and summarized by Viktor Glebovitsky (1986), who even proposed to classify the Belomorian Province as an eclogite-gneiss belt.

Anew investigations of high-pressure mineral assemblages in the Kola Peninsula began after the first report on a discovery of eclogite in the Salma localities (Konilov et al., 2005). Nowadays the most detailed studied are three eclogite localities, Uzkaya Salma, Shirokaya Salma, and the Kuru-Vaara quarry which all are the field trip objects (Fig. 3.1). Herein we outline some most important data on their petrology, geochemistry, and the results of age dating to receiving more attention on questionable problems.

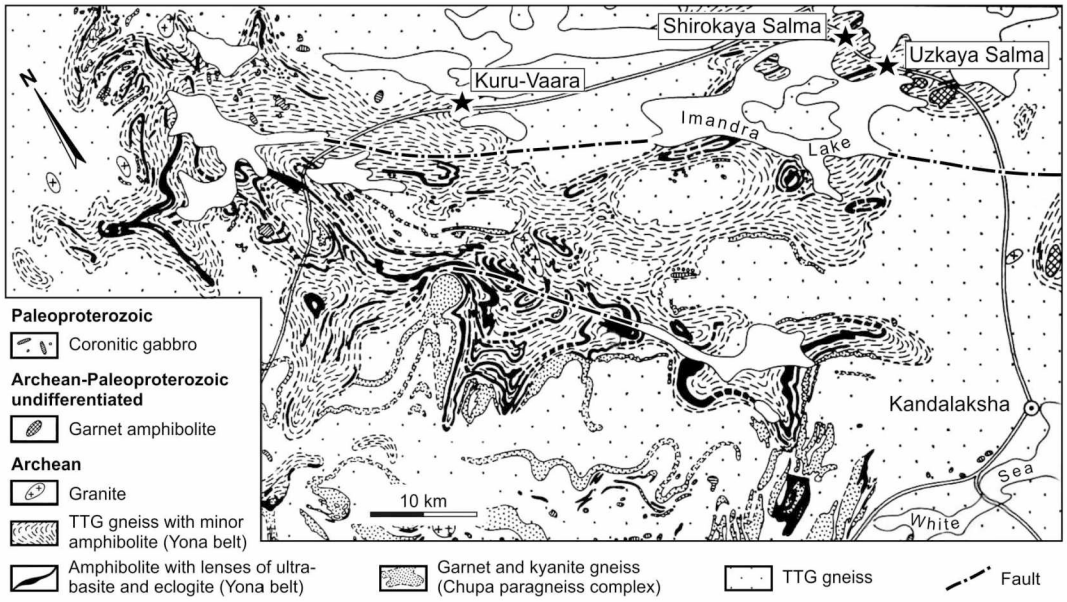

Fig. 3.1. Geological map of the northernmost Belomorian Province, after V. Pozhilenko *in* Mitrophanov et al., (1995)

This field trip aims to make a long field, petrological, geochemical and geochronological studies accessible to a wider audience. We hope also that an acquaintance with the oldest world-wide eclogite occurrences can considerably help to insight deeply into the Early Precambrian geodynamics by omparing with the much better studied eclogites from Phanerozoic fold belts.

Uzkaya Salma locality (32°22.4′ E, 67°28.3′ N)

The Uzkaya Salma eclogitic assemblage is well exposed on a roadside of the federal highway St.-Petersburg–Murmansk. This seems to be part of a large, ~ 500 m thick body which can be traced more than 4 km northeastwards along the Babinskaya Imandra and Ekostrovskaya Imandra lakes. The body is embedded in tonalite-trondhjemite-granodiorite (TTG) gneiss suite referred to here as the late Archean Belomorian gneiss series (Slabunov et al., 2006a, b). As a rule, the Belomorian grey gneisses are sheared and migmatized by later, Neoarchean or Paleoproterozoic granitic leucosomes. The most conserved TTG varieties reveal late Archean Nd model ages of 2.93–2.73 Ga, and show ε_{Nd} values of +2 – +2.3 suggesting their juvenal provenance (Timmerman, Daly, 1995).

There are several detailed publications concerned with the Uzkaya Salma eclogite locality (Mints et al., 2010a, b; Kaulina et al., 2010; Konilov et al., 2011; Li et al., 2017). The published data led to quite distinct implications on its age, and consequently, on its tectonic significance. Mints et al. (2010b) consider the Uzkaya Salma eclogite as a fragment of subducted Mesoarchean oceanic crust which was compositionally being akin to the modern low-rate spreading crust from the southern Indian Ocean. Li et al. (2017) and Yu et al. (2019a, b) advocate its Paleoproterozoic ages due to crustal stacking during the Lapland-Kola collisional orogeny.

Field observation, petrology and mineralogy

Six different high- to moderate-pressure rock types are described herein: (i) strongly retrogressed eclogite, (ii) Fe-Ti eclogitic rock, (iii) *Grt*-bearing amphibole-pyroxene shcist, (iv) kyanite-garnet-biotite plagiogranite, (v) *Grt*-bearing and *Grt*-free amphibolite, and (vi) garnetite (Fig. 3.2). In the vicinity of the Uskaya Salma locality the host Belomorian gneiss is also exposed, but its relationships with the eclogitic exposure are covered by moraine talus.

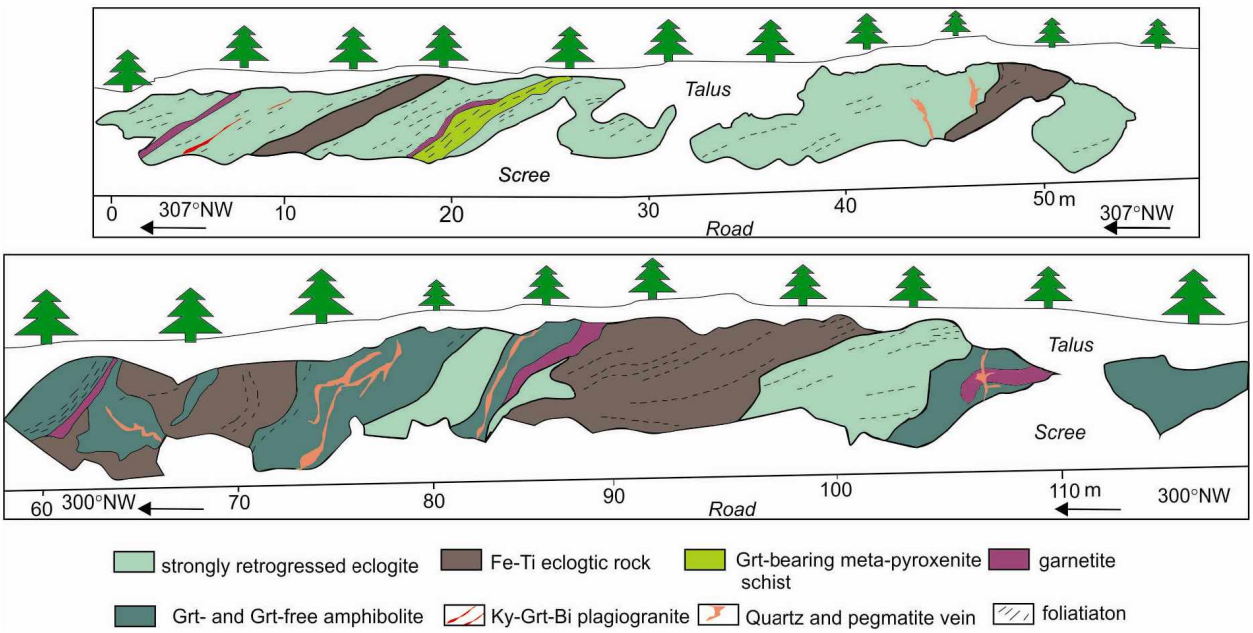

Fig. 3.2. Sketch of the Uskaya Salma eclogite occurrence complied by K. Dokukina, N. Kozlova, and O. Platonova (Mints et al., 2014)

(i) The eclogites have experienced extensive retrogression after the high-pressure metamorphism (Fig. 3.3a). The modal amount of amphibole and plagioclase has increased at the expense of pyroxene and garnet with increasing retrograde transformation. Complete transformation to the garnet-free amphibolite assemblage is found along the margins of the eclogitic mass, adjacent to intruded Paleoproterozoic pegmatite and related quartz veins, and fractures where fluid influx has occurred.

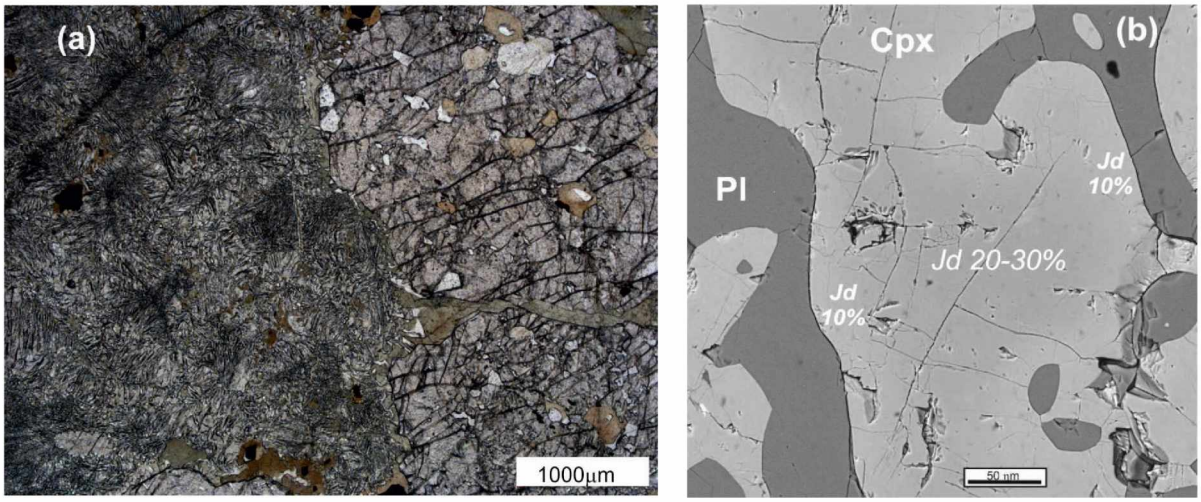

Fig. 3.3. (a) Microphotograph of a retrogressed eclogite, and (b) enlarged BSE image illustrating a relic of omphacite preserved in a symplectite area (Konilov et al., 2011)

Relics of an eclogite-facies metamorphism are very seldom and have been preserved, as a rule, as local grains armored in the symplectitic matrix (Fig. 3.3b). The majority of thin slices observed have demonstrated a complete breakdown of omphacite to *Cpx-Pl* symplectite. Symplectitic diopside intergrown mostly with sodic plagioclase (andesine) in the retrogressed eclogite have X_{Na}–values = 0.05–0.11. In rare instances bytownite, oligoclase and albite have been found in subordinate amounts; occasionally K-feldspar and Ba-bearing feldspar are also detected. In addition to that, coarse orthopyroxene grains (10–20 μm), containing 55–60 mol % of the *En* component, were occasionally found in association with the clinopyroxene-plagioclase symplectite (Li et al., 2017).

All retrogressed eclogite samples are featured by euhedral garnet which may be distinguished into two groups by both their sizes and chemical compositions (Fig. 3.4). The first are larger, 1.5–3 mm across, and reveal relatively more *Prp* but less *Alm* components, while the second are smaller-grained, ~0.5 mm across, and are usually Prp depleted but *Alm* enriched (Li et al., 2017). Furthermore, the both garnet groups display an indirect winding-like chemical zoning that is difficult to explain by a single cycle of HP metamorphism.

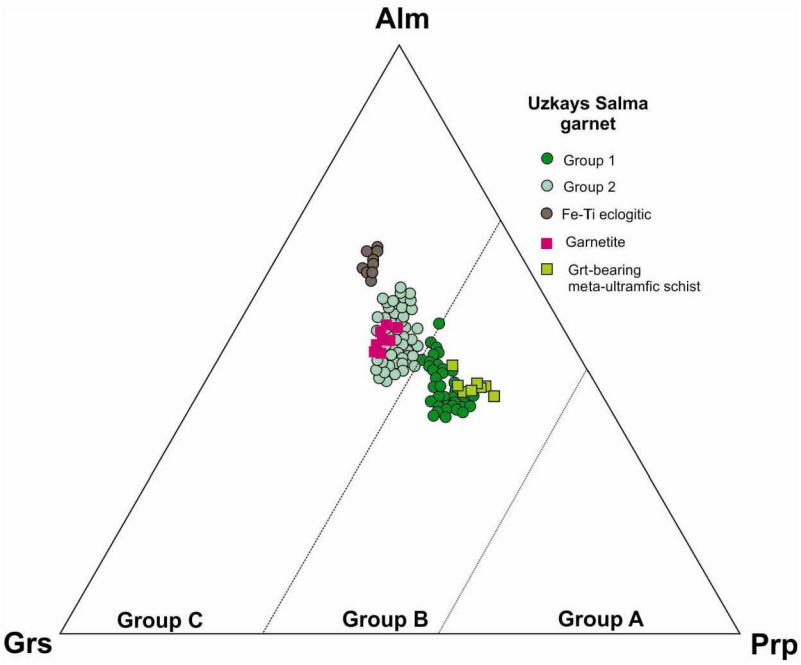

Fig. 3.4. Compositional diagrams of garnet. Data for garnet of group 1 and 2 are from Li et al. (2017). Garnet composition for Fe-Ti eclogitic rocks, ultra-mafic schist, and garnetite are from Konilov et al. (2011) with addition of unpublished analyses

(ii) As compared with the retrogressed eclogite, the Fe-Ti eclogitic rocks are demonstrably

richer in garnet and stand out because of enhanced contents of Fe-Ti oxides, causing the rocks have rusty coloring on their weathered surface. In thin sections, these consist of dominantly fine-grained (about 1 mm across), subhedral to irregular garnet (up to 50–65 % mode) embedded in the matrix phase involving vermicular or finger-like *Cpx-Pl* symplectites (~ 15–25 % mode), amphibole (up to 10–15 % mode), quartz (~5 % mode), and Fe-Ti oxides, mostly rutile and ilmenite (~ 5–8 % mode) with minor secondary chlorite (Fig. 3.5).

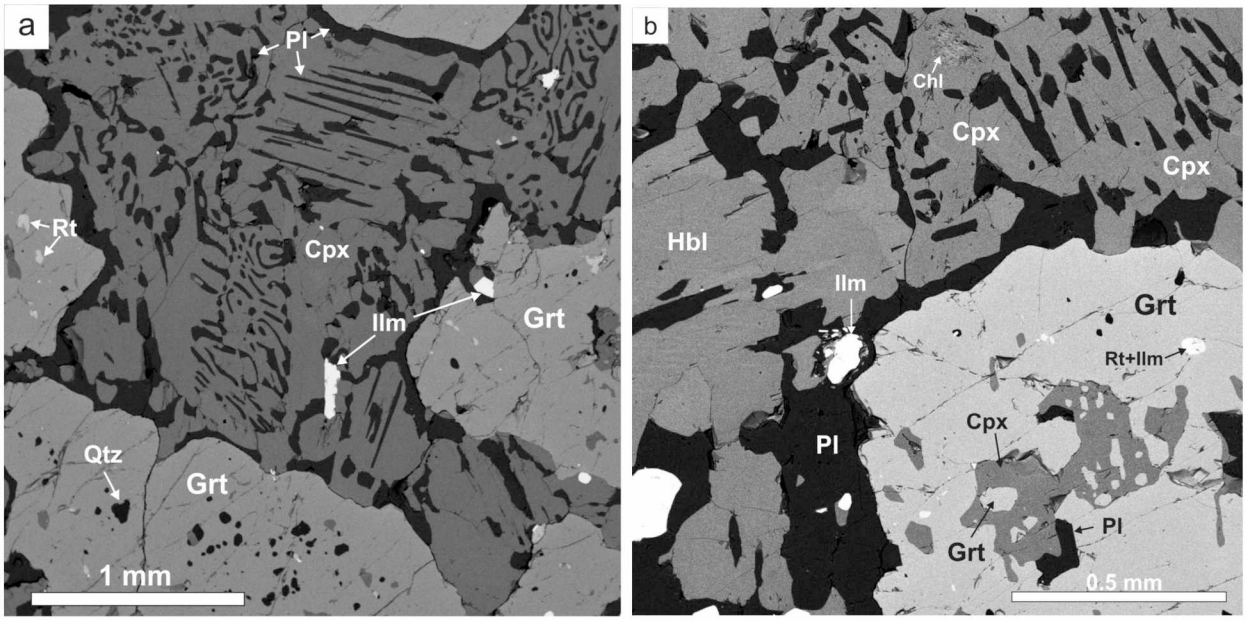

Fig. 3.5. BSE images showing mineral assemblages and textural features of a Fe-Ti eclogitic rock. (a) Coarse-grained vermicular and finger-like diopside-plagioclase symplectite typical of the Fe-Ti eclogite. Subhedral garnets contain many inclusions disseminated throughout the crystals. (b) Relationships between coarse-grained hornblende plagioclase and diopside-plagioclase symplectites. Note that all plagioclases are oligoclase and that clinopyroxene included in garnet is diopside akin in composition to diopside from the matrix (Konilov et al., 2011)

The symplectite commonly occurs as intergarnet areas, in which omphacite is lacking. It is composed of clinopyroxene (X_{Na} = 0.09–0.10), plagioclase, amphibole, with minor polygonal crystals of quartz, and Fe-Ti oxides.

Garnet is dominantly almandine and reveals no distinct compositional zoning, even though abundant garnet grains are strongly resorbed. A compositional range in the garnet is shown in Fig. 3.4. The garnet grains, as a rule, contain many inclusions, which are disseminated throughout the crystals. Quartz ranging in size from 10 to 150 μm is the most common inclusion in garnet. Rutile and ilmenite of size 50–100 μm are also ubiquitous included phases. Commonly, rutile is replaced by ilmenite, resulting in Rt + Ilm intergrowth. The most abundant and large crystals of Fe-Ti oxides occurs within the matrix. These may be as large as 500–700 μm across and are usually represented by ilmenite and magnetite. Several small isolated grains of a low-*Jd* clinopyroxene (up to 200 μm across) were found as inclusions in garnet.

(iii) *Grt*-bearing amphibole-pyroxene schist is dark green colored strongly foliated and altered *Qtz* and *Pl*-free meta-ultramafic rock (Fig. 3.6). It consist mainly of diopside with rare relics of Opx (*En* ~ 70 mol. %). Garnet is a pyrope-almandine-grossular solution with a distinct retrograde zoning (see Fig. 3.4). Minor mineral constituents are high-Al and low-Cr metamorphic spinel, chromian-magnetite, and ilmenite. Late Mg-rich chlorite and rare talc occur mostly along with fissures of schistosity.

(iv) *Ky-Grt-Bi* plagiogranite composes rare light colored veins of 0.1–40 cm thick and a few meters long. Field observations suggest that these fill isolated tension gashes within the eclogite and structurally is no way related to the surrounding TTG gneisses. At contacts between the eclogite and *Ky-Grt-Bi* plagiogranite veins the eclogite is retrograded into a garnet-bearing amphibolite (Fig. 3.7a). In outcrop scale, the veins are largely composed of medium-grained plagioclase and quartz (up to 75–80 vol. %), garnet (up to 10–15 vol. %). A weak foliation observed in the veins is defined by alignment of minor biotite. Most of the garnet crystals tend to be concentrated along with the vein contacts. In hand specimen, a small-sized kyanite is difficult to identifying.

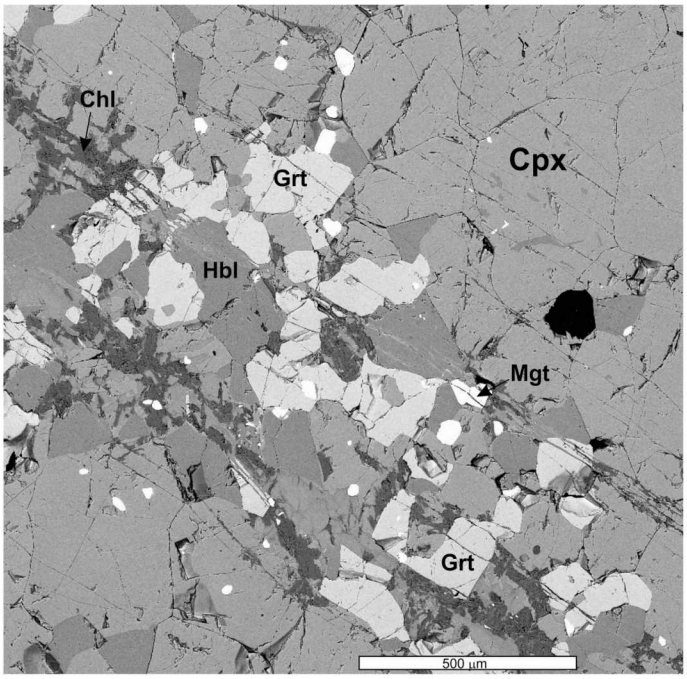

Fig. 3.6. BSE image showing mineral assemblages and textural features of a *Grt*-bearing amphibole-pyroxene schist

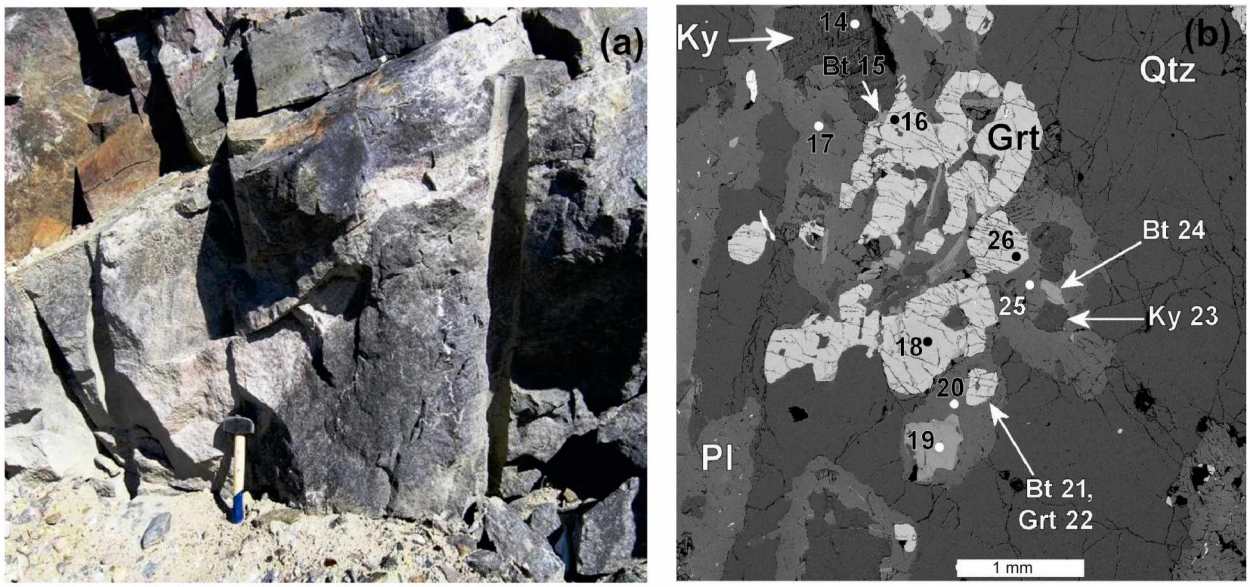

Fig. 3.7. (a) Field photo of a *Ky-Grt-Bi* plagiogranite vein (HP trondhjemite) and (b) BSE image showing its mineral assemblage

In thin section, the rock consists largely of plagioclase and quartz and contains irregular to subhedral porphyroblastic garnet and kyanite, and tabular or lamellar biotite with rutile, and zircon as accessory phases (Fig. 3.7b). Rims of ilmenite over rutile are common. Plagioclase crystals are uniquely andesine in composition but are slightly zoned from core (An_{32}) to rim (An_{39}). Kyanite occurs as isolated irregular or tabular grains of size 0.5–1 mm across. Textural relations indicate that kyanite intergrows with the plagioclase rather than it represents a relic or a late mineral phase. Garnet occurs as 0.2–1.5 mm diameter anhedral to subhedral porphyroblasts and is pyrope- and grossular-rich almandine. A retrograde zoning was observed in garnet rims. The core has an average composition of Alm_{48}–Prp_{28}–Grs_{23}–Sps_8 whereas the rim demonstrates an average composition of Alm_{52}–Prp_{26}–Grs_{21} –Sps_9. Biotite presents as isolated 0.2–0.5 mm long laths or tabular flakes and shows a strong pleochroism (yellowish-brown to dark brown or reddish brown). It is occasionally replaced by a tiny edging of late prehnite. They have Si contents between 2.6 and 2.75 apfu and Mg# between 0.67 and 0.73 that corresponds to high-Mg biotite, or phlogopite.

Both the field observation and perological studies of the Ky-Grt-Bi plagiogranite veins suggest that they could stem from a partial melt of eclogite and trapped at tension gashes that have been forming apparently during the eclogite facies metamorphism. So such Ky-Grt-Bi plagiogranite veins sealed up inside the eclogite bodies can be defined as frozen partial melts of eclogite.

(v-vi) The amphibolite and garnetite are the latest rocks among the Uzkaya Salma metamorphic suite. As can be seen from Fig. 3.2, the garnetite occurrence tends to be close spatially to amphibolite layers implying their genetic relationships. The garnetite consist of garnet (~90 %), hornblende with relics of Cpx-Pl symplectite, quartz, rutile and ilmenite (Fig. 3.8). Garnet is an almandine-grossular-pyrope solid solution (Alm_{46-49}, Grs_{24-29}, Py_{21-23}), and compositionally close to those from rims of the garnet group 2 (see Fig. 3.4).

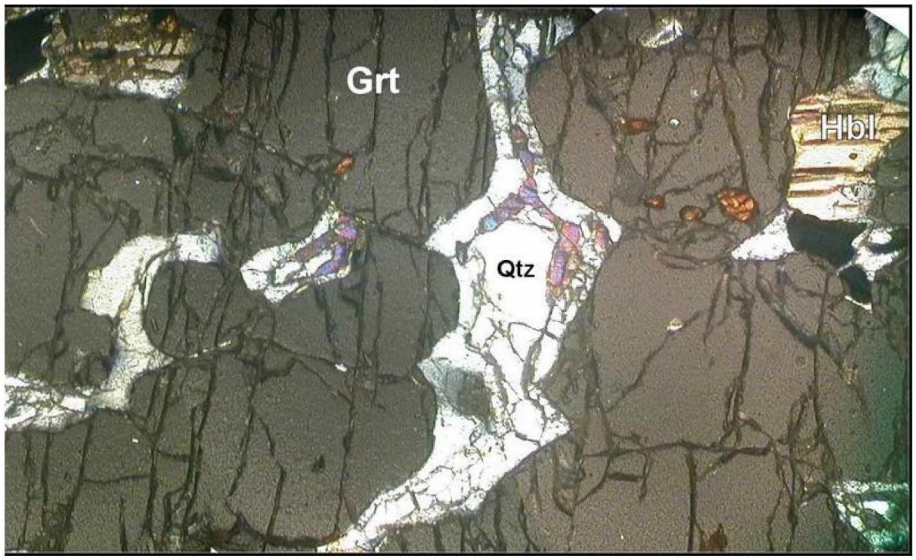

Fig. 3.8. Microphotograph of the garnetite texture

Thermobarometric estimation

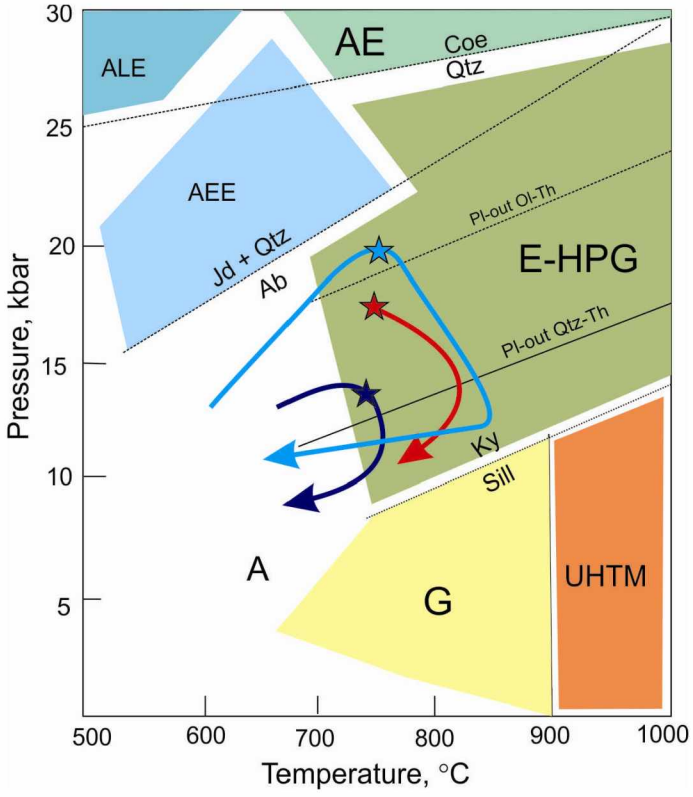

Although the thermobarometric calculations have been realized by different techniques, i.e. pseudosection modeling (Li et al., 2017; Yu et al., 2019b) and combined sets of conventional geothermobarometers (Mints et al., 2010b; Konilov et al., 2011), the peak parameters of the eclogite metamorphism are found to be in agreement to some extent; *P–T* parameters all fall in the field of Eclogite-High-Pressure Granulite metamorphism (O'Brien, Rötzler, 2003). A clear distinction exists between the post-peak trajectories from the published *P–T* paths (Fig. 3.9).

Fig. 3.9. Inferred peaks and *P–T* paths for the Uzkaya Salma eclogite: red star and array (Li et al., 2017); blue star and array (Yu et al., 2019b); deep blue star and array (Konilov et al., 2011). Petrogenetic grid is after (Brown, 2007). Abbreviation: A = Amphibolite facies, G = Granulite facies, AEE = amphibole-epidote eclogite facies, ALE = amphibole-lawsonite eclogite facies, AE = amphibole-eclogite facies; E-HPG = eclogite–high-pressure granulite metamorphism, UHTM = ultrahigh-temperature metamorphic part of the granulite facies

Zircon age dating

The Uzkaya Salma metamorphic rock suite has been dated on zircon by the SIMS and LA ICP-MS techniques. About 200 zircon grains were investigated in order to obtain an age of the eclogite-facies metamorphism which remains open to question so far. Indeed, Mints et al. (2010b) suggest a Mesoarchean age related to a subduction of Archean oceanic crust whereas Li at al. (2017) and Yu et al. (2019b) advocate the Paleoproterozoic age, *ca.* 1.9 Ga, ascribed as a result of the Lapland-Kola orogenic crustal stacking.

A wealth of the zircon dated allow us to construct a probability density plot for U-Pb data from the whole bulk of zircon in order to highlight their provenance with reference to the well-constrained tectonic events in the Belomorian Province (Fig. 3.10).

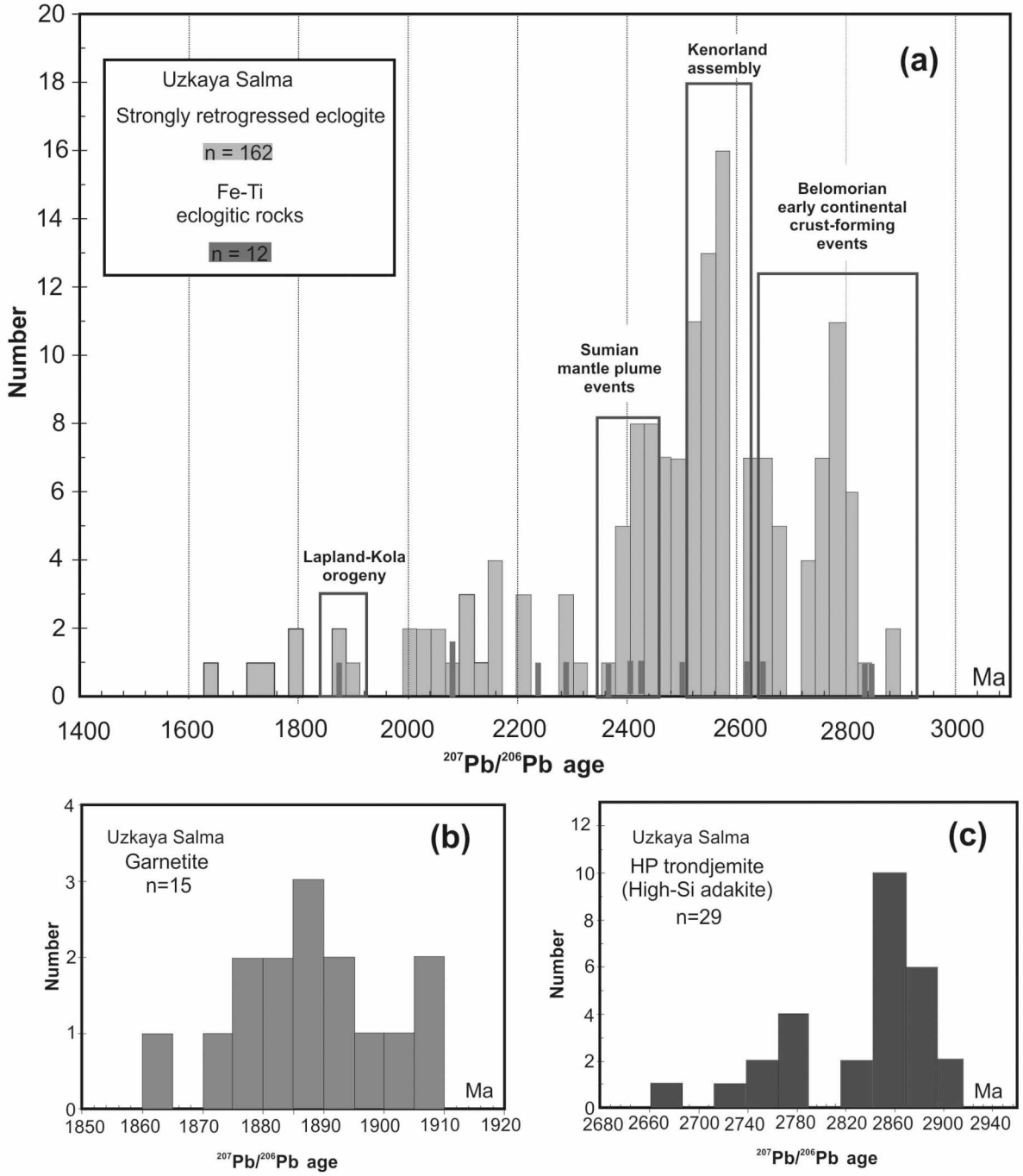

Fig. 3.10. Probability density plot for U-Th-Pb data from zircon picked from the Uzkaya Salma eclogite locality.

(a) Age data for the strongly retrogressed eclogite are from Mints et al. (2010a, b), Kaulina et al. (2010), Li et al. (2017), and Shchipansky (unpubl.). (b–c) Age data for the garnetite (b) and for HP-trodhjemite (c) are from Mints et al. (2010b)

As can be seen from the plot, the majority of isotopic ages obtained correspond to Late Archean tectonic events whereas ages falling in the time interval of the Lapland-Kola orogeny are very subordinate (Fig. 3.10a). Conversely, the Lapland-Kola isotopic ages were yielded by zircon from the garnetite rather than the strongly retrogressed eclogite (Fig. 3.10b). The result of the zircon dating of the *Ky-Grt-Bi* plagiogranite vein is of prime interest for revealing a nature of early crust-forming events in the Belomorian Province. These show only late Archean $^{207}Pb/^{206}Pb$ ages (Fig. 3.10c), and concordant ages for zircon cores yielded an age of 2866 ± 10 Ma (Mints et al., 2010a). This date is one of a few oldest zircon ages reported from the Belomorian Province (cf. Slabunov et al., 2006a, b, 2019), and thus it manifested the beginning of the formation of early continental crust. Noteworthy, the zircon cores contain inclusions of kyanite and rutile suggesting their HP syn-metamorpic origin (mostly under the garnet control) of the *Ky-Grt-Bi* plagiogranite veins.

Geochemistry

Without regard to a rate of retrograde decompositions, the strongly retrogressed eclogites are found to belong to the category of low-K tholeiitic basalts in major element composition. Mg numbers of the eclogites ranging between ~ 0.60 and ~ 0.70 indicate that their magmatic precursors were formed from a near primary upper mantle melt without significant fractionation. The sole exception is provided by a composition of the sample UzS-5 (Li et al., 2017) which displays Mg# of 0.55. Fe-Ti eclogitic rocks have a chemical composition differing drastically from the retrogressed eclogites. As compared to the latter, these are strongly enriched in Fe_2O_3 (~18–21 mass %) and TiO_2 (~1.5 and 2.5 mass %). Their Mg numbers are low, 0.36–0.41, reduced approximately by half as compared to the eclogites. Such a substantial gap in the Mg numbers suggest that the ferruginous eclogitic rocks cannot apparently be interpreted as a metamorphic equivalent derived from any basaltic protolith, such as a strongly fractionated primary mantle melt.

The chondrite normalized REE patterns and the primitive mantle normalized multi-element variation diagrams for the Uzkaya Salma retrogressed eclogite rocks are shown in Fig. 3.11. As can be easily seen, the absolute trace element abundances point toward mantle derivation for magmatic precursors of the samples, but in so doing are lower than those of the modern N-MORB (Fig. 3.11a). This may be due to higher rates of Archean mantle partial melting as compared with the modern upper mantle. It is significant that they display positive Nb anomalies (Nb/Th_N = 1.1–1.7) suggesting that basaltic protholiths of the eclogites did not originate from subduction-related mantle sources, and further still excluding major crustal contamination (Fig. 3.11b).

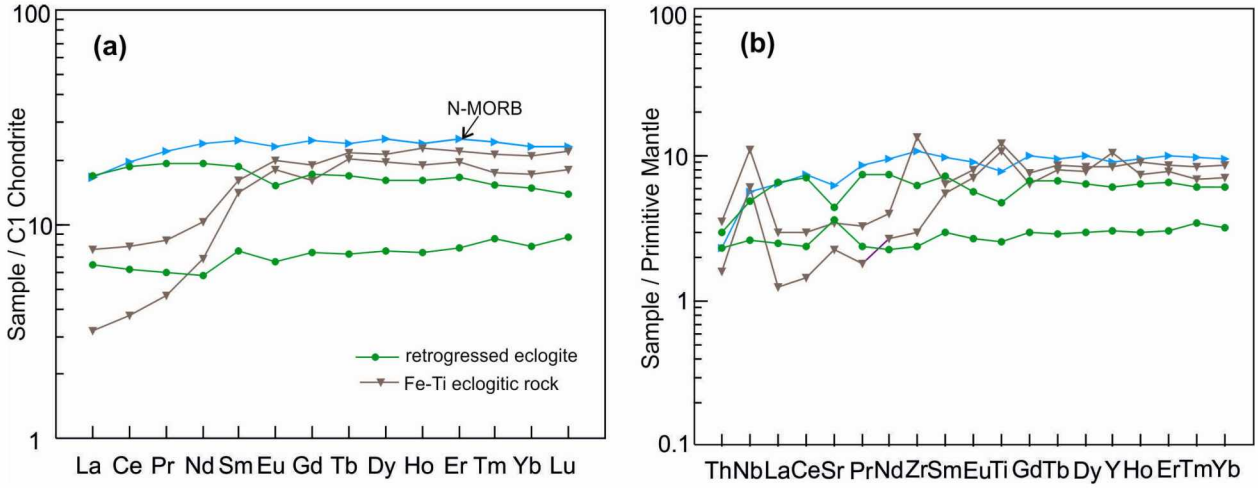

Fig. 3.11. REE patterns (a) and trace-element spidergram (b) for samples from strongly retrogressed eclogite and Fe-Ti eclogitic rocks. Chondrite is herein after Sun and McDonough (1989). Primitive mantle and N-MORB are after Hofmann (1988)

The Fe-Ti eclogitic rocks differ markedly from the retrogressed eclogites in trace element traits. These have regular LREE-depleted and HREE-enriched patterns. Their striking peculiarity is a coupled appearance of large positive HFSE anomalies. The Fe-Ti eclogitic rocks are strongly enriched in Nb (Nb_N/Th_N = 2.4–3.8) that is accompanied by positive Zr and Ti anomalies revealed in the primitive mantle normalized-diagram (see Fig. 3.11b).

Of particular interest is the geochemistry of the *Ky-Grt-Bi* plagiogranite vein. Being clearly occurred within the retrogressed eclogite, this rock bears a clear similarity in chemical composition to the mean Archean TTG as well as to the mean Phanerozoic high-Si adakite which currently is being classified as the HP trondhjemite (Moyen, 2011), or formerly the high-Si adakite (Martin et al., 2005) (Fig. 3.12). Moreover, its geochemistry is in excellent agreement with experimental data on partial melting of N-MORB-type basalt at pressure of 2.0–2.5 GPa rather than with those obtained at pressure of 1 GPa (Xiong, 2006).

In this connection, the Fe-Ti eclogitic rocks are of great interest. To highlight a petrogenetic implication of the Fe-Ti eclogitic rocks we have adopted the Pearce's approach to a case of partial melting of basaltic source, dividing the geochemical pattern into the LHS (partial melting and source composition-dependent behavior) and the RHS (garnet-dependent behavior) parts (Pearce, 2008). As can be seen from the spidergram (Fig. 3.13), a clear complementary balance exists between the TTG rocks and

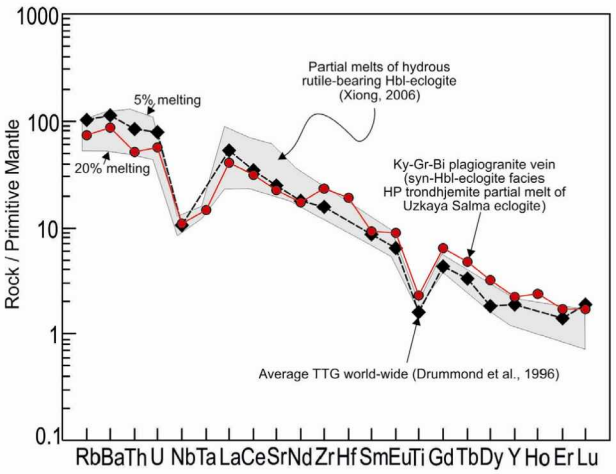

Fig. 3.12. Primitive mantle (Hofmann, 1988) normalized trace element diagram showing a close similarity between experimental melts of hydrous rutile-bearing hornblende eclogite (Xiong, 2006) and the HP trondhjemite from the Uzkaya Salma eclogite. Trace element composition of the average TTG (Drummond et al., 1996) is also shown for a comparison

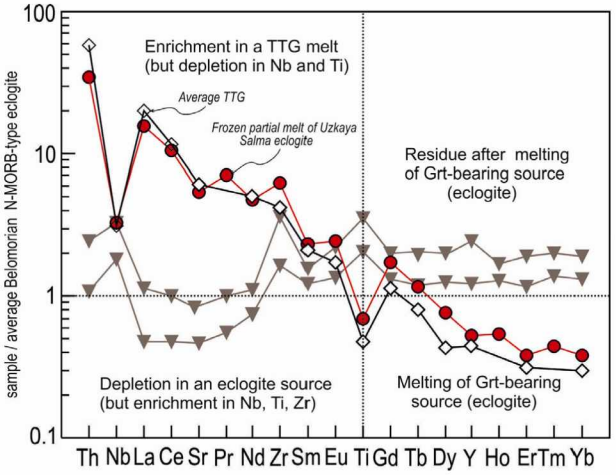

Fig. 3.13. Trace-element spidergram showing a geochemical complementary between the Fe-Ti eclogite rocks and the TTG melts. An averaged Belomorian eclogite (n = 7) is used as the normalized factor. An average TTG is from Drummond et al. (1996)

the ferruginous eclogitic rocks rich in garnet suggesting that the later constitute a Fe-Ti oxides-bearing residuum left from partial melting of the N-MORB-like Belomorian eclogites. Of the high field strength elements, only Zr (Hf) displays an unexpected behavior which is represented by marked positive anomalies. However, high Zr/Sm rations can stem from incompatibility in Zr in residual amphibole (Drummond et al, 1996) thus leading to an appearance of a Zr-oversaturated TTG melt, and consequently zircons together with Fe-Ti oxides and quartz could be precipitated within the eclogitic residue. It is vital also to note that the Fe-Ti eclogitic residue shows very low Sr/Y ratios of 1–1.8 suggesting that partial melting should have been occurred at pressures high enough to destabilize plagioclase, i.e. in the field of hornblende eclogite.

Shirokaya Salma locality (32°22.1′ E, 67°31.3′ N)

The Shirokaya Salma eclogite occurrence is located ~7 km northwards from Uzkaya Salma. This is an abandoned road metal quarry which has disclosed a fragment of a larger eclogite block embedded in migmatized and strongly sheared TTG grey gneiss (Fig. 3.14). From field observations, the eclogites appears to be less weathered as compared with the Uzkaya Salma ones.

There are several detailed publications concerning the Shirokaya Salma eclogite assemblage (Mints et al., 2010b; Kaulina et al., 2010; Konilov et al., 2011; Imayama et al., 2017; Li et al., 2018). The published data led also to quite distinct implications on its age, and consequently, on its tectonic significance. Mints et al. (2010b) considered the Shirokaya Salma eclogite with the framework model of Mesoarchean subduction whereas Imayama et al. (2017) speculated that these could have resulted from the Paleoproterozoic subduction that predated the Lapland-Kola collision. Li et al. (2018) are favorably disposed towards to a model of the Paleoproterozoic crustal collisional stacking.

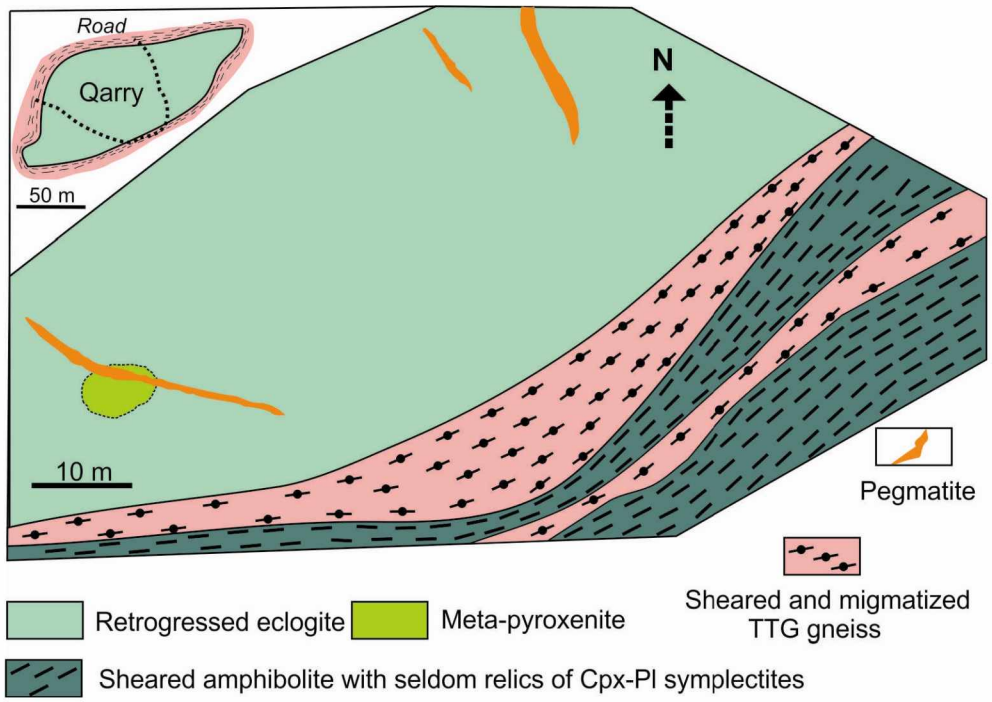

Fig. 3.14. Geological sketch of the Shirokaya Salma eclogite locality compiled by N. Kozlova and O. Planova, with some simplification after Mints et al. (2014)

Field observation, petrology and mineralogy

Apart from eclogitic varieties, the outcropped part of the quarry contains garnet-bearing and garnet free-amphibolites which are largely absorbed the earlier eclogitic mineral associations (Fig. 3.15). A strongly altered meta-pyroxenite body also occurs but its relations with meta-mafic rocks are unclear. Rare late pegmatite dikes cut the eclogite, the related amphibolite and the meta-pyroxenite. Numerous thin sromatic-type leucosome veinlets of trondhjemite compositions are characteristic of eclogitic rocks thus implying that the eclogites were prone to partial melting. The partial melting is also indicated by sporadic occurrences of Fe-Ti-enriched isolated residues throughout the eclogite body.

The most extensive research in the Shirokaya Salma eclogite occurrence has been carried out by Li with co-workers (2018). Based on a rate of preservation, they established three eclogite groups: (i) well preserved (fresh) bimineralic eclogite, (ii) partly retrograded coarse-grained eclogite, and (iii) strongly retrograded symplectitic eclogite. As the rate of preservation of the Shirokaya Salma eclogite is principally governed by its later amphibolization, herein on Figures in text we use a slightly corrected approach.

Fig. 3.15. Field photo illustrating the transformation of a retrogressed eclogite into an amphibolite with a devouring mode

The best preserved eclogite samples are shown in Fig. 3.16. As can be seen, no equilibrium exists between garnet and clinopyroxene. Moreover, this clinopyroxene reveals abundant signs of several back reactions represented by different types of symplectite. However, as a rule, a common mineral assemblage for the most samples is *Grt* + *Cpx(Di)* + *Pl* + *Hbl* + *Qtz* with accessory rutile and zircon. Rutile is often rimmed by ilmenite. Minor opaque phases, apatite, carbonate may be present. Relics of a low-*Jd* omphacite are seldom and may occur as within symplectite-dominated areas and in garnet as well. Isometrical, subhedral garnet grains are normally around 1 mm across but these rarely can be up to 3 mm in diameter. The typical composition of garnet is in the range $Alm_{44\text{-}47}Prp_{33\text{-}34}Grs_{19\text{-}21}Sps_{1}$.

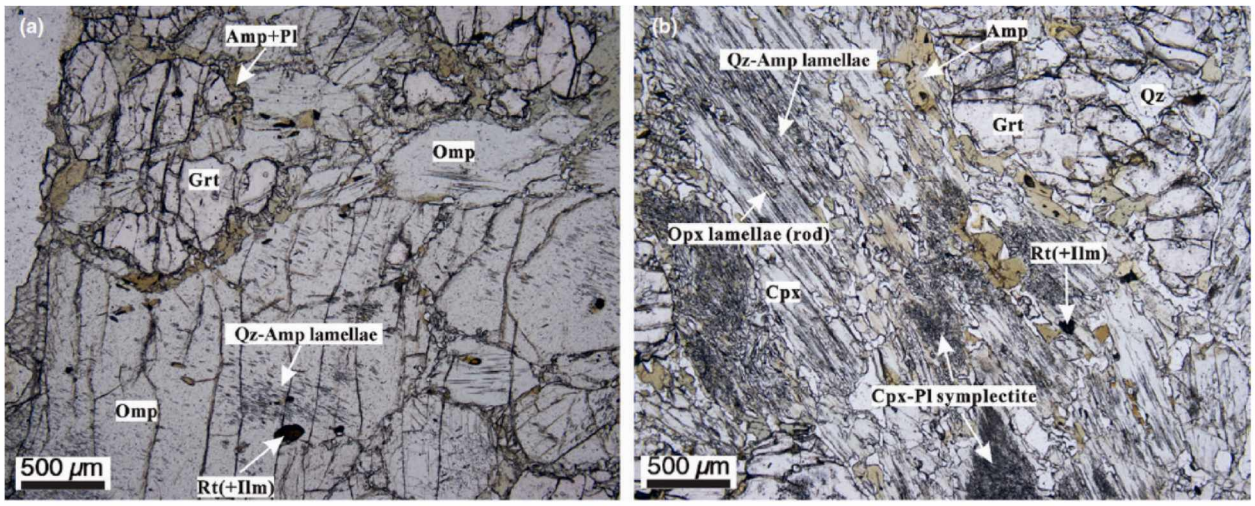

Fig. 3.16. Photomicrographs of the Shirokaya Salma eclogites: (a) least retrogressed eclogite and (b) moderately retrograded eclogite; after Li et al. (2018)

In less retrograded samples, omphacite (up to ~Jd_{30}) occurs in different proportions (~10–30 vol. %) but a low-*Jd* diopside are more widespread (Fig. 3.17). Beside rarely preserved matrix omphacite, Li et al. (2018) distinguished three types of HP *Cpx* breakdown: (i) clinopyroxene containing quartz/quartz–amphibole lamellae, (ii) clinopyroxene containing superfine needle-shaped orthopyroxene lamellae, and (iii) symplectitic to vermicular (plagioclase-bearing) clinopyroxene. Type I possesses the highest jadeite concentrations, while type II has the highest edenite and Ca-Tschermak contents; type III has the highest Ca-Eskola component but very low jadeite abundances. In the symplectitic clinopyroxene (diopside), both CaEs and *Jd* proportions are usually very low, 1–4 mol. % and 8– 11 mol. %, respectively, whereas after the reintegration procedures, they may reach up to 5–14 mol. % and 25–30 mol. %, respectively.

Garnet is commonly an almandine–pyrope–grossular solid solution. Garnet in the fresh eclogite features low grossular (Xgrs = 0.09–0.20) but moderate-high pyrope (Xprp = 0.31–0.39), whereas the garnet from the retrograded eclogite samples has different pyrope contents from (Xprp = 0.39–0.45, Xgrs = 0.16–0.22) to (Xprp = 0.29–0.37, Xgrs = 0.17–0.24). Generally, there is no clear compositional zonation in garnet grains, although a subtle decrease of the pyrope component is occasionally noticed at their rims (Fig. 3.18).

Plagioclase is predominately oligoclase–andesine (*Ab* = 68–87 mol. %). Three types of plagioclase occurrences can be distinguished: (1) kelyphitic type, forming coronas (with amphibole) around garnet. (2) lamellae-like type, forming (oriented) stout rods in clinopyroxene, often in association with orthopyroxene, and (3) symplectitic type, forming vermicular aggregates with clinopyroxene.

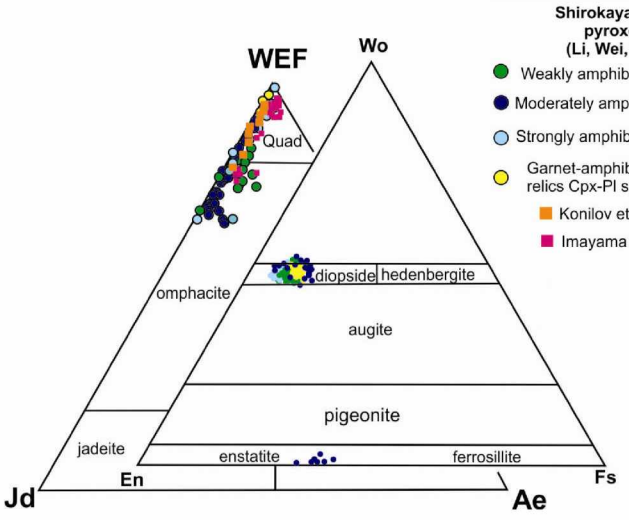

Fig. 3.17. Compositional diagrams of pyroxene

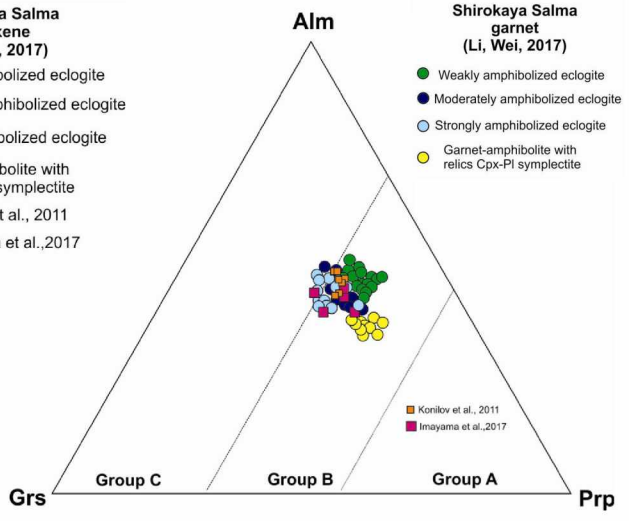

Fig. 3.18. Compositional diagram of garnet

Amphibole occurs mostly as interstitial veinlets or replacement of clinopyroxene. Some also forms composite lamellae (with quartz) in clinopyroxene. Four textural types of amphibole can be distinguished as follows: (1) inclusions in garnet, (2) kelyphitic corona with plagioclase around garnet, (3) lamellae with quartz in clinopyroxene and (4) in the matrix with interstitial occurrence and epitaxial formation. All amphiboles within garnets and the matrix plot within the compositional field of pargasite-edenite.

Thermobarometric estimation

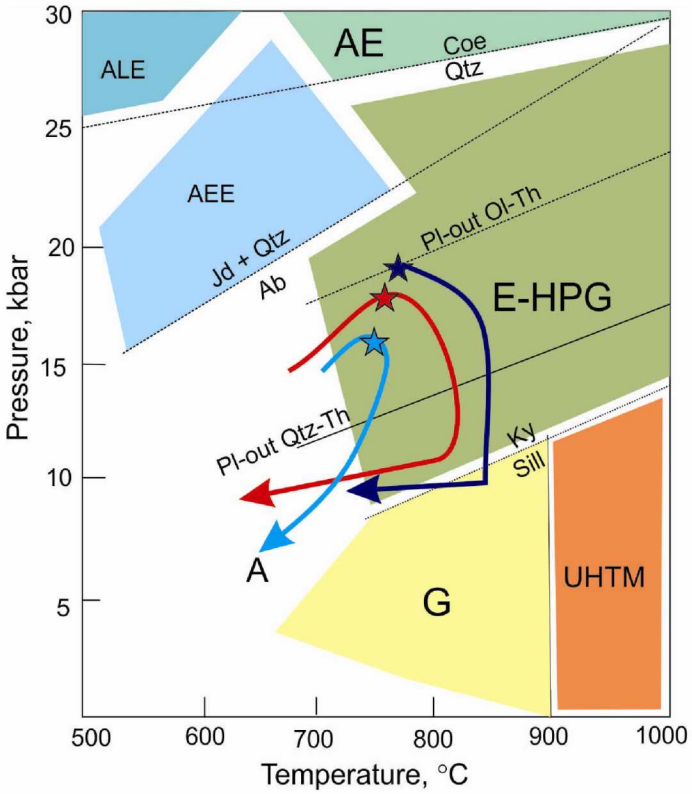

All published estimations for an inferred peak of the eclogite metamorphism correspond to the E-HPG field, even if these show some distinctions (Fig. 3.19). A clear difference exists between the post-peak trajectories that are due to a finding of *Opx*-bearing assemblages by Li et al. (2018) and Imayama et al. (2017) in comparison with an earlier work by Konilov et al. (2011).

It is vital to note that *P–T* paths involving the post-eclogite granulitization are explained in the both publications by a fast exhumation of the eclogite from deep, hotter to upper, colder crustal levels. Furthermore, the following part of the *P–T* paths includes isobaric cooling that is, as well-known, a process with a very slow cool rate, and consequently it should have been going for many tens billion years (cf. Fig. 3.9).

Fig. 3.19. Inferred peaks and *P-T* paths for Uzkaya Salma eclogite: red star and array (Imayama et al., 2017); dark blue star and array (Li et al., 2018); blue star and array (Konilov et al., 2011)

Zircon age dating

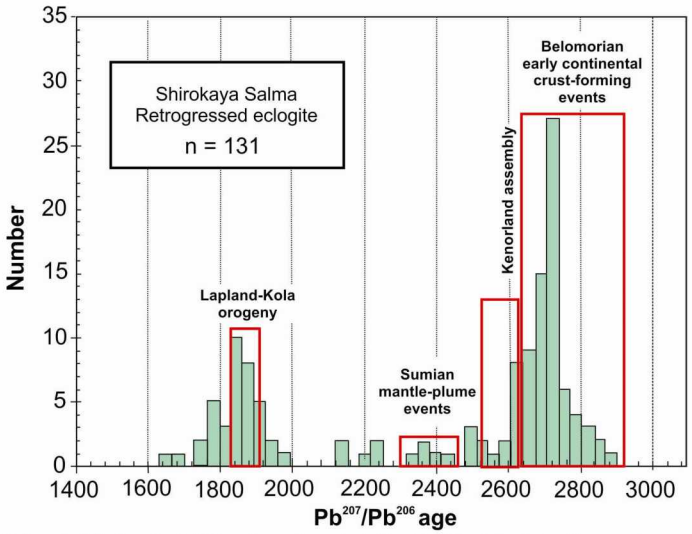

Fig. 3.20. Probability density plot for U-Th-Pb data from zircon picked from the Shirokaya Salma eclogite locality.
Data used are from: Mints et al. (2010), Kaulina et al. (2010), and Imayama et al. (2017)

Results of zircon dating from the Shirokaya Salma area were published in several articles (Mints et al., 2010b, 2015; Kaulina et al., 2010; Konilov et al., 2011), and more recently by Imayama et al. (2017). 131 dating points of zircon were reported in the aggregate. The results are shown on a probability density plot (Fig. 3.20). As evident from the plot, the majority of isotopic ages obtained correspond to Meso-Neoarchean tectonic events while the Lapland-Kola orogenic reworking is also revealed by the ages. Based on a single finding of omphacite inclusion in a rim of zircon dated at *ca.* 1.87 Ga ago Imayama et al. (2017) have suggested that this date corresponds to the peak of the HP eclogite metamorphism. However, earlier Kaulina et al. (2010) depicted within a similar zircon rim

inclusions of *Pl* (An_{56}), *Ep*, and *Cpx* (Jd_5) with *Pl* (An_{30}) ascribing the crystallization of such a kind of Paleoproterozoic zircon to final stages of an eclogite decompression path. Coupled together with inclusions of *Qtz*, *Grt*, and *Hbl* discovered in zircon rims (Imayama et al., 2017), it testifies that the late zircon rims originated in the course of a decompression stage rather than during the peak metamorphism.

Geochemistry

Eclogite-hosting grey gneisses represent the TTG suite typical of those from grey gneisses terrains worldwide.

The least retrogressed eclogite samples bear the major element composition in keeping with a low-K tholeiite basalt. As compared with the modern N-MORB, they are richer in magnesium revealing Mg numbers ranging between ~ 0.58 and ~ 0.62. Their off-arc affinity is clearly outlined by the trace-element abundances as compared with the averaged N-MORB composition (Fig. 3.21). As seen from Figure 3.21 the least retrogressed eclogite samples display significant positive Nb anomalies; their Nb_N/Th_N ratios are in range of 1.8 to 2.3 indicative of melts uncontaminated by crustal material or subduction input (Jochum et al., 1991).

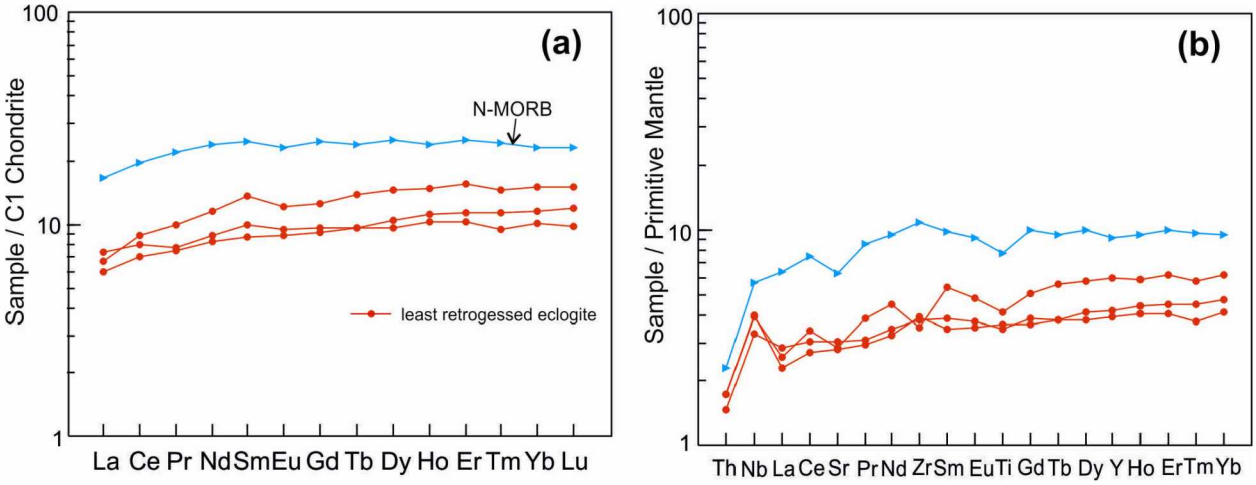

Fig. 3.21. REE patterns (a) and trace-element spidergram (b) for samples from the least retrogressed eclogite. Chondrite is after Sun and McDonough (1989). Primitive mantle and N-MORB are after Hofmann (1988)

It is important to keep in mind that the oceanic geochemical affinity only emerges in the least retrogressed eclogites. Some eclogitic samples display an appearance of trace element behavior characteristic of an island arc tholeiite provenance. This could have been resulted from two different processes. The first involves incipient melting which is undistinguishable with the naked eye. This led to the manifestation of a LREE enriched pattern and negative Nb, Sr, Zr, and Ti anomalies. On the other hand, even with incipient melting an eclogitic residue could have just originated as clearly corroborated by complimentary REE and multi-elementary patterns (Fig. 3.22a–b). The second apparently depends upon a rate of late alterations. Fig. 22c–d illustrates a generation of arc signatures for an eclogite protolith of MORB affinity depending on prolonged retrogression from the eclogite- to the amphibolite-facies conditions by the case study from the Shirokaya Salma samples. In the limiting case when the eclogite was completely transformed into an amphibolite, the REE patterns have been changed drastically while two samples of the eclogite show no evidence for any REE behavior change (Fig. 3.22c). But the multi-elementary patterns mark the appearance of sensible changes revealing negative Nb and Ti anomalies indicative of arc-related or crustal contaminated melts, which they are not (Fig. 3.22d). In fact, this clearly demonstrates that the retrogression of the eclogites proceeded in an open isotope-geochemical system during an exhumation-related overprinting. Hence using mineral isochrons and even zircon dating to constraint an age of eclogite metamorphism is bound to be applied with caution because the Belomorian eclogites were obviously repeatedly re-equilibrated via fluid-induced element transfer under retrograde *P–T* conditions.

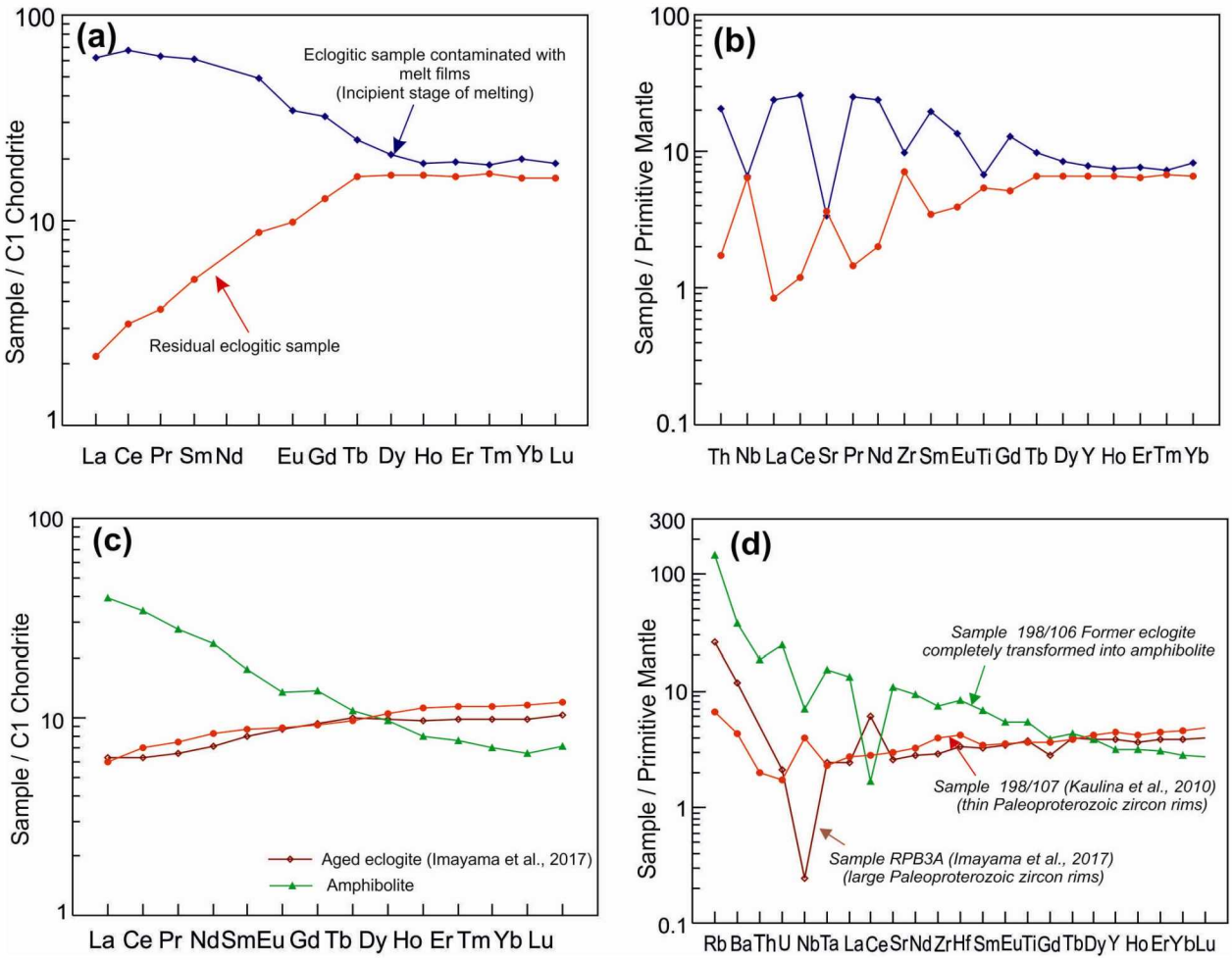

Fig. 3.22. Change in geochemical behaviors in the eclogite samples depending on their melting (a–b), and rate of their late alteration (c–d). See text for explanation

Kuru-Vaara quarry

The section of the Kuru-Vaara quarry is of crucial importance for elucidating the architecture and nature of the early continental crust, at least, for substantial part of the Belomorian Province. The quarry, where ceramic pegmatites are currently mined, is the totally outcropped portion of the Belomorian crust up to 1200 m across its strike and to a depth of ~ 100 m. Its eight benches are oriented along the strike (~330°) of commercial pegmatite veins of 5–6 m in the average thickness; the veins dip northeastwards at 40–60°. Such a kind of the rock exposure has allowed geological investigations to determine relative age relationships between various metamorphic and igneous lithologies.

Great interest has been expressed by many geologists owing to our discovery of numerous relic eclogite bodies scattered throughout the quarry. All these are embedded in TTG gneisses as meta-mafic blocks consisting mainly of *Grt*-bearing or *Grt*-free amphibolites in which relic eclogite-facies mineral assemblages have been occasionally preserved. A structural design of this rock association can be defined as a block-in-matrix fabric characteristic of a tectonic mélange zone where the matrix is composed of TTG gneisses. To highlight the well-known genetic relationship between the eclogites and TTG melts we classify this structure as an 'eclogite-TTG gneiss' mélange (Fig. 3.23). We have identified more that 50 blocks of former eclogite with relic HP mineral assemblages. These form small bodies (1–3 m across) which typically have lens- or boudin-shaped morphology and are concordant with deformational fabrics of the host gneisses.

By now several articles devoted to the Kuru-Vaara eclogitic rocks have been published. Most of them centers exclusively on the petrology and radiometric age dating of case samples studied (Skublov et al., 2010, 2011b; Herwartz et al., 2012; Mel'nik et al., 2013; Mel'nik, 2015; Liu et al., 2017). All these investigators advocate a Paleoproterozoic age of *ca.* 1.9 Ga for the peak eclogite metamorphism.

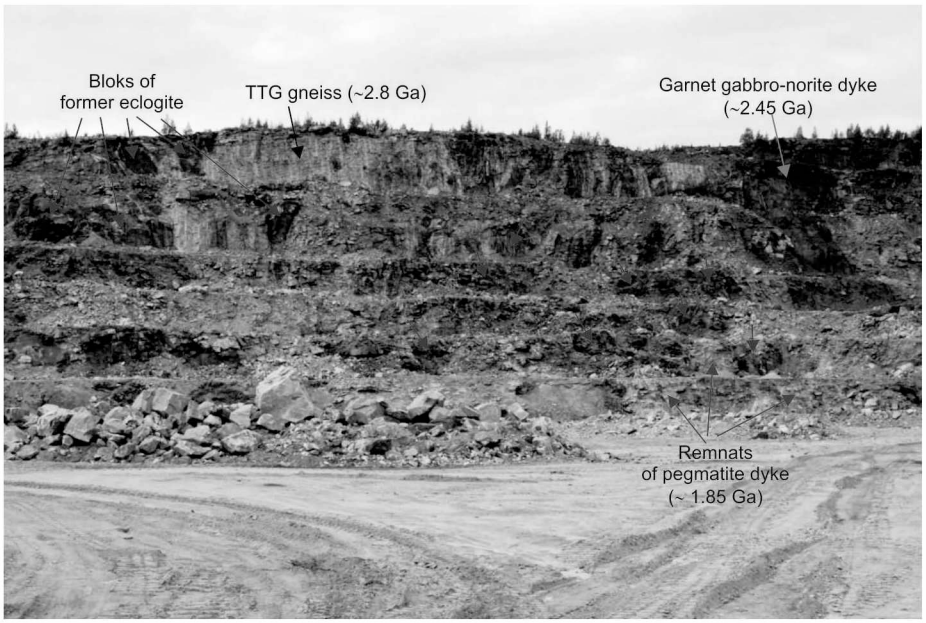

Fig 3.23. Field photo illustrating a structural design of the southern Kuru-Vaara quarry

However, the geological framework of the quarry and geochemical affinities of eclogitic and related rocks can best be appreciated from (Shchipansky et al, 2012 a, b; Balagansky et al., 2015). The detailed field observations and crucial bracketing ages obtained suggest the formation of the eclogite-TTG mélange in the Archean rather than the Paleoproterozoic.

Short geological outline

The study area is composed of TTG gneisses, amphibolites (many contain relics of eclogites), a coronitic/garnet gabbro–norite dike, and abundant ceramic pegmatite (Fig. 3.24). A single block of alumina-rich paragneiss occur in the northernmost part of the quarry. Rare meta-ultramafic lithologies have also been recognized. Apart the Early Precambrian rocks, several thin Devonian olivine melilitite dikes occur.

It can be subdivided into northwestern and southeastern domains which are separated by the Central Shear Zone (Balagansky et al., 2015). In the southeastern domain most of the TTG gneisses and amphibolites have been strongly and repeatedly folded, boudinaged, and migmatized. In this case, metatexite and diatexite are common. In contrast, in the northwestern domain, most of the TTG gneisses are sheared, display prominent stretching lineations, and contain microcline porphyroblasts. Southern-type and northern-type eclogites occur in the northwestern and southeastern domains, respectively (Shchipansky et al., 2012a, b). Gabbro–amphibolites without indications of relic eclogite assemblage occur in the northwestern domain.

The TTG gneisses are peraluminous (A/CNK index = 1.1–1.27), have Al_2O_3 contents of 13.7 to 17.4 wt.% (Mg# = 0.40–0.65 and $La_N/Yb_N > 10$), and are classified as calc-alkalic magnesian granitoid. A magmatic zircon from a HP-trondhjemitic gneiss yielded an age of 2805 ± 11 Ma (U–Pb SIMS; Shchipansky et al. 2012b), which coincides with the ages of similar TTG gneisses in the northern Belomorian Province. Metatexite and diatexite are common in these rocks.

Two main types of meta-mafic rocks occur in the quarry: (i) amphibolite with relic eclogitic mineral assemblages (former eclogite), and (ii) locally gabbro-textured amphibolite.

(i) The first are often intensively foliated, boudinaged, and migmatized. They occur, as a rule, concordantly with the foliated host gneiss (Fig. 3.25a).

(ii) The second are almost non-migmatized and moderately foliated (Fig. 3.25b). Metatexite and diatexite can be distinguished in the type 1 amphibolites. The size of the bodies varies from tens of meters to several hundred meters. Although the amphibolites were experienced largely strong ductile deformations, they do preserve occasionally structural indications for their provenance as intrusions into the TTG frame. Because of this, we have combined the amphibolite bodies of this type into the group of post-eclogite intrusions which remain undated yet.

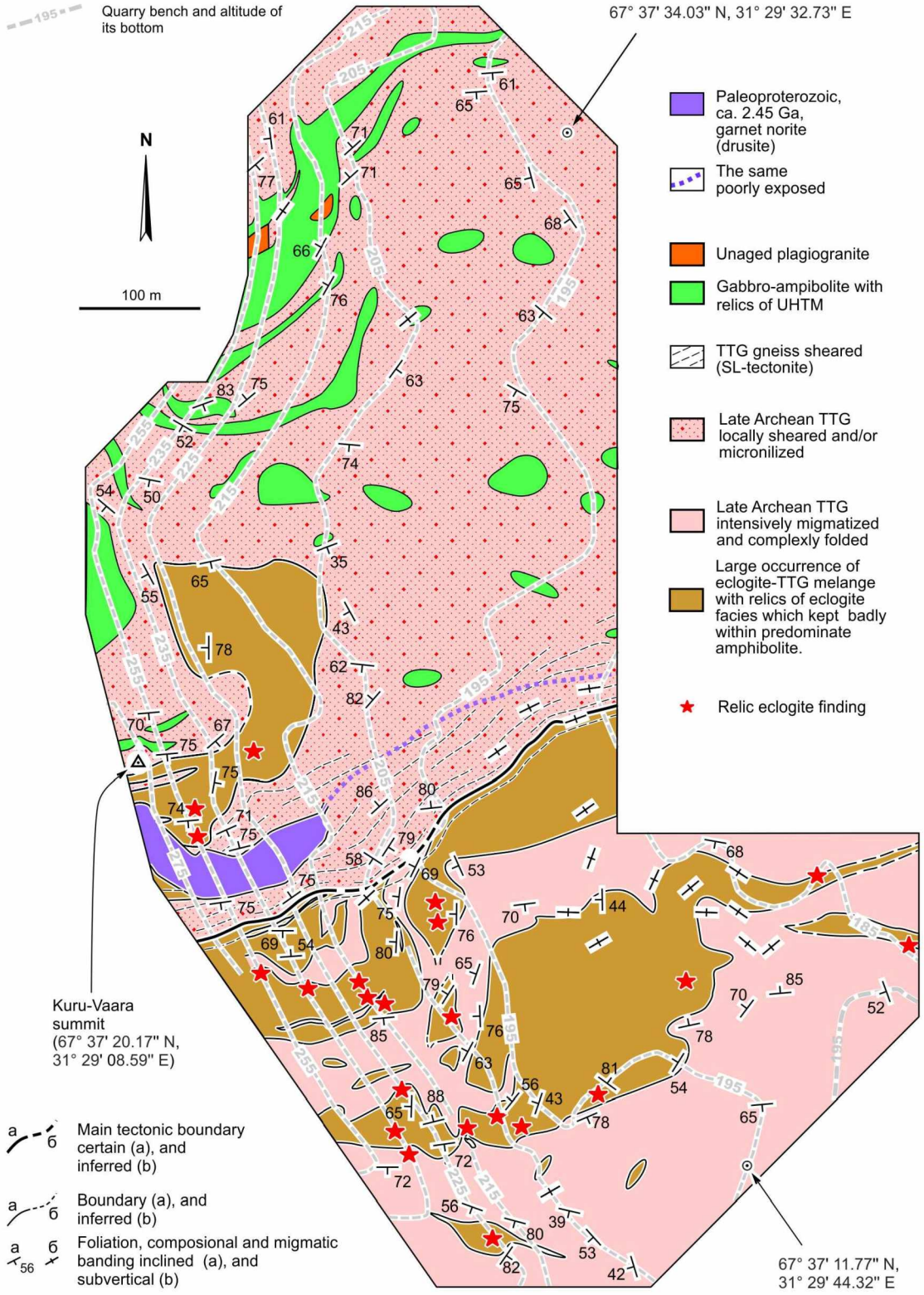

Fig. 3.24. Geological map of the Kuru-Vaara quarry (Balagansky et al., 2015)

The coronitic/garnet gabbronorite dike cuts the TTG gneisses and the amphibolites in the Central Shear Zone. The thickest part of the dike preserves chilled margins in some places. Its internal domains consist of amphibolized medium-grained gabbronorites with locally preserved igneous minerals, such as orthopyroxene (X_{Mg} = 0.86), which contains inclusions of olivine (Fo_{83}) with Cr-spinel (Cr# = 66), clinopyroxene (Fig. 3.26a). Brownish plagioclase (bytownite) is the latest igneous mineral. The internal domains contain up to 7 % olivine. Biotite is a subordinate mineral. Accessories include ilmenite,

sulphides, zircon, and baddeleyite (Fig. 3.26b). The reaction coronas around olivine reveal a multi-zonal texture. The inner zone consists of a prismatic grain of secondary Opx (X_{Mg} = 0.86). The intermediate zone is made up of *Grt-Hbl* symplectite (Fig. 26d). The outer zone shows up as merely edenite with spinel inclusion. The SIMS dating of magmatic zircon from the gabbronorite dike yielded an age of 2443 ± 22 Ma (Mel'nik, 2015) that seems to be a bracketing age for the older eclogite-TTG mélange.

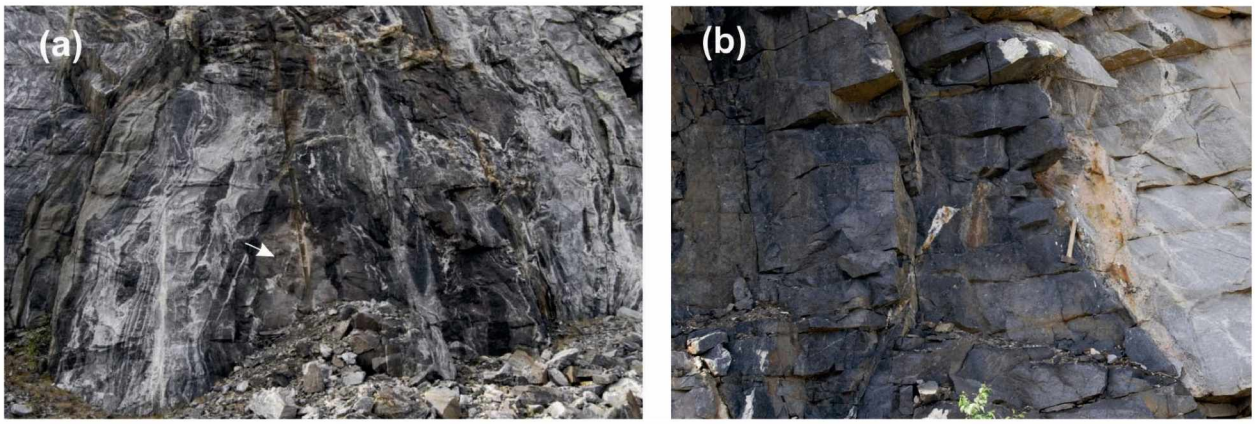

Fig. 3.25. Field photos demonstrating two types of the meta-mafic rocks: (a) block containing relic eclogitic assemblage; (b) eclogite-free amphibolite block

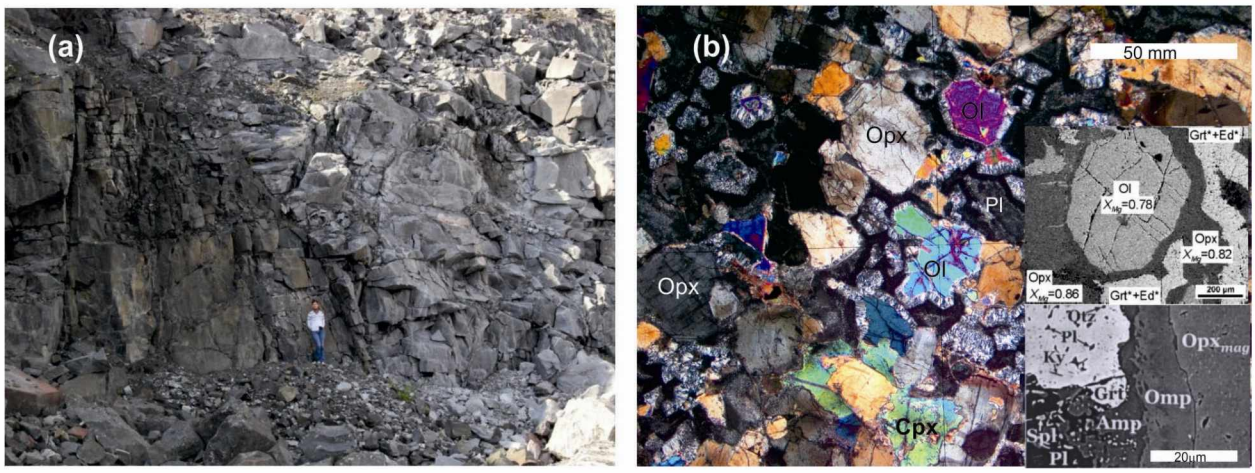

Fig. 3.26. Garnet/coronitic gabbronorite dike: (a) field photo illustrating its structural relationship with the country TTG gneiss and (b) microphotograph displaying the textural feature of the coronitic gabbronorite; magmatic minerals are indicated by symbols. Insets in the right lower part of Figure outline the common coronitic mineralogy (upper box, after Balagansky et al. (2015)) and the tiniest and rarely observed halo of omphacite (*Jd* = 25–30 mol. %) (lower box, after Mel'nik (2015))

A high-alumina paragneiss block is composed of garnet, biotite, kyanite, cordierite, plagioclase, and quartz; K-feldspar and muscovite are lacking. Accessories are represented by pyrrhotite, rutile, graphite and zircon. Garnet porphyroblasts compose 20–25 % the rock and contain inclusions of quartz, kyanite, biotite and rutile. Their cores are enriched in pyrope (25–30 %), whereas the rims contain 17–20 %. The grossular content varies from 9–10 % in the cores to 6–8 % in the rims, and the spessartine content is almost constant (2–3 %). The Al content in biotites is almost constant (1.52–1.58 apfu for Al_{tot}), whereas X_{Mg} varies from 0.6 to 0.8. The Ti content is 0.08–0.16 apfu. The plagioclase composition changes significantly. Large matrix grains are almost unzoned (An_{35-45}), while the anorthite content in rims varies from 55 % to 70–90 %. Cordierite forms rims around some grains of garnet and biotite, and its composition is constant (X_{Mg} = 0.77–0.80). No minerals that could be indicative of eclogite-facies metamorphism have been found. Reliable *P–T* conditions have been calculated only for the latest retrograde metamorphic event when cordierite rims formed. These rims were formed at 580–610 °C and 5.0–5.5 kbar. From an earlier mineral assemblage *Ky+Gr+Bi+Pl+Qtz*, *P–T* estimations have been just roughly yielded as being in broad range of 640–720 °C and 7.5–9 kbar.

Eclogites and Related Rocks

Although strictly speaking, "eclogite" is defined as a bimineralic assemblage of garnet and omphacitic clinopyroxene, herein we use this term for simplicity since a true eclogite mineral assemblage has not been no preserved at all even in a scale of thin slice. For the most part, the eclogite occurrences are relic areas preserved as a strongly altered symplectitic eclogite wrapped by an amphibolite mineral assemblage. Throughout the quarry there are only a few blocks where a rate of preservation seems to be better.

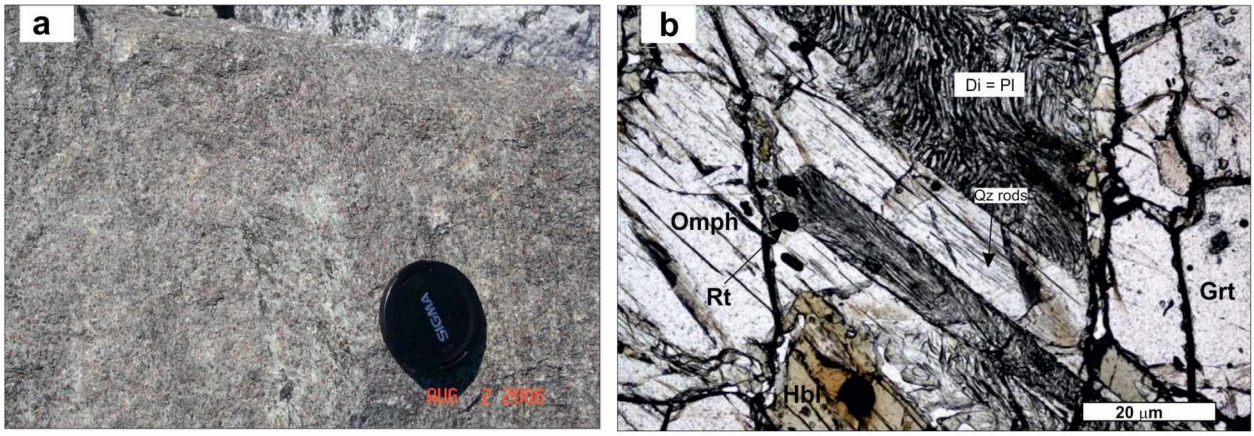

Fig. 3.27. Striking example of the best preserved eclogite: (a) its field photo and (b) microphotograph illustrating the primary eclogite-facies mineral assemblage

Nevertheless, two texturally different types among eclogites may be distinguished: southern and northern (Shchipansky et al. 2012a). The southern type is represented by a coarse-grained eclogite, whereas the northern type is relatively a fine-grained eclogite (Fig. 3.28). Seemingly, the southern eclogite is akin to the Uzkaya Salma eclogite while the northern eclogite looks like the Shirokaya Salma/Gridino ones. Typical mineral textures of the both types are illustrated in Fig. 3.28. Among the southern type eclogites are known kyanite-bearing varieties. They have been described by Konilov et al. (2011) and more more detailed by Liu et al. (2017) (Fig. 3.29).

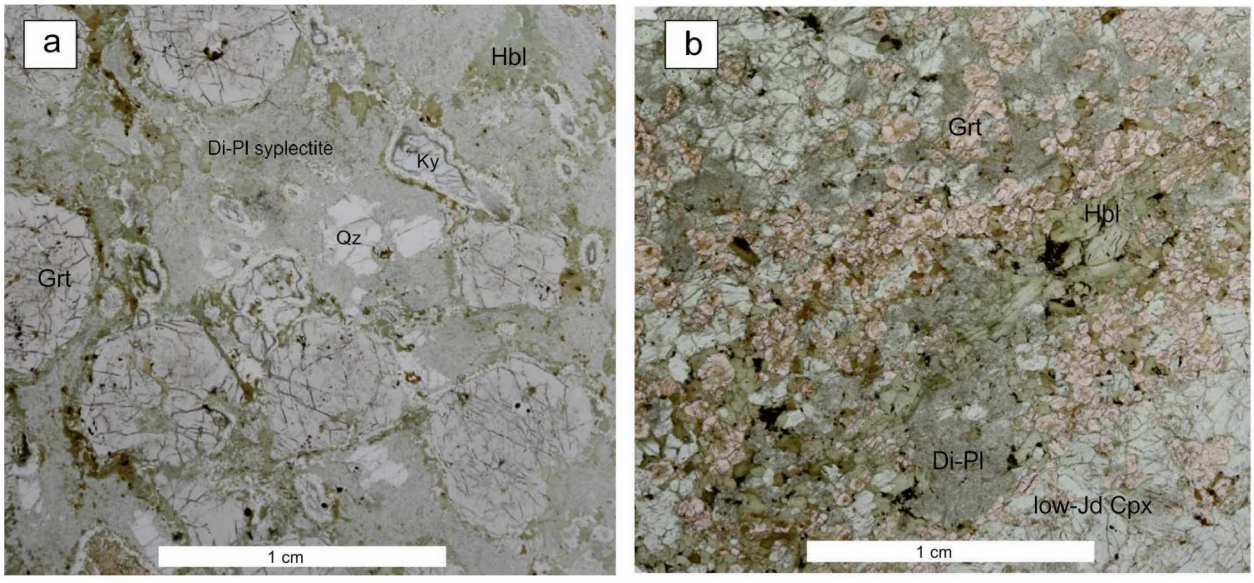

Fig. 3.28. Texturally different types of the eclogites, (a) southern-type, (b) northern type

Both types contain orthopyroxene as a minor constituent which occurs mostly within *Di-Pl* symplectitic areas. A relic clinopyroxene from both eclogite types reveals acicular rods of quartz indicative of a high-Si *Cpx* breakdown that is largely thought as circumstantial evidence that eclogites could have stemmed from UHP metamorphic depths, i.e. from the mantle depths. In this connection, it is vital that many eclogite blocks are tightly bound to meta-ultramafic rocks.

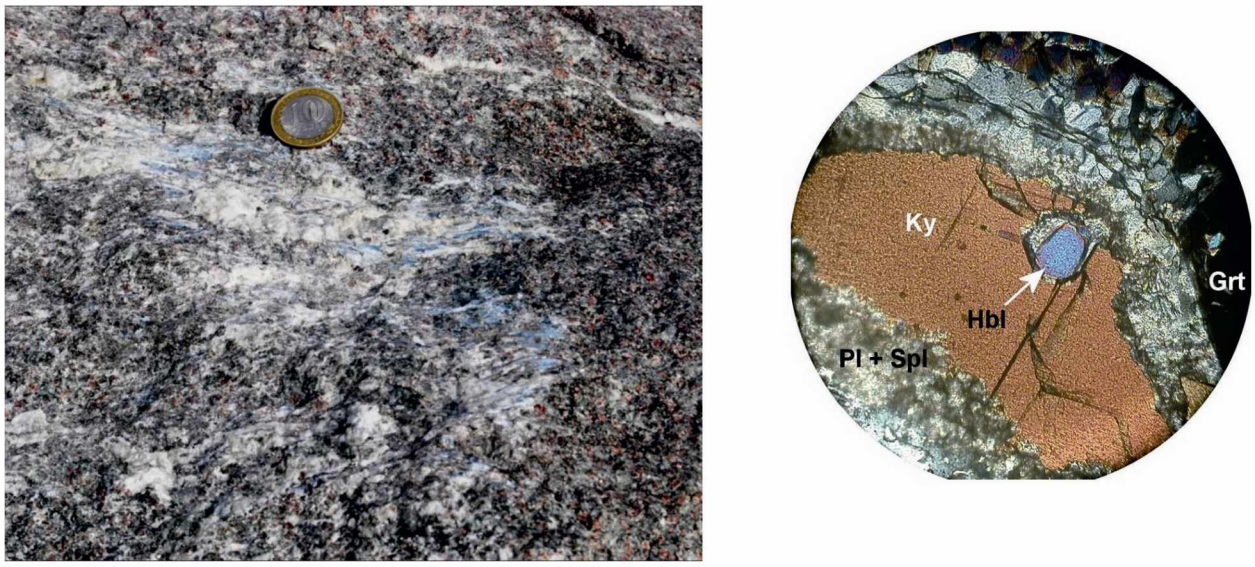

Fig. 3.29. Field photo and microphotograph illustrating a kyanite-bearing eclogite

These occur as small bodies (1–3 m across) that have lens- or boudin-shaped patterns on the map and are concordant with respect to deformational structures of the host TTG gneisses. As a rule, meta-ultramafics have blackwall reaction zones consisted mainly of amphibole along with the enclosing gneisses. Although the original mineral assemblages and hence the origin of these rocks have been largely obscured by subsequent metamorphic alterations, their modal chemistry shows a variety of ultramafic compositions involving both a phlogopite-bearing pyroxenite and peridotite lithologies. In addition, rare garnet websterite lenses occur along with meta-ultramafics (Fig. 3.30).

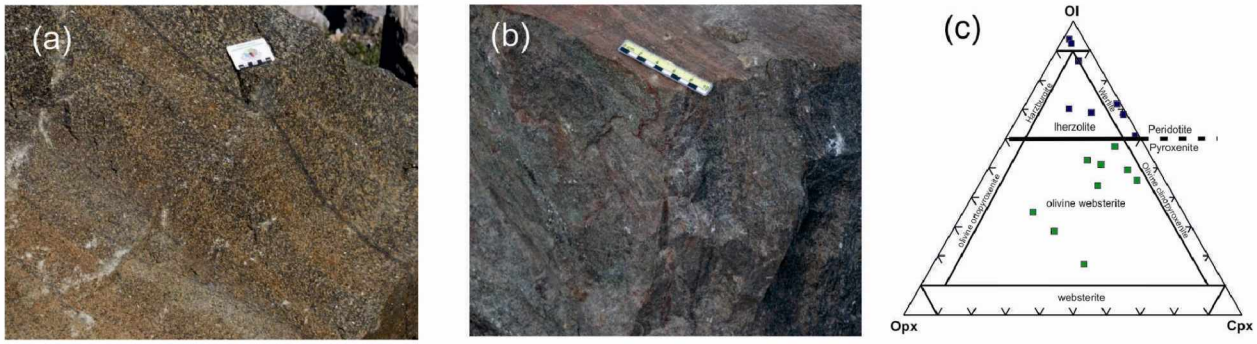

Fig. 3.30. Mantle-derived rocks; field photos of (a) phlogopite meta-peridotite and (b) garnet websterite; (c) CIPW norm composition

As can be seen from Figs. 3.28 and 3.29, the southern and northern eclogites differ substantially. A clear difference of mineral compositions exists also between these types. Garnet from the southern eclogite is pyrope-rich (up to 58 mol. % Prp), whereas garnet from the northern eclogite is moderately enriched in Prp and strongly enriched in Alm (Fig. 3.31). Both garnets reveal a slightly different chemical zoning manifested by wave line incoherent behaviors of end-member components (Shchipansky et al., 2012a). They both contain a large variety of inclusions, from low-*PT* minerals as pumpellyite, cummigtonite and plagioclase to high-*PT* orthopyroxene and clinopyroxene; amphibole inclusions are common. However, garnet from the southern eclogite bears inclusions of kyanite and zoisite, whereas garnet from the northern eclogite contains dolomite and Fe-Ni sulfides.

Omphacite from the southern eclogite is richer in the jadeite end-member (up to 34 mol. %) as compared with a low-Jd clinopyroxene from the northern counterpart (Fig. 3.32). Orthopyroxene is also richer in the edenite end-member in the southern eclogite (76–81 mol.%) as opposed to those from the northern eclogite (67–71). It is vital to note that beside orthopyroxene, Liu et al. (2017) have described sapphirine-bearing assemblages in the kyanite-bearing eclogite, suggesting a HT/UHT (up to 940–990 °C) granulite-facies overprint.

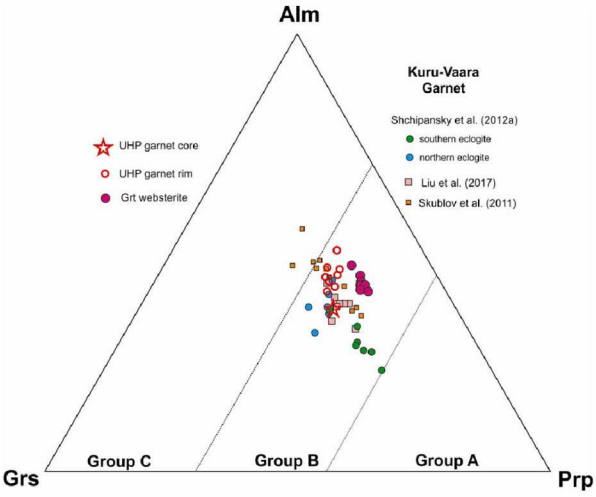

Fig. 3.31. Compositional diagram of garnet

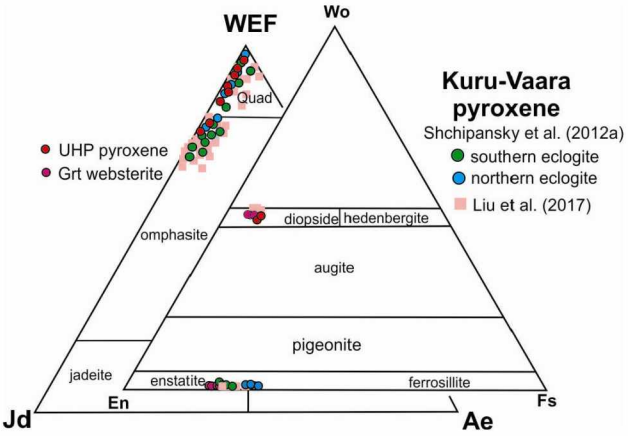

Fig. 3.32. Compositional diagrams of pyroxene

Meta-peridotite lithologies have modal compositions corresponding to a lherzolite, and they consist mainly of secondary olivine, antigorite, orthopyroxene, diopside, phlogopite, Mg-chlorite, metamorphic spinel (Cr# up to 18), and rare pentlandite (Fig. 3.33). Ca-amphibole is locally observed testifying that the latest re-equilibration of earlier ultra-mafic mineral assemblages occurred under amphibolite-facies conditions. In some blocks fine grains of garnet are rarely present but most garnet was completely replaced by tiny mineral aggregates whose compositions cannot be resolved by probe analyses. The meta-pyroxenite lithologies are compositionally close to the meta-peridotite, except that clinopyroxene predominates over othopyroxene in the first case. The garnet websterite consists roughly of 30–50 %, garnet (30–50 %), othopyroxene (30–40 %), clinopyroxene (20–30 %), phlogopite (up to 10 %) and minor Mg-rich calcite, low-Cr spinel and ilmenite. Amphibole is obviously a late metamorphic mineral which penetrates largely into previous mineral assemblages. Noteworthy that all the mantle-derived rocks are phlogopite-bearing and contain no phengite.

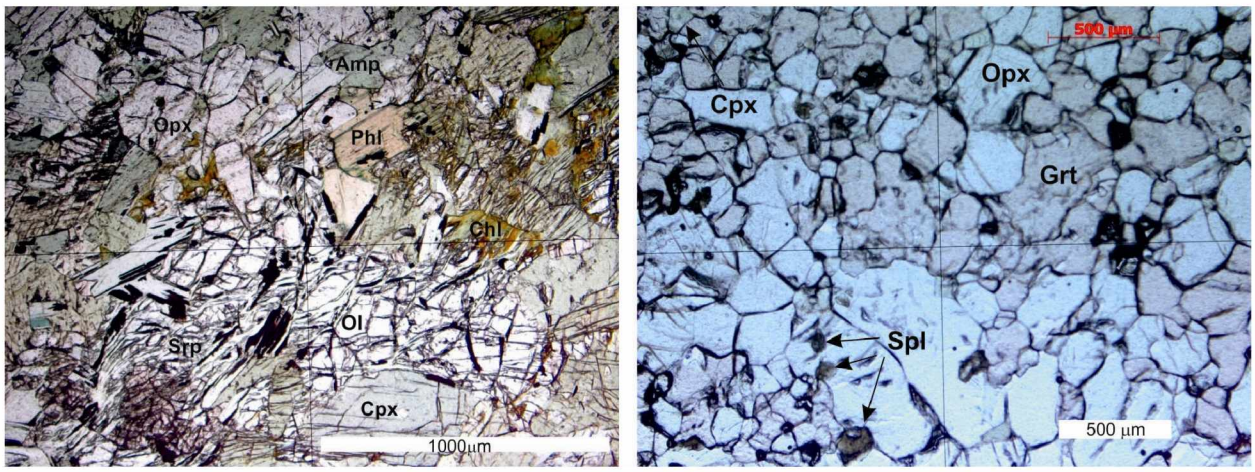

Fig. 3.33. Microphotographs of meta-peridote (left panel) and garnet websterite (right panel)

Thermobarometric estimation

Published estimations for the inferred peak of the eclogite-facies metamorphism are slightly different. We have proposed that a peak condition for the Kuru-Vaara eclogite could have occurred at pressures exceeding, at least, 20 kbar (Shchipansky et al., 2012a). Beside the high-Si Cpx breakdown mentioned above, we have recently found additional evidences for plausible UHP conditions at the metamorphic peak. These are: (i) topotactically oriented rutile needless occasionally occurred in garnet, and (ii) poly-carbon phases armored also in garnet. Although they are consisted of graphite, carbonate and CO_2, some crystals have clear cubic features, thus, implying that these are pseudomorphs after diamond (Fig. 3.34).

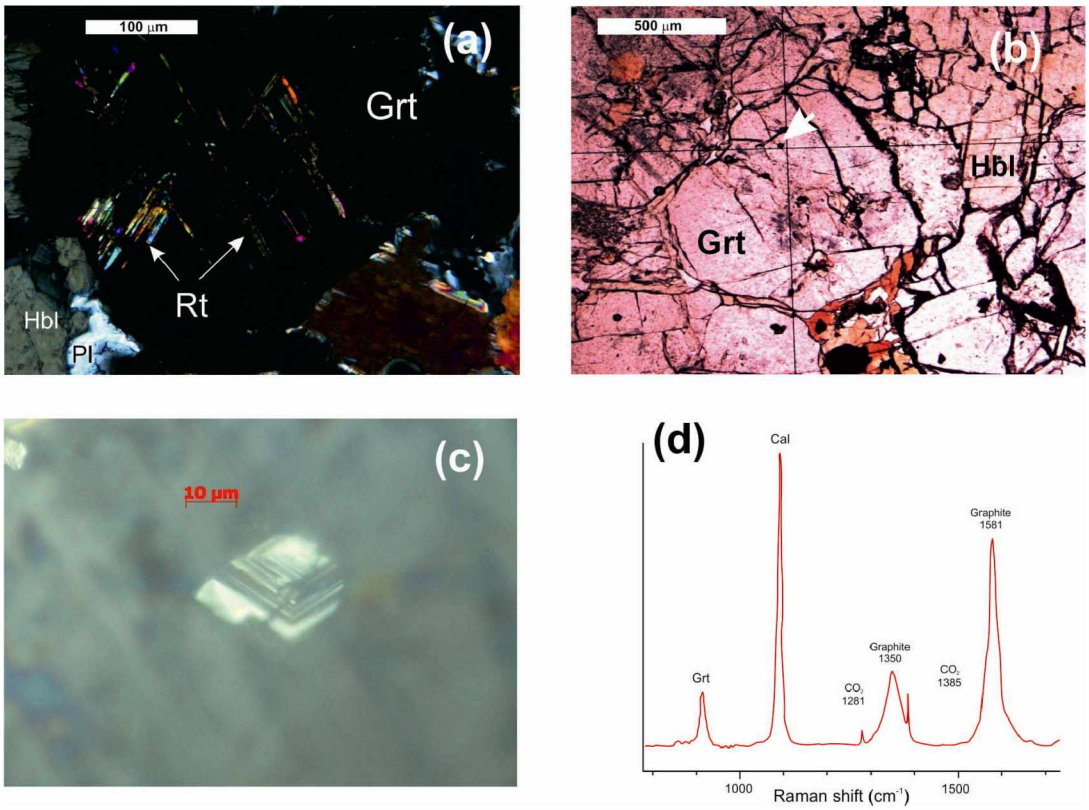

Fig. 3.34. Toward to evidence for UHP metamorphism: (a) microphoto of parallel-oriented *Ru* needles in *Grt*; (b) location of a poly-carbon phase in *Grt*; (c) microphoto (reflective light) of this phase beneath the thin section surface; its shape suggests a pseudomorph after *Dia*; (d) Raman spectrum

Liu et al. (2017) estimated the maximum pressure at 18–20 kbar and temperature in the range of 720–820 °C. A substantial discrepancy is found in post-peak trajectories that are due to a finding by Liu et al. (2017) HT/UHT mineral assemblages (Fig. 3.35). They have suggested that the essential increase in temperature during the exhumation may have been caused by a thermal relaxation and have not considered this suggestion in any detail.

It should be noticed that the post-granulitic exhumation path is of a greater extent in comparison with the adiabatic slope. It leads to concluding that the Paleoproterozoic exhumation of the Belomorian eclogites should have been fast. In fact, the granulitization of eclogites should have led to their dehydration and densification, so they might have become much denser at crustal depths than the enclosing TTG gneisses. As a result, it is difficult if not possible to attain physical conditions for exhumating eclogites through buoyancy mechanisms. Moreover, the post-granulitic exhumation path reveals a nearly isobaric thermal cooling, thus, implying that a conductive thermal relaxation was a primary constituent in the crustal history of the Belomorian eclogites.

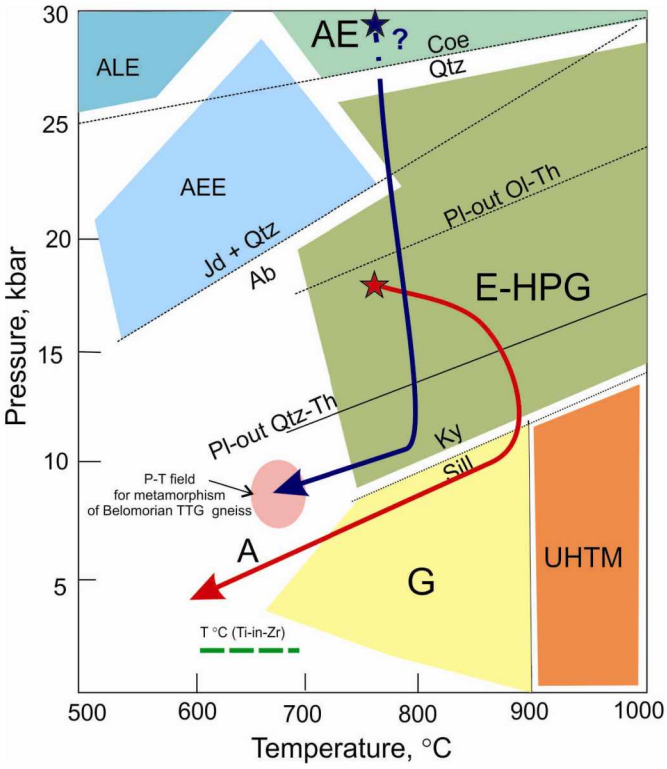

Fig. 3.35. Inferred peaks and *P-T* paths for the Kuru-Vaara eclogite: red star and array from (Liu et al, 2017) and dark blue star and array from (Shchipansky et al., 2012b); data on the temperature range determined by the Ti-in-Zr geothermometer from Skublov et al. (2011), Mel'nik et al. (2013) and Shchipansky et al. (2012b); for detail explanation see the text

Zircon age dating

Results of a SIMS zircon dating from the Kuru-Vaara eclogites were published in several articles (Skublov et al., 2010, 2011; Shchipansky et al., 2012a; Mel'nik et al., 2013). These results are shown on a probability density plot (Fig. 3.36). A recent publication by Liu et al. (2017) includes both SIMS and LA-ICP-MS results. Because this work was focused on dating the latest zircons, ages published in it have not shown in the plot.

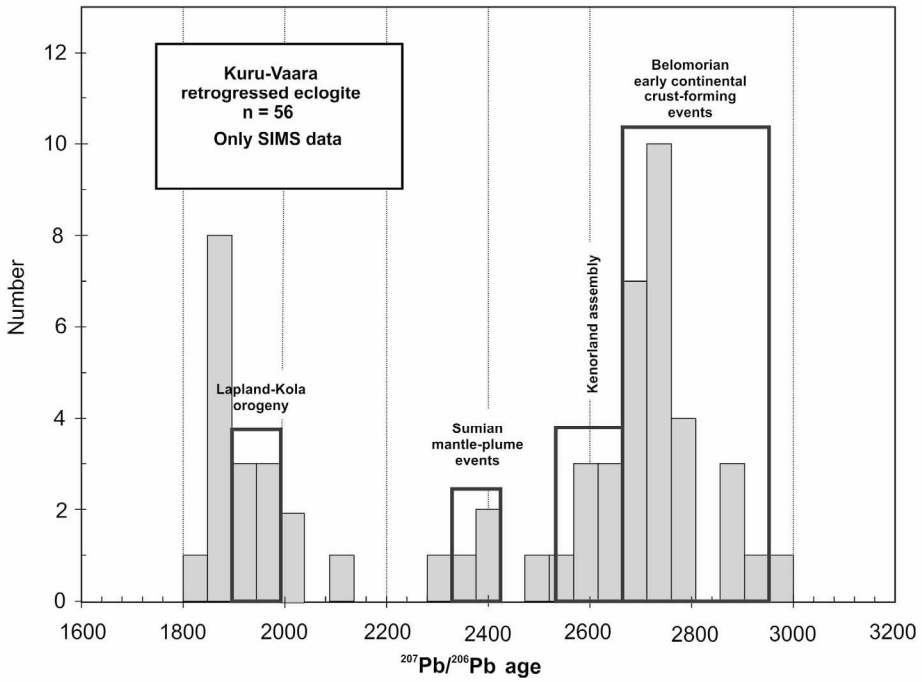

Fig. 3.36. Probability density plot for U-Th-Pb data from zircon picked from the Kuru-Vaara eclogite

As evident from the plot, the majority of isotopic ages obtained correspond to late Archean tectonic events. Some zircons reveal the Sumian (early Paleoproterozoic) mantle plume impingement. Zircon ages corresponding to the Lapland-Kola orogenic events are also present. Note that the Lapland-Kola metamorphic 'peak' zircon age falls within a time span of 1880–1840 Ma and thus are rather close to an age of the ceramic pegmatite than to an age reported for the Lapland-Kola collision. Interestingly, all publications that advocate a Paleoproterozoic age of the Belomorian eclogite are based on a simple approach: 'eclogitic' zircons of that age have very low Th/U ratios (0.0001–0.1) and their MREE and HREE pattern are flat. It may well be appreciable for a mono-cycle metamorphism typical of the Phanerozoic orogenic belts but its application to zircon from ancient, deeply eroded orogenic belts seems to be inadequate. In such a situation, observed modification of zircon were not formed in response to major high-grade metamorphic events recorded in the rock mineralogy because they crystallized after the a high-grade metamorphism when newly-formed zircon was formed in response to a later post-peak fluid infiltration (Harley, Kelly, 2007; Harley at al., 2007). In addition, all Archean zircons from the Belomorian eclogite experienced re-equilibrations through the coupled dissolution-reprecipitation mechanism and such zircons have to be used for geochemical tracing with caution (Geisler et al., 2007). The crystallization of later zircon overgrowths needs a zirconium source from external fluids in many instances (Martin et al., 2008).

In fact, the available data on Ti-in Zr temperature from the 'eclogitic' zircons from the Kuru-Vaara quarry show a temperature range from ~ 700 to 600 ºC and the average value of 650–660 °C falls too far from the inferred temperature peak of the eclogite metamorphism (see Fig. 3.35). Moreover, such a kind of 'eclogitic' zircons is known from the Ivrea-Verbano Zone in the Southern Alps. They are termed as stubby zircons which precipitated after the peak of metamorphism over 60 Ma at the transition between amphibolite and granulite facies (Guergouz et al., 2018). A detailed petrographic study of the Kuru-Vaara eclogite has revealed that a wealth of the so-called 'eclogitic' zircons are related to zones where amphiboles predominate. Thus, these should also be referred to as stubby zircons formed after the metamorphic peak (Fig. 3.37).

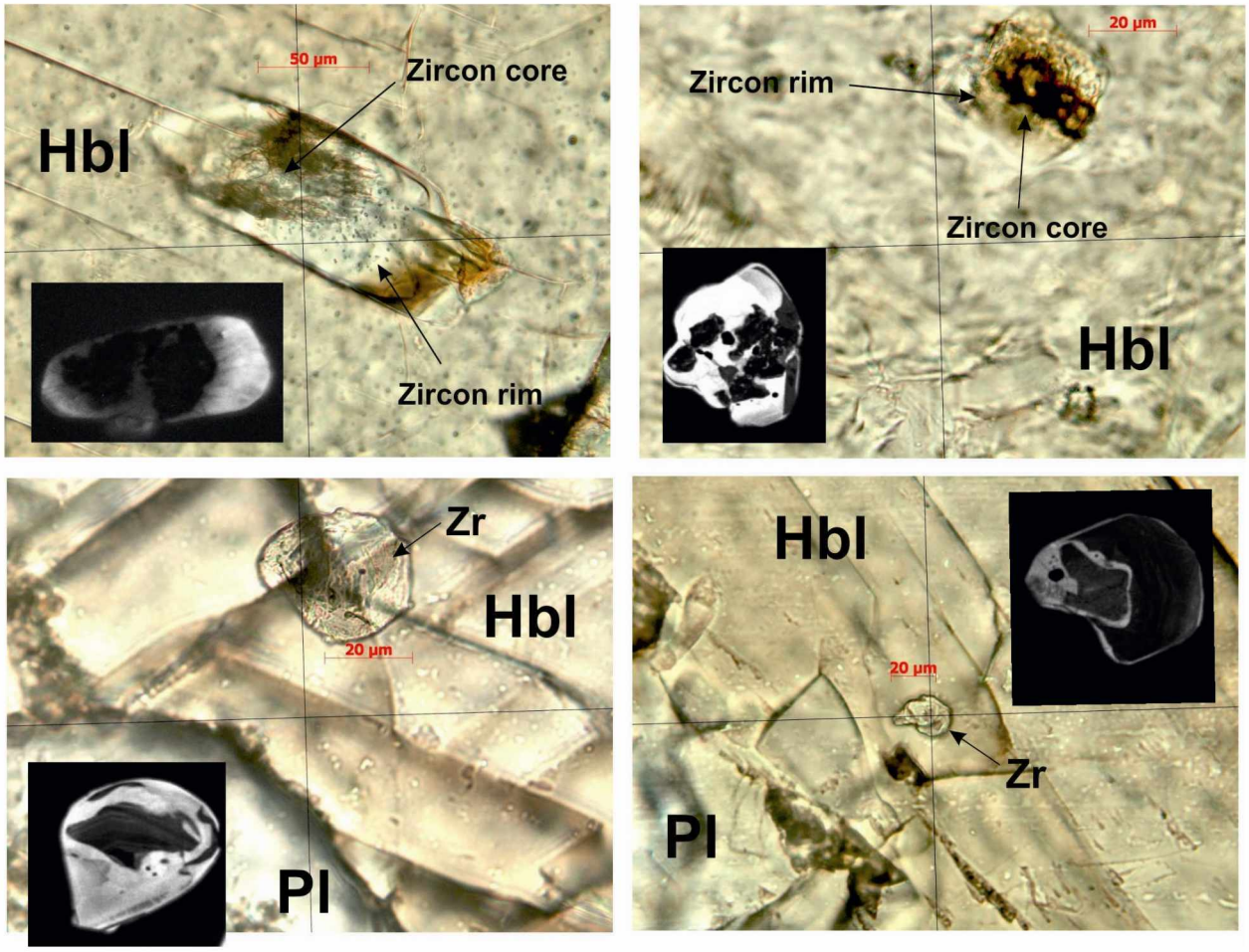

Fig. 3.37. Microphotographs illustrating that stubby zircons from the Kuru-Vaara eclogite are related to late amphiboles; insets demonstrate CL images of zircons picked for a SIMS dating

Furthermore, data on Lu-Hf ages (Herwartz et al., 2012) from a strongly resorbed garnet from the Kuru-Vaara eclogite are not consistent with the criteria imperative to obtain a correct isochron which could result in a false Lu-Hf age rather than a true Lu-Hf age (Kelly et al., 2011).

Geochemistry

Chemically, all representative samples of the studied well-preserved eclogites correspond to primitive (Mg#[Mg_2+/(Mg^{+2} + Fe^{+2})] = 0.6–0.7) olivine-normative low-K and high-Mg tholeites or even picrites (MgO ~ 12–14 wt.%) (Shchipansky et al., 2012b). This evidences that their mafic protoliths were formed from primary mantle melts without the following substantial fractional crystallization.

As can be seen from mantle-normalized patterns of trace elements, the eclogites are more similar in composition to melts derived from the primitive mantle rather than to melts produced through the partial melting of the modern depleted upper mantle (Fig. 3.38a). It is noteworthy that the both types of eclogites show pronounced positive Nb anomalies indicative of melts uncontaminated by crustal material or subduction input (Jochum et al., 1991). If so, a precursor for the Kuru-Vaara eclogite was obviously a Mesoarchean subducting oceanic crust. Petrological modeling for eclogite precursor melts (Shchipansky, 2012) revealed that the eclogitic protoliths are compositionally consistent with experimental and parameterized primary melts for a late Archean oceanic crust, which should have been formed by partial melting of an ambient peridotite mantle which was hotter than the modern ambient mantle by 150–200 K (e.g. Herzberg et al., 2010). Contrary to the eclogites, the both post-eclogitic gabbro-amphibolites and the Paleoproterozoic garnet gabbronorite bear clear crustal contamination geochemical signs (Fig. 3.38b).

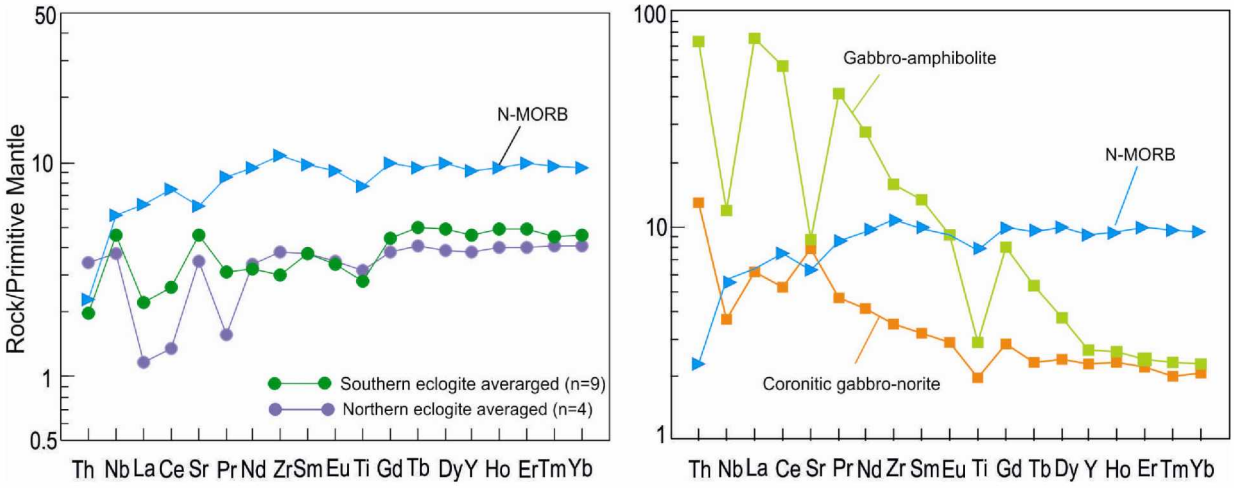

Fig. 3.38. Geochemical contrast between eclogite and post-eclogite lithologies: (a) Primitive mantle-normalized (Hofmann 1988) trace element patterns of the eclogites; (b) the same diagram for coronitic gabbronorite and gabbro-amphibolite samples. N-MORB is shown for comparison

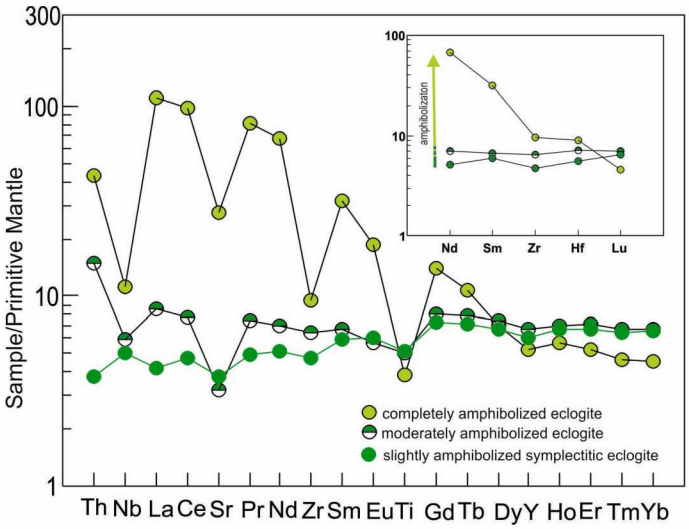

Fig. 3.39. Change in geochemical behaviors as a result of the complete transformation of eclogite into amphibolite; inset demonstrates abundance patterns for trace elements used for mineral chronometry (cf. Balagansky et al., 2015; Shchipansky, Slabunov, 2015)

It is important to keep in mind that the oceanic geochemical affinity has been distinguished only in the least retrogressed eclogites. Fig. 3.39 illustrates apparent arc signatures for an oceanic MORB protolith resulted from a prolonged retrogression of a southern eclogite block during the transition from eclogite-facies to the amphibolite-facies conditions. As can be seen, this symplectitic eclogite has loosed oceanic geochemical traits and have got arc-like geochemical signatures. This case clearly demonstrates that the retrogression of eclogites proceeded in an open system during an exhumation-related overprinting. Hence it is ineffective to use mineral isochron dating to constraint age of the eclogite-facies metamorphism because the eclogites have apparently been re-equilibrated via a fluid-induced element transfer under retrograde *P–T* conditions at crustal levels.

Towards the early continental crust-forming geodynamics

When were the Kuru-Vaara eclogites formed? A zircon age dating alone gives no way of settling the question. Nevertheless, the geology of the quarry makes possible to resolve this question by various means.

(1) *When did the HT/UHT granulitization occur?* All authors suggest that this process post-dated the eclogite-facies metamorphism. If so, the HT/UHT event should have been inevitably coupled with partial melting of previously exhumed eclogites. There are preserved only a few small domains in south-western part of the Kuru-Vaara quarry where one can observe primary relationships between leucosome and eclogite that are clearly suggestive of an *in situ* HPT melting (Fig. 3.40a). Fig. 3.40b evidently illustrates a result of an open isotope-geochemical reworking which resulted in the formation of an amphibolite with remnants of an unclear garnet-free plagiogranite rather than a HP granulite assemblage similar to that shown in Fig. 3.40a. Chemically, the garnet plagiogranite is trondhjemite akin to some extent to a HP trondhjemite, except that it contains unusually high, 900–1000 ppm content of *Zr* indicative of hot inheritance-poor granite (Miller et al., 2003). Indeed, the picketed zircon population shows no evidence, with one exception, for inherited zircon, as well as for so-called 'eclogitic' rims. SIMS dating yielded a concordant age of 2460±5 Ma that correspond well to the Sumian mantle plume impingement.

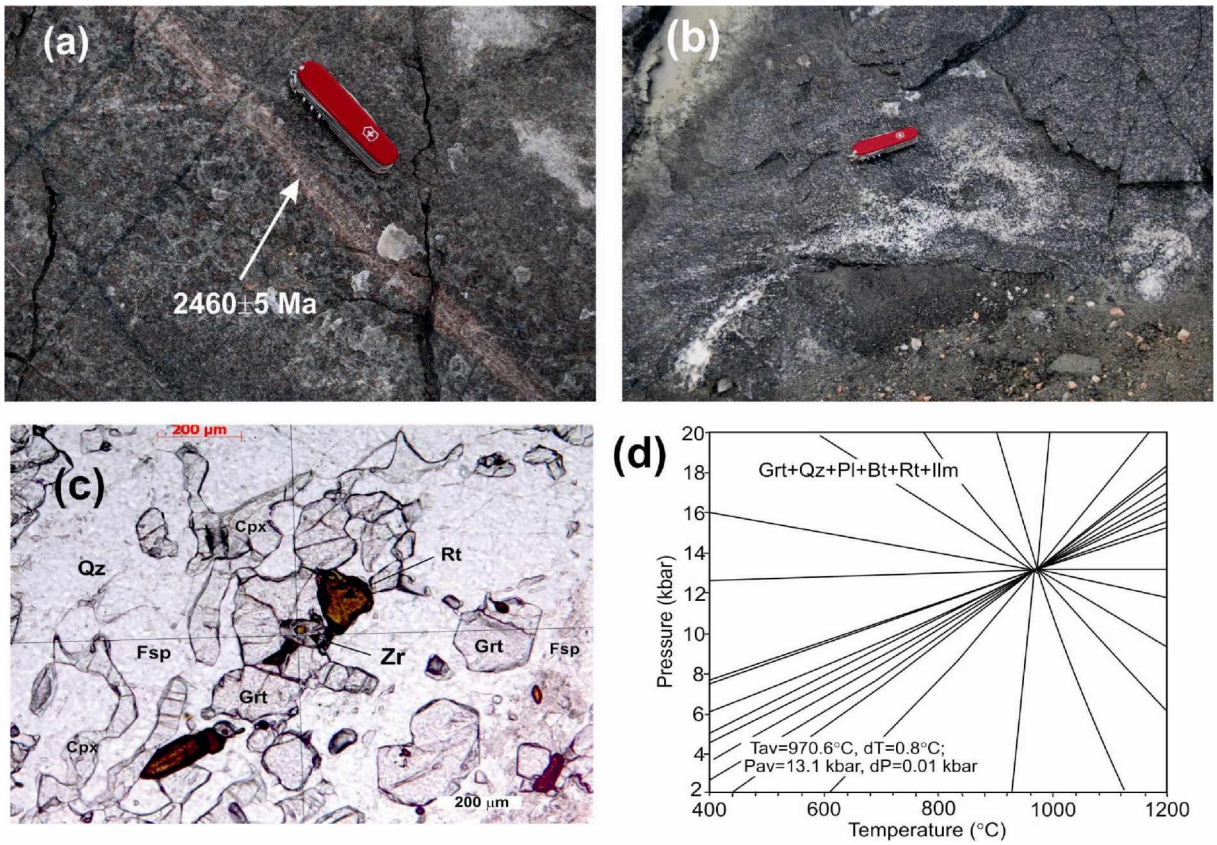

Fig. 3.40. Granulitization of a symplectite eclogite: (a) field photo illustrating a stromatic leucosome (partial melting *in situ* with the garnet melanosome) and its concordant U-Pb SIMS zircon age; (b) field photo showing a final result of reworking of the pre-existed assemblage from (a) in an open system; (c) microphotograph illustrating the mineral assemblage and its texture of the UHT garnet-plagiogranite leucosome; note that a zircon grain is equilibrated with garnet; (d) *P–T* diagram produced for the UHT leucosome by using the Berman's TWQ software and database; all possible reactions for selected end-member components area shown but there are only four linearly independent reactions (after Azimov et al., 2014)

The leucosome melt was formed mostly under control of garnet and rutile (Fig. 3.40c) under water-undersaturated conditions at T ~ 950 °C and P ~ 13 kbar (Fig. 3.40d). This result is of outstanding significance because the granulitization of the eclogite has been reported from the mentioned above Uzkaya and Shirokaya Salma localities. So, the eclogites from all these localities were formed in the late Archean rather than the Paleoproterozoic.

(2) *When did the HP/UHP metamorphism occur?* In order to constrain a bracketing age for the eclogite emergence, we have dated zircon from different leucosomes observed in a banded, strongly retrogressed eclogite block in the southern part of the quarry. The result obtained is illustrated in the Fig. 3.41. As can be seen, a low-P partial melting of eclogite produced a trondhjemitic leucosome dated at 2829 ± 11 Ma, which indicates an older age of eclogite-facies metamorphism. A later granitic leucosome was dated at 1888 ± 8 Ma and was formed during the Lapland-Kola orogenic

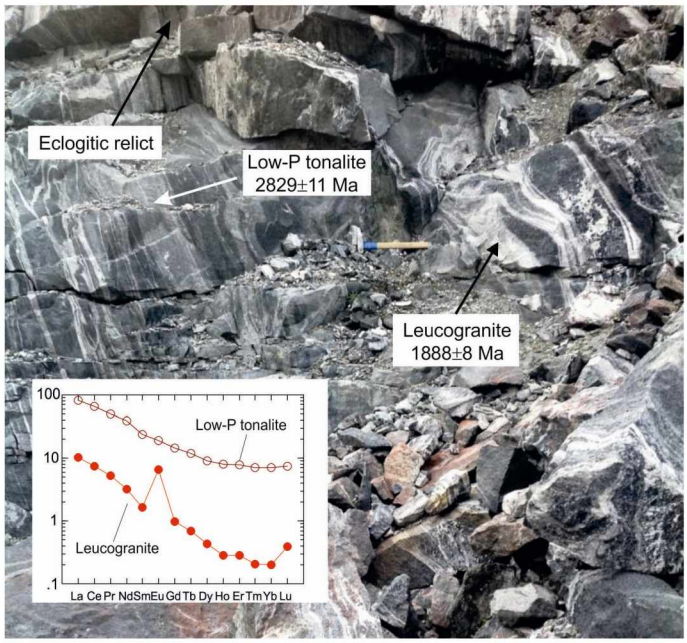

Fig. 3.41. Field photo illustrating older and younger leucosomes that constrain an age of the eclogite emergence and its following alteration during the Lapland-Kola orogenic reworking; inset highlights a clear distinction between REE patterns from the late Archean and Paleoproterozoic leucosome melts

reworking. So, the HP/UHP metamorphism should have been occurred prior to the exhumation of eclogites at a mid-crustal level where they must have endured low- to moderate pressure partial melting producing, thus, tonalite melts. As a whole, zircon ages of the Belomorian TTG gneisses that host eclogites may be considered as bracketing ages for eclogitic blocks (see Fig. 3.12–3.13).

(3) *Where did the eclogites come from?* They came from a Mesoarchean oceanic crust which was being subducted into the mantle at some time. This inference is obvious from the coupled geochemical behaviors of available geochemical data on whole rock and zircon implying that the Belomorian eclogitic protoliths stemmed from an oceanic crust rather than the basalt to eclogite phase transition in a lower tectonically thickened crust (Fig. 3.42).

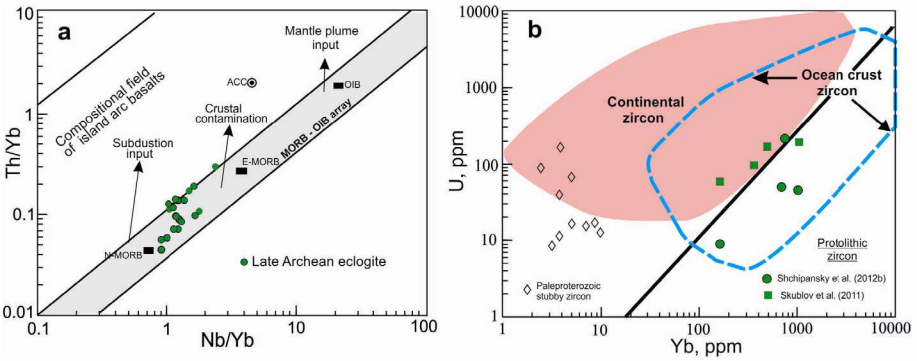

Fig. 3.42. Geochemical evidence for an oceanic crust provenance of the Belomorian eclogites: (a) Th-Nb proxy diagram for searching of Archean oceanic crust (Pearce, 2008) indicating that these eclogites match MORB-OIB array; (b) U vs. Yb discrimination diagram with the dividing line (Grimes et al., 2007) for SIMS dated zircons from the Kura-Vaara eclogites illustrating that Mesoarchean protolithic zircons stemmed from an oceanic crust

(4) *Did the eclogites visit the mantle?* Yes, they were in the mantle. In fact, there are several locations in the quarry where one can observe mechanically coupled eclogite and mantle meta-peridotite (Fig. 3.43). It comes no surprise that such a kind of eclogite lenses contain vestigial UHP mineral assemblages involving diamond along with other minerals suggestive of deep and cold subduction in the late Archean (see Shchipansky et al., 2019).

Fig. 3.43. Coupled occurrence of eclogite and meta-peridotite; left panel is a field photo demonstrating lenses of an eclogitic remnant enclosed in a meta-peridotite block; right panels illustrate photomicrographs of the occurrence of diamond coated by graphite within a high-Si clinopyroxene at transmitted light (top) and reflective light (bottom)

Acknowledgements

We appreciate the past and present management of the Kol'sky Pegmatit enterprise and the Kuru-Vaara quarry for permission to conduct long-term fieldworks in the quarry, logistics, and help. We thank the Russian Foundation for Basic Research for a prolonged financial support without which our search for and study of the Belomorian eclogites and related rocks would have not been possible (RFBR grants 06-05-65237, 12-05-01080, 13-05-91162, 16-05-00479 and 16-05-01031). This communication has been partly prepared in the framework of research projects of Geological Institute of the RAS (#AAAA-A17-117030610104-2) and the Kola Science Center of the RAS (#0226-2019-051).

REFERENCES

Anderson, E.D., Moecher, D.P. (2016) Omphacite breakdown reactions and relation to eclogite exhumation rates Omphacite breakdown reactions and relation to eclogite exhumation rates. Contributions to Mineralogy and Petrology 154: 253-277.

Azimov, P.Ya., Shchipansky, A.A., Slabunov, A.I. (2014) Relicts of the UHT-HP metamorphism in the Belomorian Mobile Belt, Fennoscandian Shield. In: Supercontinents at the Early Precambrian history. St.-Petersburg, IGGD RAS 6-8. [in Russian].

Azimov, P.Ya., Slabunov, A.I., Stepanova, A.V., Serebryakov, N.S., Babarina, I.I. (2017) The Paleoproterozoic High-Pressure Granulites in the Belomorian Province of the Fennoscandia: the petrological evidences for continent-continent collision. In: Early Precambrian vs Modern Geodynamics. Slabunov A.I., Svetov S.A., Baltibaev Sh.K. (Eds). Extended Abstracts and Field Trips Guide. Petrozavodsk: KarRC RAS 13-17.

Babarina, I.I., Sibelev, O.S. (2015) Deformation events in the Gridino zone, Belomorian Province, Fennoscandian Shield: Relationships between mafic dike swarms and eclogite-bearing mélange. International Geology Review 57: 1607-1618.

Babarina, I.I., Stepanova A.V. Azimov, P.Ya., Serebryakov, N.S. (2017) Heterogeneous basement reworking during Paleoproterozoic collisional orogeny within the Belomorian province, Fennoscandian Shield. Geotectonics 51(5): 463-478.

Balagansky, V.V. (2002) Main stages of the Palaeoproterozoic tectonic evolution of the northeastern Baltic Shield, Doctoral dissertation, Russian Academy of Sciences, Apatity 1-326 [In Russian].

Balagansky, V.V., Glaznev, V.N., Osipenko, L.G. (1998) Early Proterozoic evolution of the northeastern Baltic Shield: Terrane analysis. Geotectonics 32: 81-93.

Balagansky, V., Shchipansky A., Slabunov, A., Gorbunov, I., Mudruk. S., Sidorov, M., Azimov, P., Egorova, S., Stepanova, A., Voloshin, A. (2015) Archean Kuru-Vaara eclogites in the northern Belomorian Province, Fennoscandian Shield: crustal architecture, timing and tectonic implications. International Geology Review 57: 1543-1565.

Balagansky, V.V., Maksimov, O.A., Gorbunov, I.A., Kartushinskaya, T.V., Mudruk, S.V., Sidorov, M Yu., Sibelev, O.S., Slabunov, A.I. (2019) Older and younger eclogites in the Belomorian province, Fennoscandian shield: an example from the Gridino area. In. Abstract Volume of the 13th of International Eclogite Conference. C. Mattinson et al. (Eds.). Petrozavodsk: KarRC RAS 10

Berezin, A.V., Skublov, S.G., Marin Yu.B., Mel'nik, A. E., Bogomolov, E.S. (2013) New Occurrence of Eclogite in the Belomorian Mobile Belt: Geology, Metamorphic Conditions, and Isotope Age. Doklaby Earth Sciences 448 (Part 1): 43-53.

Berezin, A.V., Travin, V.V., Marin, Yu.B., Skublov, S.G., Bogomolov, E.S. (2012) New U–Pb and Sm–Nd Ages and P–T Estimates for Eclogitization in the Fe-Rich Gabbro Dyke in Gridino Area (Belomorian Mobile Belt). Doklady Earth Sciences 444 (Part 2): 760-765.

Berman, R.G. (1988) Internally-consistent thermodynamic data for minerals in the system Na_2O–K_2O–CaO–MgO–FeO–Fe_2O_3–$A1_2O_3$–SiO_2–TiO_2–H_2O–CO_2. Journal of Petrology 29: 445–522.

Berman, R.G. (1991) Thermobarometry using multiequilibrium calculations: a new technique with petrologic applications. Canadian Mineralogist 29: 833-855.

Berman, R.G., Aranovich, L.Ya. (1996) Optimized standard state and solution properties of minerals: I. Model calibration for olivine, orthopyroxene, cordierite, garnet, and ilmenite in the system FeO–MgO–CaO–Al_2O_3–TiO_2–SiO_2. Contributions in Mineralogy and Petrology 126: 1-24.

Berthelsen, A., Marker, M (1986) Tectonics of the Kola collision suture and adjacent Archaean and Early Proterozoic terrains in the northeastern region of the Baltic Shield. Tectonophysics 126: 31–55.

Bibikova, E.V. (1989) Uranium–Lead Geochronology of Early Evolution Stages of Ancient Shields. Moscow, Nauka Publishing 1-179. [in Russian].

Bibikova, E.V., Bogdanova, S.V., Glebovitsky, V.A., Claesson, S., Skiöld, T. (2004) Evolution of the Belomorian Belt: NORDSIM U-Pb Zircon Dating of the Chupa Paragneisses, Magmatism, and Metamorphic Stages. Petrology 12: 195-210.

Bibikova, E., Skiöld, T., Bogdanova, S., Gorbatschev, R., Slabunov, A. (2001) Titanite-rutile thermochronometry across the boundary between the Archaean Craton in Karelia and the Belomorian Mobile Belt, eastern Baltic Shield. Precambrian Research 105: 315-330.

Bibikova, E.V., Slabunov, A.I., Bogdanova, A.I., Skiöld, T., Stepanov, V S., Borisova, E.Yu. (1999) Early magmatism of the Belomorian Mobile Belt, Baltic Shield: lateral zoning and isotopic age. Petrology 7(2): 123-146.

Bogdanova, S.V. (1996) High-grade metamorphism of 2,45–2,4 Ga age in mafic intrusions of the Belomorian Belt in the northeastern Baltic Shield. In: Precambrian Crustal Evolution in the North Atlantic Region. Brewer T.S. (Ed.) Geological Society. Special Publication 112: 69-90.

Bogdanova, S.V., Gorbatschev, R., Garetsky, R.G. (2005) East European Craton. In: Encyclopedia of Geology. Vol. 2. Selley, R.C., Cocks, L.R.M., Plimer, I.R. (Eds.). Amsterdam: Elsevier 34-49.

Boland, J., van Roermund, H. (1983) Mechanisms of exsolution in omphacites from high temperature, type B, eclogites. Physics and Chemistry of Minerals 9: 30-37.

Brown, B. (2007) Metamorphic Conditions in Orogenic Belts: A Record of Secular Change. International Geology Review 49: 193-234.

Brown, M., Johnson, T. (2018) Secular change in metamorphism and the onset of global plate tectonics. American Mineralogist 103: 181-196.

Brunsmann A., Franz G. Heinrich W. (2002) Experimental investigation of zoisite–clinozoisite phase equilibria in the system CaO–Fe2O3–Al2O3–SiO2–H2O. Contributions to Mineralogy and Petrology 143: 115-130.

Corfu, F., Hanchar, J.M., Hoskin, P.W.O., Kinny, P. (2003) Atlas of zircon textures. Reviews in Mineralogy and Geochemistry 53: 469-500.

Daly, J.S., Balagansky, V.V., Timmerman, M.J., Whitehouse, M.J. (2006) The Lapland-Kola Orogen: Palaeoproterozoic collision and accretion of the northern Fennoscandian lithosphere. In: European Lithosphere Dynamics. Gee, D.G., and Stephenson, R.A. (Eds.) Memoirs 32. London: Geological Society 579-598.

Daly, J.S., Balagansky, V.V., Timmerman, M.J, Whitehouse, M.J., de Jong, K., Guise, P., Bogdanova, S., Gorbatschev, R. , Bridgwater, D. (2001) Ion microprobe U–Pb zircon geochronology and isotopic evidence supporting a trans-crustal suture in the Lapland Kola Orogen, northern Fennoscandian Shield. Precambrian Research 105: 289-314.

Deer, W.A., Howie, R.A., Zussman, J. Epidote group (1986). In: Disilicates and ring silicates. Deer, W.A., Howie, R.A., Zussman, J. (Eds.) 2nd end. Longman Scientific and Technical. London 2-179.

Dokukina, K.A., Mints, M.V., Konilov, A.N., Bayanova, T.B., Kaulina, T.V , Serov, P.A., Travin, A.V. (2012a). The Belomorian eclogite province: the sequence of events and the age of magmatic and metamorphic rocks of the Gridino eclogite association. Russian Geology and Geophysics 53(10): 1023-1054.

Dokukina K.A., Dokukin P.A. (2015). Tectonic breccias of the Belomorian eclogite province (Gridino area): evidences of paleoseismic dislocations in a Mesoarchean subduction zone. GeoScience 2: 17-39. [in Russian].

Dokukina, K.A., Kaulina, T.V , Konilov, A.N., Mints, M.V , Van, K.V., Natapov, L.M , Belousova, E.A., Simakin, S.G., Lepekhina, E.N. (2014) Archaean to Palaeoproterozoic high-grade evolution of the Belomorian eclogite province in the Gridino area, Fennoscandian Shield: Geochronological evidence. Gondwana Research 25: 585-613.

Dokukina, K.A., Konilov, A.N. (2011). Metamorphic evolution of the Gridino mafic dyke swarm (Belomorian eclogite province, Russia). In: Ultrahigh-Pressure Metamorphism. 25 Years after the discovery of coesite and diamond. Dobrzhinetskaya, L., Cuthbert, S., Faryad, W., Wallis, S. (Eds.), Amsterdam: Elsevier 579-621.

Dokukina, K.A., Konilov, A.N., Van, K.V , Mints, M.V., Simakin, S.G. (2012) Origin of early paleoproterozoic zircons in rocks of the Archean eclogite association of Gridino (Belomorian eclogite province). Doklady Earth Sciences 445: 832-839.

Dokukina, K., Mints, M. (2019) Subduction of the Mesoarchaean spreading ridge and related metamorphism, magmatism and deformation by the example of the Gridino eclogitized mafic dyke swarm, the Belomorian Eclogite Province, eastern Fennoscandian Shield. Journal of Geodynamics 123: 1-37.

Drummond, M S., Defant, M.J., Kepezhinskas, P.K. (1996) Petrogenesis of slab derived tonalite-dacite adakite magmas. Philosophical Transactions of the Royal Society Edinburgh 58: 205-215.

Egorova, S.V (2017) Paleoproterozoic gabbronorites of the Belomorian and Karelian Provinces of the Fennoscandian Shield: comparative analysis of the composition, forming conditions and metamorphic transformations. Extended abstract of Candidate's Dissertation in Geology and Mineralogy. Moscow 1-24. [in Russian].

Eskola, P. (1921) On the eclogites of Norway. Skrifter Utgitt av det Norske Videnskaps-Akademii Oslo, Klasse 1, 8: 1-118.

Fedorov, E.S. (1896) A new group of igneous rocks. Izv. Mosk. Sel'skokhoz. Inst. 1: 12-29. [in Russian]

Geisler, T., Schaltegger, U., Tomaschek, F. (2007). Re-equilibration of zircon in aqueous fluids and melts. Elements 3: 43-50.

Glebovitsky, V A. (1986) Tectonic regime of metamorphism and evolution of the geothermal state of the lithosphere. In: Magmatic and Metamorphic Formations in the Earth's History. Vasilenko V. B. (Ed). Nauka Publ., Novosibirsk 59-63. [in Russian].

Glebovitsky, V.A., Miller, Yu.V., Drugova, G.M., Mil'kevich, R.I., Vrevskii, A.B. (1996) The structure and metamorphism of the Belomoride–Lapland collision zone. Geotectonics 30: 53-63.

Glebovitsky V A. (Ed). (2005) Precambrian of the Baltic Shield. St. Petersburg, Nauka Publ. 1-711. [In Russian].

Glebovitsky, V A., Sedova, I.S. (2005) Metamorphism of the Belomorian Mobile Belt. In: Early Precambrian of the Baltic Shield. Glebovitsky V.A. (Ed). St. Petersburg, Nauka Publ. 251-287. [In Russian].

Grimes, C.B., John, B.E., Kelemen, P.B., Mazdab, F.K., Wooden, J.L., Cheadle, M.J., Swapp, S., Hanghøj, K., Schwartz, J.J. (2007) Trace element chemistry of zircons from oceanic crust: a method for distinguishing detrital zircon provenance. Geology 35: 643-646.

Guergouz, C., Martin, L., Vanderhaeghe, O., Thébaud, N., Fiorentini, M. (2018) Zircon and monazite petrochronologic record of prolonged amphibolite to granulite facies metamorphism in the Ivrea-Verbano and Strona-Ceneri Zones, NW Italy. Lithos 308-309: 1-18.

Hanmer, S., Passchier, C. (1991) Shear-sense indicators: a review. Geological Survey of Canada. Paper 90–17: 72.

Harley, S.L. Kelly, N.M. (2007a) The impact of zircon–garnet REE distribution data on the interpretation of zircon U-Pb ages in complex high-grade terrains: an example from the Rauer Islands, East Antarctica. Chemical Geology 241: 62-87.

Harley S.L. Kelly, N.M. (2007). Zircon – Tiny but Timely. Elements 3: 13-18.

Harley, S.L., Kelly, N.M., Möller, A. (2007b) Zircon behavior and the thermal histories of mountain chains. Elements 3: 25-30.

Herzberg, C., Condie, K., Korenaga, J. (2010) Thermal history of the Earth and its petrological expression. Earth and Planetary Science Letters 292: 79–88.

Herwartz, D., Nagel, T.J., Münker, C., Scherer, E.E., Froitzheim, N. (2011). Tracing two orogenic cycles in one eclogite sample by Lu–Hf garnet chronometry. Nature Geoscience 4: 178-183.

Herwartz, D., Skublov, S.G., Berezin, A. V., Mel'nik A.E. (2012) First Lu-Hf garnet ages of eclogites from the Belomorian mobile belt (Baltic Shield, Russia). Dokl. Earth Sci. 443: 377-380.

Hofmann, A.W. (1988) Chemical differentiation of the Earth: The relationship between mantle continental crust and oceanic crust. Earth and Planetary Science Letters 90: 297-314.

Holland, T.J.B. (1980) The reaction albite = jadeite + quartz determined experimentally in the range 600–1200 °C. American Mineralogist 65: 129-134.

Hölttä, P., Balagansky, V., Garde, A.A., Mertanen, S., Peltonen, P., Slabunov, A., Sorjonen-Ward, P., Whitehouse, M. (2008) Archean of Greenland and Fennoscandia. Episodes 31(1): 13-19.

Hölttä, P., Heilimo, E., Huhma, H., Kontinen, A., Mertanen, S., Mikkola, P., Paavola, J., Peltonen, P., Semprich, J., Slabunov, A., Sorjonen-Ward, P. (2012) The Archaean of the Karelia Province in Finland. In: The Archaean of the Karelia Province in Finland. Hölttä, P. (Ed). Geological Survey of Finland, Special Paper 54: 21-73.

Hölttä, P., Heilimo, E., Huhma, H., Kontinen, A., Mertanen, S., Mikkola, P., Paavola, J., Peltonen, P., Semprich, J., Slabunov, A., Sorjonen-Ward, P. (2014) The Archaean Karelia and Belomorian Provinces, Fennoscandian Shield. In: Evolution of Archean Crust and Early Life. Dilek, Y., Furnes, H. (Eds). Modern Approaches in Solid Earth Sciences 7: 55-102.

Imayama, T., Oh, C.-W., Baltybaev, S.K., Park, C.-S., Yi, K., Jung, H. (2017) Paleoproterozoic high-pressure metamorphic history of the Salma eclogite on the Kola Peninsula, Russia. Lithosphere 9: 855-873.

Jochum, K.P., Arndt, N.T., Hofmann, A.W. (1991) Nb-Th-La in komatiites and basalts: constrains on komatiite petrogenesis and mantle evolution. Earth and Planetary Science Letters 107: 272-289.

Kamzolkin V.A., Ivanov S.D., Konilov A.N. (2015) Empirical phengitic geobarometer: substantiation, calibration and practical application. Proceedings of the Russian Mineralogical Society 5: 1-14. [In Russian].

Kartushinskaya, T.V., Balagansky, V.V., Gorbunov, I.A., Larionov, A.N., L'vov, P.A. (2018) U-Pb age of inherited zircons from leucosomes in grey gneisses of the Salma and Gridino study areas, Belomorian Province. Transactions of Karelian Research Centre of RAS 11: 17-33.

Kaulina, T.V., Mitrofanov, F.P., Apanasevich, E.A., Zhavkov, V.A., D'yakov, S.N., Sherstennikova, O.G. (2005) U-Pb dating of garnet. In: Mitrofanov, F.P. (Ed.) New Data on Geology and Mineral Deposits of the Kola Peninsula. Kola Science Centre RAS, Apatity 60-64. [In Russian].

Kaulina, T.V., Yapaskurt, V.O., Presnyakov, S.L., Savchenko, E.E., Simakin, S.G. (2010) Metamorphic evolution of the Archean eclogite-like rocks of the Shirokaya and Uzkaya Salma (Kola Peninsula). Geochemistry International 48(9): 871-890.

Kelly E.D., Carlson, W.D., Connelly J.N. (2011). Implications of garnet resorption for the Lu–Hf garnet geochronometer: an example from the contact aureole of the Makhavinekh Lake Pluton, Labrador. Journal of Metamorphic Geology 29: 901-916.

Kohn, M.J., Kelly, N.M. (2018) Petrology and Geochronology of Metamorphic Zircon, Microstructural Geochronology: Planetary Records Down to Atom Scale, Geophysical Monograph 232: 35-61.

Konilov, A.N., Shchipansky, A.A., Mints M.V. (2005) Archaean eclogites from the central part of the Belomorian Mobile Belt, Kola Peninsula, Russia. Mitteilungen der Österreichischen Mineralogischen Gesellschaft 150: 70.

Konilov, A.N., Shchipansky, A. A., Mints, M. V., Kaulina, T. V., Dokukina, K.A., Natapov, L. M., Belousova, E. A., Griffin, W. L., O'Reilly, S. Y. (2011) The Salma eclogites from the Belomorian Province, Russia: evidence for HP/UHP metamorphism through the subduction of the Mesoarchean oceanic crust. In: Ultrahigh_Pressure Metamorphism: 25 Years after the Discovery of Coesite and Diamond. L. Dobrzhinetskaya, S. W. Faryad, S. Wallis, S. Cuthbert (Eds.). Elsevier, Amsterdam 635-682.

Konilov, A.N., Shchipansky, A., Mints, M.V., Volodichev, O.I. (2004) Petrology of eclogites of the Belomorian province. In: 32nd International Geological Congress. Scientific Sessions: abstracts (part 1) 108.

Korsakova M.A., Myskova T.N., Ivanov N.M. (2011) Sumian granitoid complexes in the southeastern North Karelian zone. In: Geology and useful minerals of Karelia, No 14. Golubev A.I. (Ed.). Petrozavodsk: KarRC RAS 57-71. [In Russian].

Kozlovsky, V.M., Aranovich, L.Ya. (2008) Geological and structural conditions of eclogitization of Paleoproterozoic basic dikes in the Eastern Belomorian Mobile Belt. Geotectonics 42(4): 305-317.

Kozlovsky, V.M., Aranovich, L.Ya. (2010) Petrology and Thermobarometry of Eclogite Rocks in the Krasnaya Guba Dike Field, Belomorian Mobile Belt. Petrology 18(1): 27-49.

Kretz, R. (1983) Symbols for rock-forming minerals. American Mineralogist 68: 277-279.

Krivolutskaya, N.A., Belyatsky, B.V., Smolkin, V.F., Mamontov, V.P., Fanygin, A.S., Svirskaya, N.M. (2010) Geochemical Specifics of Massifs of the Drusite Complex in the Central Belomorian Mobile Belt: II. Sm–Nd Isotopic System of the Rocks and the U–Pb Isotopic System of Zircons. Geochemistry International 48: 1064-1083.

Kulikov, V.S., Bychkova, Ya.V., Kulikova, V.V., Ernst, R. (2010) The Vetreny Poyas (Windy Belt) subprovince of southeastern Fennoscandia: An essential component of the ca. 2.5–2.4 Ga Sumian large igneous provinces. Precambrian Research 183: 589-601.

Kulikov, V.S., Svetov, S.A., Slabunov, A.I., Kulikova, V.V., Polin, A.K., Golubev, A.I., Gorkovets, V.Ya., Ivashchenko, V.I., Gogolev, M.A. (2017) Geological map of Southeastern Fennoscandia (scale 1:750 000): a new approach to map compilation. Transactions of the Karelian Research Centre of the Russian Academy of Sciences 2: 3-41

Lahtinen, R. Garde, A.A. Melezhik, V.A. (2008) Paleoproterozoic evolution of Fennoscandia and Greenland. Episodes 31 (1): 1-9.

Lahtinen, R., Huhma, H. (2019) A revised geodynamic model for the Lapland-Kola orogen. Precambrian Research 330: 1-19.

Larikova T.L. (2000) Genesis of Drusitic (Corona) Textures around Olivine and Orthopyroxene during Metamorphism of Gabbroids in Northern Belomorie, Karelia. Petrology 8(4): 384-402.

Li, X.L., Zhang, L.F., Wei, C.J., Slabunov, A.I. (2015) Metamorphic PT path and zircon U-Pb dating of Archean eclogite association in Gridino complex, Belomorian province, Russia. Precambrian Research 268: 74-96.

Li, X., Zhang, L., Wei, Ch., Slabunov, A.I., Bader, T. (2017). Neoarchean-Paleoproterozoic granulite-facies metamorphism in Uzkaya Salma eclogite-bearing mélange, Belomorian Province (Russia). Precambrian Research 294: 257-283.

Li, X., Zhang, L., Wei, Ch., Slabunov, A.I., Bader, T. (2018) Quartz and orthopyroxene exsolution lamellae in clinopyroxene and the metamorphic P–T path of Belomorian eclogites. Journal of Metamorphic Geology 38: 1-22.

Liu, F.L., Zhang, L.F., Li, X.L., Slabunov, A.I., Wei, C.J., Bader, T. (2017) The metamorphic evolution of Paleoproterozoic eclogites in Kuru-Vaara, northern Belomorian Province, Russia: Constraints from P-T pseudosections and zircon dating. Precambrian Research 289: 31-47.

Maksimov, O.A. (2019) Geology and petrology of eclogites in the Samylino area (Belomorian province of the Fennoscandian Shield). Transactions of the Karelian Research Centre of the Russian Academy of Sciences 2: 88-94. [In Russian].

Martin, H., Smithies, R.H., Rapp, R., Moyen J.-F., Champion, D. (2005) An overview of adakite, tonalite-trondhjemite-granodiorite (TTG) and sanukitoid: relationships and some implications for crustal evolution. Lithos 79: 1-24.

Martin, L.A.J., Duchêne, S, Deloule, E, Vanderhaeghe, O. (2008) Mobility of trace elements and oxygen in zircon during metamorphism: Consequences for geochemical tracing. Earth and Planetary Science Letters 267: 161-174.

Mezger, K., Hanson, G.N., Bohlen, S.R. (1989) U-Pb systematics of garnet: dating of the growth of garnet in the Late Archean Pikwitonei granulite domain at Cauchon and Natawahuman lakes, Manitoba, Canada. Contributions to Mineralogy and Petrology 101: 136-148.

Mel'nik, A.E. (2015). Eclogites from the northern-western part of the Belomorian mobile belt: Geochemistry and Age of the metamorphism. PHD thesis, St.-Petersburg, Institute of Precambrian Geology and Geochronology RAS 1-20.

Mel'nik, A.E., Skublov, S.G., Marin, Y.B., Berezin, A.V., Bogomolov, E.S. (2013) New data on the age (U–Pb, Sm–Nd) of garnetites from Salma eclogites of the Belomorian mobile belt. Doklady Earth Sciences 448: 78-85.

Miller, Yu.V., Mil'kevich, R.I. (1995) The Fold-and-Nappe Structure of the Belomorian Zone and Its Relationshipwith the Karelian Granite–Greenstone Domain. Geotektonika 6: 80–93. [In Russian].

Miller, C.F., McDowell, S.M., Mapes R.W. (2003). Hot and cold granites? Implications of zircon saturation temperatures and preservation of inheritance. Geology 31: 529-532.

Mitrofanov, F.P., Pozhilenko, V.I., Smolkin, V.F., et al. (1995) Geology of Kola Peninsula. KSC RAS 1-145.

Mints, M.V., Belousova E.A., Konilov, A. N., Natapov, L.M., Shchipansky, A.A., Griffin, W.L., O'Reilly, S.Y., Dokukina, K.A., Kaulina T.V. (2010a) Mesoarchean subduction processes: 2.87 Ga eclogites from the Kola Peninsula, Russia. Geology 38: 739-742.

Mints, M.V., Suleimanov, A.K., Babayants, P.S., Belousova, E.A., Blokh, Yu.I., Bogina, M.M., Bush, W.A., Dokukina, K.A., Zamozhniaya, N.G., Zlobin, V.L., Kaulina, T.V., Konilov, A.N., Mikhailov, V.O., Natapov, L.M., Piip, V.B., Stupak, V.M., Tihotsky, S.A., Trusov, A.A., Philippova, I.B., Shur, D.Yu. (2010b) Deep Structure, Evolution and Mineral Deposits of the Early Precambrian Basement of the East European Platform: an Interpretation of the Data From 1-EU Geotraverse, the 4B and Tatseis Profiles. GEOKART, GEOS., Moscow v. 1: 1-408, v. 2: 1-400. [in Russian].

Mints, M.V., Dokukina, K.A. (2019 in press) The Belomorian eclogite province (Eastern Fennoscandian Shield, Russia): Meso- or Neoarchaean or Late Paleoproterozoic? Geodynamics & Tectonophysics.

Mints, M.V., Dokukina, K.A., Konilov, A.N. (2014) The Meso-Neoarchaean Belomorian eclogite province: tectonic position and geodynamic evolution. Gondwana Research 25: 561-584.

Mints, M.V., Dokukina, K.A., Konilov, A.N., Philippova, I.B., Zlobin, V.L., Babayants, P.S., Belousova, E.A., Blokh, Yu.I., Bogina, M.M., Bush, W.A., Dokukin, P.A., Kaulina, T.V., Natapov, L.M., Piip, V.B., Stupak, V.M., Suleimanov, A.K., Trusov, A.A., Van, K.V., Zamozhniaya, N.G. (2015) East European Craton: Early Precambrian history and 3D models of deep crustal structure. The Geological Society of America Special Paper 510: 1-433.

Mints, M.V., Eriksson, P.G. (2016) Secular changes in the relationships between platetectonic and mantle-plume engendered processes during Precambrian time. Geodynamics & Tectonophysics 7(2): 173-232.

Mints, M.V., Kaulina, T.V., Konilov, A.N., Krotov, A.V., Stupak, V.M. (2007) The thermal and geodynamic evolution of the Lapland Granulite Belt: implications for thermal structure of the lower crust during granulite-facies metamorphism. Gondwana Research 12: 252-267.

Mints, M.V., Konilov, A.N., Dokukina, K.A. (2014) Belomorian eclogite province, Salma association, Kola Peninsula: Uzkaya and Shirokaya localities. In: Precambrian high-grade mobile belts; Bolomorian mobile belt in eastern Fennoscandian Shield. Field Guidebook. Petrozavodsk, KRC RAS 39-63.

Moyen, J.-F. (2011) The composite Archaean grey gneisses: Petrological significance, and evidence for a non-unique tectonic setting for Archaean crustal growth. Lithos 123: 21-36.

Morgunova, A.A., Perchuk, A.L. (2012). UHP metamorphism in an Archaean-Proterozoic mobile belt, Gridino complex, Karelia, Russia). Doklady Earth Sciences (Moscow) 443: 358-362.

Mudruk, S.V., Balagansky, V.V., Gorbunov, I.A., Raevsky, A.B. (2013) Alpine-type tectonics in the Paleoproterozoic Lapland-Kola Orogen. Geotectonics 47: 251-265.

Nakamura N. (1974). Determination of REE, Ba, Fe, Mg, Na and K in carbonaceous and ordinary chondrites. Geochimica et Cosmochimica Acta. 38: 757-775.

Nesterova, N.S., Kirnozova, T.I., Fugzan, M.M. (2011) New U-Pb titanite age data on the rocks from the Karelian craton and the Belomorian mobile belt, Fennoscandian shield. Geochemistry international 49(12): 1161-1167.

Nomenclature of the micas: final report of mica subcommittee of the Commission on new minerals and mineral names of the International Mineralogical Association (CNMMN IMA) (1998) Proceedings of the Russian Mineralogical Society 5: 55-65. [In Russian].

O'Brien, P. J., Rötzler, J. (2003) High-pressure granulites: Formation, recovery of peak conditions, and implications for tectonics. Journal of Metamorphic Geology 21: 3-20.

Pearce, J.A. (2008) Geochemical fingerprinting of oceanic basalts with applications to ophiolite classification and the search for Archean oceanic crust. Lithos 100: 14-48.

Peltonen, P., Kontinen, A. (2004) The Jormua ophiolite: a mafic-ultramafic complex from an ancient ocean-continent transition zone. In: Precambrian Ophiolites and Related Rocks. Kusky, T., Veenstra, V., Condie, K. (Eds). Elsevier, Amsterdam 35-71.

Perchuk, A.L., Morgunova, A.A. (2014). Variable P–T paths and HP-UHP metamorphism in a Precambrian terrane, Gridino, Russia: Petrological evidence and geodynamic implications. Gondwana Research 25: 614-629.

Powell, R. (1985) Regression diagnostics and robust regression in geothermometer/geobarometer calibration: the garnet-clinopyroxene geothermometer revised. Journal of metamorphic Geology 3: 231-243.

Sharov, N.V., Slabunov, A.I., Isanina, E.V., Krupnova, N.A., Roslov, Y.V., Shchiptsova, N.I. (2010). Seismic simulation of the Earth's crust on the profiles DSS – CDP Kalevala-Kem'-White Sea. Geophysical journal (Ukraina) 32: 21-34. [In Russian].

Sibelev, O.S. (2012) Gridino mélange zone (Belomorian mobile belts): geology and crustal architecture. In: Geology and useful minerals of Karelia. No15. Golubev A.I. (Ed.). Petrozavodsk: KarRC RAS 28-37. [In Russian].

Sibelev, O.S., Babarina, I.I., Slabunov, A.I., Konilov, A.N. (2004) Archean eclogite-bearing mélange in the Gridino zone (Belomorian mobile belt) on Stolbikha Island: structure and metamorphism. In: Geology and useful minerals of Karelia, No 7. Golubev A.I. (Ed.). Petrozavodsk: KarRC RAS 5-20. [In Russian].

Shchipansky, A.A. (2012) Subduction geodynamics in Archean and formation of diamond-bearing lithospheric keels and early continental crust of cratons. Geotectonics 46(2): 122-141.

Shchipansky, A.A., Babarina, I.I., Konilov, A.N., Krylov, K.A., Samsonov, A.V., Bogina, M.M., Bibikova, E.V., Slabunov A.I. (2004). 2.8 Ga boninite-hosting partial suprasubduction zone ophiolite sequences from the North Karelian greenstone belt, NE Baltic Shield, Russia. In: Precambrian ophiolites and related rocks. Kusky, T.M. (Eds.). Developments in Precambrian Geology 13. Amsterdam: Elsevier 425-486.

Shchipansky, A.A., Khodorevskaya, L.I., Konilov, A.N., Slabunov, A.I. (2012a) Eclogites from the Belomorian Mobile Belt (Kola Peninsula): geology and petrology. Russian Geology and Geophysics 53: 1-21.

Shchipansky, A.A., Khodorevskaya, L.I., Slabunov, A.I. (2012b) The geochemistry and isotopic age of eclogites from the Belomorian Belt (Kola Peninsula): evidence for subducted Archean oceanic crust. Russian Geology and Geophysics 53: 262-280.

Shchipansky, A.A., Sidorov, M.Yu., Balagansky, V.V. (2019) Vestigial UHP mineral assemblages in the Archean rocks from the Kuru-Vaara quarry, Belomorian Province, Kola Peninsula, Russia. In. Abstract Volume of the 13th of International Eclogite Conference. C. Mattinson et al. (Eds.). Petrozavodsk: KarRC RAS 78.

Shchipansky, A.A., Slabunov A.I. (2015) Provenance of 'Svecofennian zircons' in the Belomorian mobile belt, Baltic shield, and some geodynamic implications. Geochemistry International 53: 869-891.

Skublov, S.G., Astaf'ev, B.Yu., Berezin, A.V., Marin, Yu.B., Mel'nik, A.E., Presnyakov, S.L. (2011a) New data on the age of eclogites from the Belomorian Mobile Belt at Gridino settlement area. Doklady Earth Sciences 439: 1163-1170.

Skublov, S.G., Berezin, A.V., Mel'nik, A.E. (2011b) Paleoproterozoic eclogites in the Salma area, Northwestern Belomorian mobile belt: Composition and isotopic geochronologic characteristics of minerals and metamorphic age. Petrology 19: 470-495.

Skublov, S.G., Balashov, Y.A., Marin, Y.B., Berezin, A.V., Mel'nik, A.E., Paderin, I.P. (2010) U-Pb age and geochemistry of zircons from Salma eclogites (Kuru-Vaara deposit, Belomorian Belt). Doklady Earth Sciences 432: 791-798.

Skublov, S.G., Berezin, A.V., Berezhnaya, N.G. (2012) General relations in the trace-element composition of zircons from eclogites with implications for the age of eclogites in the Belomorian Mobile Belt. Petrology 20: 427-449.

Skublov, S.G., Berezin, A.V., Mel'nik, A.E., Astafiev, B.Yu., Voinova, O.A., Alekseev, V.I. (2016) Protolith Age of Eclogites from the Southern Part of Pezhostrov Island, Belomorian Belt: Protolith of Metabasites as Indicator of Eclogitization Time. Petrology (Moscow) 24: 594-607.

Slabunov, A.I. (2008) Geology and geodynamics of the Archean mobile belts exemplified on Belomorian Province of the Fennoscandian Shield. Petrozavodsk: KarRC RAS: 1-296. [In Russian].

Slabunov, A.I., Azimov, P.Ya., Glebovitsky, V.A., Zhang, L., Kevlich, V.I. (2016) Archean and Paleoproterozoic migmatization in the Belomorian Province, Fennoscandian Shield: petrology, geochronology and geodynamic setting. Doklady Earth Sciences 467(1): 71-74.

Slabunov, A.I., Guo, J., Balagansky, V.V., Lubnina, N.V., Zhang, L. (2017) Early Precambrian Crustal evolution of the Belomorian and Trans-North China orogens and supercontinents reconstruction. Geodynamics & Tectonophysics 8(3): 569-572.

Slabunov, A.I., Lobach-Zhuchenko, S.B., Bibikova, E.V., Balagansky, V.V., Sorjonen-Ward, P., Volodichev, O.I., Shchipansky, A.A., Svetov, S.A., Chekulaev, V.P., Arestova, N.A., Stepanov, V.S. (2006a) The Archean of the Baltic Shield: Geology, Geochronology, and Geodynamic Settings. Geotectonics 40: 409-433.

Slabunov, A.I., Lobach-Zhuchenko, S.B., Bibikova, E.V., Sorjonen-Ward, P., Balagansky, V.V., Volodichev, O.I., Shchipansky, A.A., Svetov, S.A., Chekulaev, V.P., Arestova, N.A., Stepanov, V.S. (2006b). The Archaean nucleus of the Fennoscandian (Baltic) Shield. Geological Society, London, Memoirs 32 627-644.

Slabunov, A.I., Shchipansky, A.A., Stepanov, V.S., Babarina, I.I. (2019) A tectonic remnant of the Mesoarchean oceanic lithosphere in the Belomorian Province, Fennoscandian Shield. Geotectonics 53(2): 205-230.

Slabunov A.I., Volodichev O.I., Li Xiaoli, Maksimov O.A. (2015) Archean zoisitites of the gridino eclogitebearing melange, Belomorian province of the Fennoscandian shield: geology, U-Pb zircon ages and geodynamic setting. Transactions of the Karelian Research Centre of the Russian Academy of Sciences 7: 85-103.

Slabunov, A.I., Volodichev, O.I., Skublov, S.G., Berezin, A.V. (2011). Main Stages of the Formation of Paleoproterozoic Eclogitized Gabbro-Norite: Evidence from U–Pb (SHRIMP) Dating of Zircons and Study of Their Genesis. Doklady Earth Sciences 437: 396-400.

Slabunov, A.I., Volodichev, O.I., Stepanova, A.V., Sibelev, O.S., Stepanov, V.S., Babarina, I.I. (2008) Archean eclogites and Paleoproterozoic eclogitized gabbroids, Gridino area, White Sea. In: Karelian Craton transect (Finland, Russia): Precambrian greenstone belts, ophiolites and eclogites. Peltonen, P., Hölttä, P., Slabunov, A. (Eds.) 33 IGC, The Nordic Countries. Oslo Archean eclogites and Paleoproterozoic eclogitized gabbroids, Gridino area, White Sea 36-53.

Stepanov, V.S. (1981) Basic magmatism of the Precambriam of the western Belomorian Region. Leningrad: Nauka 1-216. [In Russian].

Stepanov, V.S., Stepanova, A.V. (2005) Dyke field Gridino: geology, geochemistry, petrology. In: Belomorian mobile belt and its analogues: geology, geochronology, geodynamics and metallogeny. Field trip guide book and Extended abstracts. Petrozavodsk: KarRC RAS 285-288. [In Russian].

Stepanova, A.V., Larionov, A.N., Bibikova, E.V., Stepanov, V.S., Slabunov, A.I. (2003) Early Proterozoic (2.1 Ga) Fe-tholeiite magmatism in the Belomorian Province of the Baltic Shield: geochemistry and geochronology. Doklady Earth Sciences 390: 528-532

Stepanova, A., Stepanov, V. (2010) Paleoproterozoic mafic dyke swarms of the Belomorian Province, eastern Fennoscandian Shield. Precambrian Research 183(3): 602-616.

Stepanova, A.V., Samsonov, A.V., Salnikova, E.B., Puchtel, I.S., Larionova, Y.O., Larionov, A.N., Stepanov, V.S., Shapovalov, Y.B., Egorova, S.V. (2014) Palaeoproterozoic Continental MORB-type Tholeiites in the Karelian Craton: Petrology, Geochronology, and Tectonic Setting. Journal of Petrology 55(9): 1719-1751.

Stepanova, A.V., Stepanov, V.S., Larionov, A.N., Azimov, P.Ya., Egorova, S.V., Larionova, Yu.O. (2017) 2.5 Ga Gabbro-anorthosites in the Belomorian Province, Fennoscandian Shield: Petrology and Tectonic Setting. Petrology 25(6): 566-591.

Sudovikov, N.G. (1936) Report on the geology over the South-Western part of Kola Peninsula. Leningrad Geological Trust 10, 1-38. [in Russian].

Sun S., McDonough W.F. (1989) Chemical and isotopic sistematics og oceanic basalts: implications for mantle composition and processes. In: Magmatism in the Ocean basins. Sanders A.D., Norry M.J. (Eds.) Special Publication 42. London 313-345.

Timmerman, M.J., Daly, J.S. (1995) Sm-Nd evidence for late Archaean crust formation in the Lapland–Kola Mobile Belt, Kola Peninsula, Russia and Norway. Precambrian Research 72: 97-107.

Travin, V.V. (2015) The Structural Position and Age of Eclogitization in the Area of Gridino Village in the Belomorian Mobile Belt. Geotectonics 49(5): 425-438.

Travin, V.V., Kozlova, N.E. (2005) Local shear deformations as a cause of eclogitization: evidence from the Gridino mélange zone, Belomorian mobile belt. Doklady Earth Sciences 405: 1275-1278.

Travin, V.V., Kozlova, N.E. (2009). Eclogitization of basites in early Proterozoic shear zones in the area of the village of Gridino, Western Belomorie. Petrology 17: 684-706.

Travin, V.V., Stepanov V.S., Dokukina K.A. (2005). Characteristics and conditions of the formation of tectonites in the Izbnaya Luda Island (Gridino Village area, northwestern Belomorian region) In: Geology and mineral deposits of Karelia. No 8. Golubev A.I. (Ed.) Petrozavodsk: KarRC RAS 40-49. [in Russian].

Tuisku, P., Makkonen, H.V. (1999). Spinel-bearing symplectites in Palaeoproterozoic ultramafic rocks from two different geological settings in Finland: Thermobarometric and tectonic implications. GFF 121: 293–300.

Volodichev, O.I. (1977) Metamorphic Evolution of the Polycyclic Belomorian Complex in Recurrence and Direction of Regional Metamorphism. Leningrad: Nauka 57-79. [In Russian].

Volodichev, O.I. (1990) The Belomorian Complex of Karelia (Geology and Petrology). Leningrad: Nauka 1-248. [In Russian].

Volodichev, O.I., Parfenova, O.V., Kuzenko, T.I. (2008) Paleoproterozoic eclogites of the Belomorian mobile belt (on eclogitization of gabbro in a lherzolite-gabbronorite dyke). In: Geology and mineral deposits of Karelia. No 11. Golubev A.I. (Ed.). Petrozavodsk: KarRC RAS 37-61. [in Russian].

Volodichev, O., Slabunov, A., Bibikova, E., Konilov, A. (2003) Archean eclogites from the Belomorian Mobile Belt in the Fennoscandian /Baltic Shield, Russia. In: The Alice Wain Memorial Western Norway Eclogite Symposium. Abstract volume 157-158.

Volodichev, O.I., Slabunov, A.I., Bibikova, E.V., Konilov A.N., Kuzenko, T.I. (2004) Archean Eclogites in the Belomorian Mobile Belt, Baltic Shield. Petrology 12(6): 540-560.

Volodichev, O.I., Slabunov, A.I., Sibelev, O.S., Skublov, S.G., Kuzenko, T.I. (2012) Geochronology, Mineral Inclusions, and Geochemistry of Zircons in Eclogitized Gabbronorites in the Gridino Area, Belomorian Province. Geochemistry International 50(8): 657-670.

Volodichev, O.I., Slabunov, A.I., Stepanov, V.S., Sibelev, O.S., Travin, V.V., Stepanova, A.V., Babarina, I.I. (2005) Archean and Paleoproterozoic eclogites and Paleoproterozoic druzites, Gridino area, White sea. In: Belomorian mobile belt and it's analogues: geology, geochronology, geodynamics and metallogeny. Field Guidebook and Extended abstracts. Petrozavodsk: KRC RAS 60-80.

Volodichev, O.I., Slabunov, A.I., Stepanova, A.V., Stepanov, V.S., Sibelev, O.S. (2011). Archean and Paleoproterozoic eclogites from the Gridino area, White Sea. In. Granulite and eclogite complexes in the Earth's evolution. Extended abstracts and field guide. A guide of scientific field trips. Petrozavodsk: KarRC, RAS 21-46.

Volodichev O.I., Slabunov A.I., Stepanova A.V., Stepanov V.S., Sibelev O.S. (2014) Archean eclogites and Paleoproterozoic eclogitized gabbroids, Gridino area, White sea. In: Precambrian high-grade mobile belts. Belomorian mobile belt in the eastern Fennoscandian Shield. Field Guidebook. Petrozavodsk: KRC RAS 7-32.

Watson E.B., Wark D.A., Thomas J.B. (2006a) Crystallization thermometers for zircon and rutile. Contributions to Mineralogy and Petrology 151: 413-433.

Watson E.B., Hayden L.A., Wark D.A., Cherniak D.J., Thomas J.B., Manchester J.E. (2006b) New crystallization thermometers for zircon, rutile and sphene; calibrations, diffusion considerations, and applications. Northeastern Section — 41st Annual Meeting. Abstracts with Programs, Geological Society of America 38: 5.

Xiong, X.L. (2006) Trace element evidence for growth of early continental crust by melting of rutile-bearing hydrous eclogite. Geology 34: 945-948.

Yu, H.L., Zhang, L.F., Wei, C.J., Li, X.L., Guo, J.H. (2017) Age and P–T conditions of the Gridino-type eclogite in the Belomorian Province, Russia. Journal of Metamorphic Geology 35: 855-869.

Yu, H., Zhang, L., Lanari, P., Rubatto, D., Li, X. (2019a) Garnet Lu–Hf geochronology and P-T path of the Gridino-type eclogite in the Belomorian Province, Russia. Lithos 326–327: 313-326.

Yu, H., Zhang, L., Zhang L., Chunjing Wei Ch., Li, X., Guo J., Bader, T., Qi, Y. (2019b) The metamorphic evolution of Salma-type eclogite in Russia: Constraints from zircon/titanite dating and phase equilibria modeling. Precambrian Research 326: 363-384.

Научное издание
Scientific publication

EARLY PRECAMBRIAN ECLOGITES
of the Belomorian Province, Fennoscandian Shield

Field Guidebook

Печатается по решению Ученого совета
Института геологии КарНЦ РАН

Печатается в авторской редакции

Дизайн обложки: *А.И. Слабунов, А.В. Пилицына*
Design of a cover: *Alexander Slabunov & Anfisa Pilitsyna*

Подписано в печать 28.05.19. Формат $60\times84^{1}/_{8}$.
Гарнитура Times New Roman. Уч.-изд. л. 8,95. Усл. печ. л. 9,53.
Тираж 150 экз. Заказ 558

Федеральный исследовательский центр
«Карельский научный центр Российской академии наук»
Редакционно-издательский отдел
185003, г. Петрозаводск, пр. А. Невского, 50